Syn-eruptive incision of Koko Crater, Oahu, Hawaii by condensed steam and hot cohesive debris flows: a re-interpretation of the type locality of "surge-eroded U-shaped channels"

by

Jessica Keri Bluth

B.S., State University of New York at Binghamton, 2001

Submitted to the Graduate Faculty of

Arts and Sciences in partial fulfillment

of the requirements for the degree of

Master of Science

University of Pittsburgh

2004

UNIVERSITY OF PITTSBURGH

FACULTY OF ARTS AND SCIENCES

This dissertation was presented

by

Jessica Keri Bluth

It was defended on

June 25, 2004

and approved by

Dr. Michael Ramsey

Dr. Charles Jones

Dr. Ian Skilling
Committee Chairperson

Syn-eruptive incision of Koko Crater, Oahu by condensed steam and hot cohesive debris flows: a re-interpretation of the type locality of "surge-eroded U-shaped channels"

Jessica K. Bluth, M.S.

Department of Geology and Planetary Science
University of Pittsburgh, 2004

Phreatomagmatic fall, low-concentration PDC deposits and remobilized equivalents dominate the products of craters (tuff cones/rings) of Koko fissure, south-east Oahu. At Koko crater, Fisher (1977) described "U-shaped" channels, which he interpreted as due to erosion by low-concentration PDCs (surges), with minor modification by stream and debris flows. Similar channels on tuff cones and rings elsewhere in the world have been interpreted as "surge-eroded" by subsequent authors. However, no evidence for erosion by PDCs was observed during recent fieldwork, which suggested rather the following model. An important observation is that initial incision is always correlated with the emplacement of vesiculated ash layers (derived from Hanauma Bay), and is only very rarely associated with other facies. Incision of the vesiculated ash by run-off generated an initial and widespread network of sinuous, narrow (<15 cm) and shallow (<15 cm) rills. The strong correlation of rills with vesiculated ash and the lack of obvious water-escape structures in these ashes implies that run-off was mostly derived from associated steam-rich plumes. Initial steam and rain-fed incision was probably also enhanced in these very fine-grained cohesive deposits as a consequence of lowered infiltration rates. The rill network developed locally into deeper channels (i.e. gullies) during steam and rain-fed run-off, and by significant erosion during emplacement of vesiculated (hot) debris flows, derived from remobilized vesiculated ash. Pyroclastic density currents from Hanuama Bay traveling laterally across the flank of Koko Crater, perpendicular to the gully axes, provided the bulk of the gully fills, but gave rise to little or no modification of their margins. Rill and gully development by

rainfall alone could explain similar examples of incision of low-concentration PDC deposits elsewhere in the world, but the possibility of steam-fed rills and erosion by hot debris flows should be considered. Low-concentration PDCs do not seem to be able to erode their substrate in all cases.

Acknowledgements

No great accomplishment can ever be attributed to the efforts of just one person. I would like to extend sincere gratitude to the following individuals for their assistance in the preparation of this thesis.

First and foremost, to my committee members:
Ian Skilling, for being an overall inspiring mentor...and not getting mad about the GPS unit.

Mike Ramsey, who has taught me (maybe unknowingly) that there is no limit to success when you truly love what you do.

Charlie Jones, for providing excellent criticisms of this thesis and for always offering a friendly face and a good story.

And also:
To my parents, Hedy and Neil Bluth, without whom this achievement would have never been possible.

To Brian Bluth, who always managed to provide me with confidence when it was really necessary.

To Sally Kuhn, my friend and trusty field assistant, who helped me through that day in Hawaii when I was reminded to never turn my back on the ocean.

To Erich Zorn, for pulling me through the most difficult moments with praise and encouragement (and caffeine and sugar).

To Brian Games, for his help with sample preparation.

To the graduate students and staff (past and present) in the department of Geology and Planetary Science at the University of Pittsburgh, who have provided support and friendship throughout the duration of my graduate studies.

TABLE OF CONTENTS

LIST OF TABLES

LIST OF FIGURES

1. Introduction

Incisional structures occur in sequences of phreatomagmatic fall and low-concentration pyroclastic density current (PDC) deposits that comprise the lowermost southeastern flanks of Koko Crater, Oahu, Hawaii (Figures 1 and 2). Cross-sections of the incisional structures are well exposed in the cliff faces at the base of this tuff cone. This research evaluates the erosional mechanisms by which the incisional structures were produced.

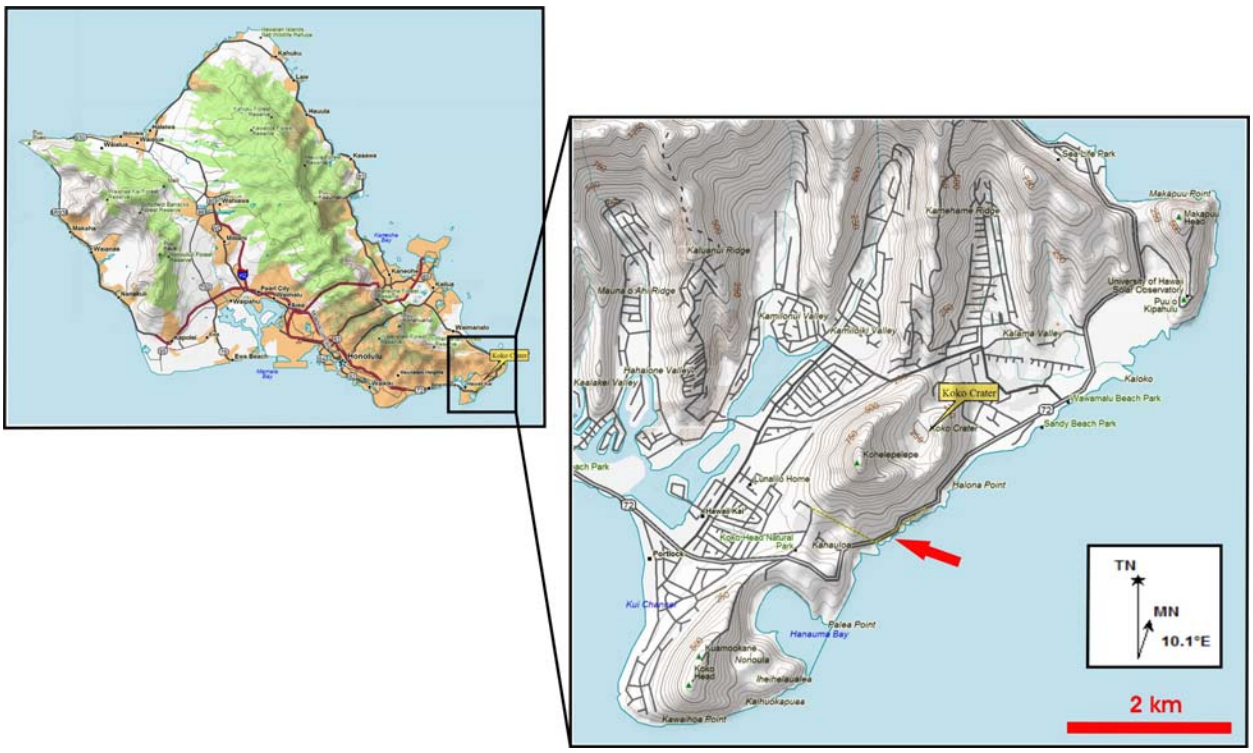

Figure 1. Map of southeastern Oahu.
Arrow indicates the location of the study area at the southeastern base of Koko Crater.

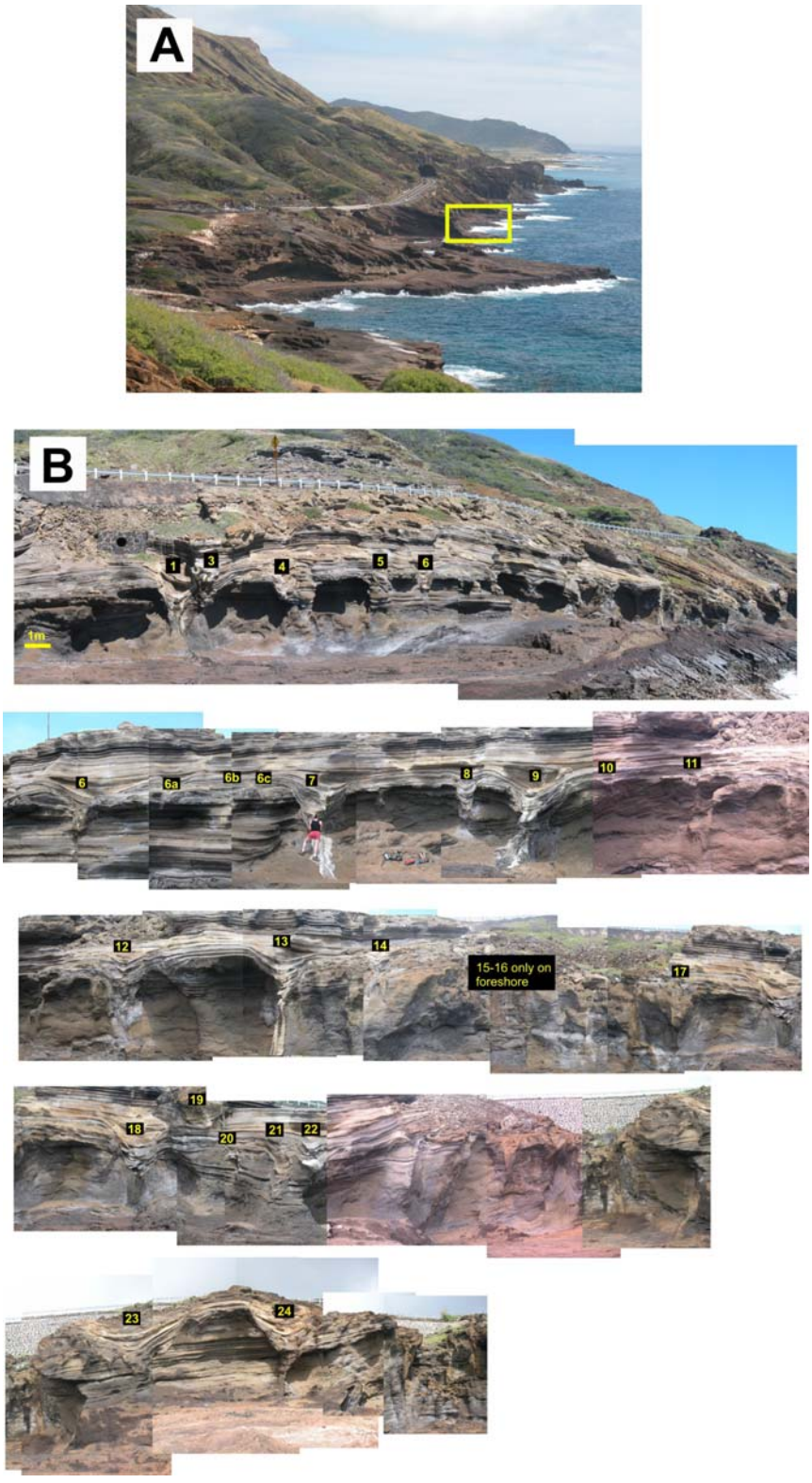

Figure 2. Southeastern base of Koko Crater

(A) Box indicates the portion of the coastline along which the incisional structures are exposed. (B) Composite of the study area with numbered incisional structures.

1.1. Purpose of study

The incisional structures along the SE flanks of Koko Crater have been studied by Fisher (1977). Fisher termed the structures "U-shaped channels" and suggested that they formed during the following sequence of events: (1) Small V-shaped fluvial channels develop on the steep outer slopes of the tuff cone; (2) Debris flows, derived from the collapse/slumping of oversteepened walls of the initial "stream channels," slightly modify the pre-existing channels into somewhat more rounded (U-shaped) forms. Debris flow material was composed of water-saturated Koko Crater tephra; (3) The subsequent passage of base surges ("wet" low-concentration pyroclastic density currents) erupted from Hanauma Bay, approximately 2 km southeast of Koko Crater (Figure 1), erode and partially or completely reshape the original channels into semi-circular U-shapes. Where mudflow or alluvial deposits do not intervene between the channels and outlying tephra, primary incision was attributed to the passage of base surges. Fisher (1977) suggested that incision by base surges was not always dependent upon the presence of pre-existing drainage.

The principal purpose of this study is to re-evaluate these very widely cited conclusions. Similar channels or incisional structures within low-concentration PDC (surge) deposits elsewhere have often been attributed to erosion by pyroclastic surge currents (e.g. Leys, 1983; Cas and Wright, 1987; Francis, 1993; Bull and Cas, 2000; Leat and Thompson, 1988; Wohletz, 1998).

An alternative model for the formation of the incisional structures at SE Koko Crater is presented here and involves the following scenario: (1) Wet fallout and PDC (surge) deposits from Hanauma Bay drape the steep flanks of southeast Koko Crater. An initial network of rills (incisional structures < 15 cm wide and deep) is generated in beds of fine-grained, cohesive ash by condensing steam and enhanced rain-fed runoff; (2) Coalescence of these ash-bearing rills

and slope failure of these deposits generate debris flows of hot (vesiculated) ash. Erosion of the substrate by these flows enlarge the rills into gullies (incisional structures > 15 cm wide and deep). Debris flow material was composed of water-saturated Hanauma Bay tephra; (3) Additional modification to gullies is provided by periodic marginal failure, prolonged surface flow, and probably pipe formation. Later phreatomagmatic deposits (fallout and low concentration PDCs) from Hanauma Bay mantled this area and largely filled the gully structures, but did not erode the substrate.

2. Geology

2.1. Introduction

This study was conducted at the southeastern base of Koko Crater, a basanitic tuff cone situated along the Koko Rift in southeastern Oahu, Hawaii (Figures 4 and 5). Oahu is composed of two large, highly eroded shield volcanoes constructed from tholeiitic basalt flows during the mid- to late-Pliocene and early Pleistocene epochs (Self and Moberly, 1997; Doell and Dalrymple, 1973; Langenheim and Clague, 1987). Koko Crater is one of approximately forty volcanic centers in southeastern Oahu that represent post-erosional, rejuvenation-stage volcanism that supplied Oahu with the vast majority of its presently exposed pyroclastic deposits. Along the Koko Rift, Koko Crater is one of about eight tuff rings and tuff cones. Some of these vents may have been active simultaneously while others may have erupted several thousand years apart. The proximity of these craters is such that some are mantled with ejecta from neighboring vents. Koko Crater is one such example. Seacliffs at the lower southeastern flanks of this crater expose sequences of tephra ejected from the Koko Crater vents that are overlain by base surge and airfall deposits originating from the nearby Hanauma Bay vents approximately 2 km to the southwest (Figure 4).

2.2. Regional geology: Oahu

The island of Oahu is located in the northwestern portion of the Hawaiian Archipelago. Like the other constituent islands in the Hawaiian chain, Oahu is situated on a northwest-southeast trending ridge and is a site of (former) hot spot volcanic activity. Presently covering

4052 km^2 (604 mi^2), Oahu comprises two shield volcanoes, Koolau in the east and Waianae in the west (Figure 3). Waianae is the older volcano, and its subaerial component was constructed in the late Teritary (Pliocene) between 3.9 and 2.5 Ma (Self and Moberly, 1997). Koolau began as a seamount above the Hawaiian hotspot about 3 million years ago. It emerged above sea level at 2.7 Ma and continued shield building until 1.7 Ma in the early Quaternary (Pleistocene) (Doell and Dalrymple, 1973; Langenheim and Clague, 1987). The two volcanoes surfaced as separate islands that gradually merged as successive outpourings of lava from Koolau filled the intervening ocean. The Schofield Plateau is the resultant plain between the two edifices which now slopes gently to the ocean (Figure 3). Lavas from Koolau bank against the northeastern lower flanks of Waianae, suggesting the latter volcano went extinct prior to coalescence.

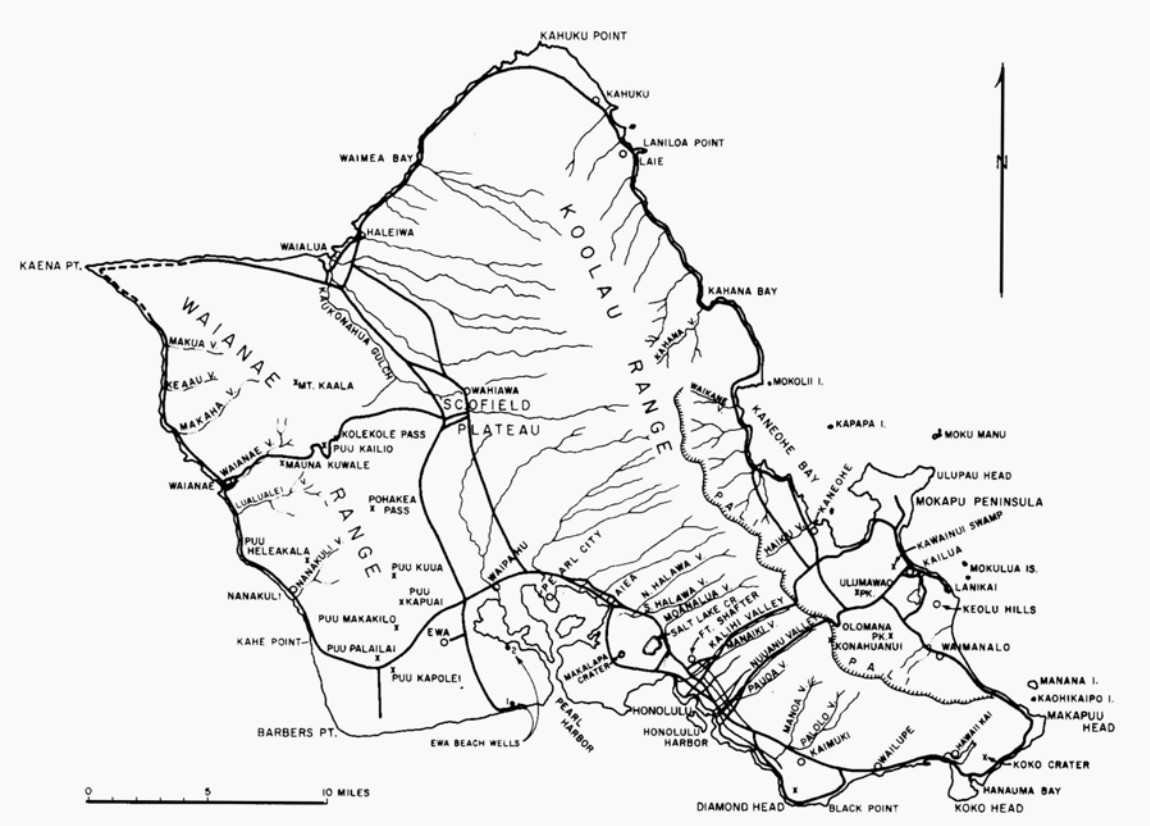

Figure 3. Map of Oahu
After Macdonald and Abbott (1970)

Waianae and Koolau volcanoes are composed of successive, thin flows of tholeiitic (and later alkalic) lavas dipping 5-15˚ away from source craters and rifts. These flows are mostly of the pahoehoe type, with lesser aa flows and thin, very minor lenses and beds of tuff (Wentworth, 1926; Stearns and Vaksvik, 1935; Macdonald and Abbott, 1970; Moberly and Walker, 1987). Both volcanoes presently stand as elongated ridges rather than rounded domes. This form is partly attributed to the trends of the rifts from which lavas emanated but it is also a product of erosion. Waianae and Koolau have suffered extensive erosion by chemical and physical agents since shield-building activity ceased. It is estimated that probably half of Koolau volcano has been eroded away in the last 1.5 million years, mostly from the eastern (windward) side (Gramlich et al., 1971). Stream erosion has carved deep valleys into the flanks, some exceeding 600 m (2000 ft) in depth. The valleys mostly originate from cirque-like headwalls and are characterized by very steep margins and relatively straight courses. Extensive vertical seacliffs have been cut by marine erosion, and marginal portions of the volcanic masses have slumped in large-scale mass-wasting events (Moore, 1964).

2.2.1. Honolulu Volcanic Series

Volcanism was sporadically renewed at the southeastern portion of the Koolau Range at approximately 600 to 800 Ka following extensive erosion and isostatic subsidence of at least 350 m (1200 ft) (Macdonald and Abbott, 1970; Gramlich et al., 1971; Self and Moberly, 1997). Erupted materials from this rejuvenation stage comprise the Honolulu Volcanic Series (Stearns and Vaksvik, 1935) and represent nearly all the known pyroclastic deposits on Oahu as well as lava flows of nepheline basalts, nepheline basanites, melilite-nephelinite basalts, and alkalic olivine basalts (Gramlich et al., 1971). The number of volcanic centers and eruptive events are

debatable as the production of nested craters (such as the Koko Head and Hanauma Bay tuff rings) and the masking of vents by subsequent proximal eruptions has made identification difficult in some cases. It is generally estimated, however, that the Honolulu Volcanic Series consists of as many as 40 volcanic centers and 30 separate eruptions (Hay and Iijima, 1968; Macdonald and Abbott, 1970; Self and Moberly, 1997). Ages of the eruptions (including lava flows and pyroclastics) have been relatively and absolutely determined through stratigraphic analysis and the employment of C^{14} and K-Ar radiometric dating techniques (Winchell, 1947; Gramlich et al., 1971; Easton and Olson, 1976). The youngest volcanic materials on Oahu were erupted from a group of about eight vents along the Koko rift at the southeastern end of the island. Koko Crater is among this group.

2.3. Local geology: Koko Crater

Koko Crater is a basanitic tuff cone. It is situated along the Koko Rift in southeastern Oahu, a 12 km-long linear fissure that extends southwest from Manana Island to a submarine cone about 3 km past Koko Head (Figure 4). Eruptions along Koko Rift took place approximately 35-30 Ka (in the late Pleistocene) as part of the renewed volcanism of the Koolau Range and are believed to represent the youngest events on the island (Gramlich et al., 1971; Stearns, 1985; Self and Moberly, 1997). The resulting craters comprise a group of at least eight tuff rings and tuff cones (Wentworth, 1926).

With a maximum elevation of 368 m (1208 ft), Koko Crater is the tallest tuff cone on Oahu and topographically dominates the southeastern coastline. Built around two vents, the cone is horseshoe-shaped when viewed from above and conspicuously asymmetric in cross-section. The asymmetry is due to the preferential piling of ejecta on the southwestern (leeward)

side by the northeasterly trade winds during eruption (Figure 5). The outer slopes are deeply incised by radial gulches that have produced steep valleys separated by sharp ridges.

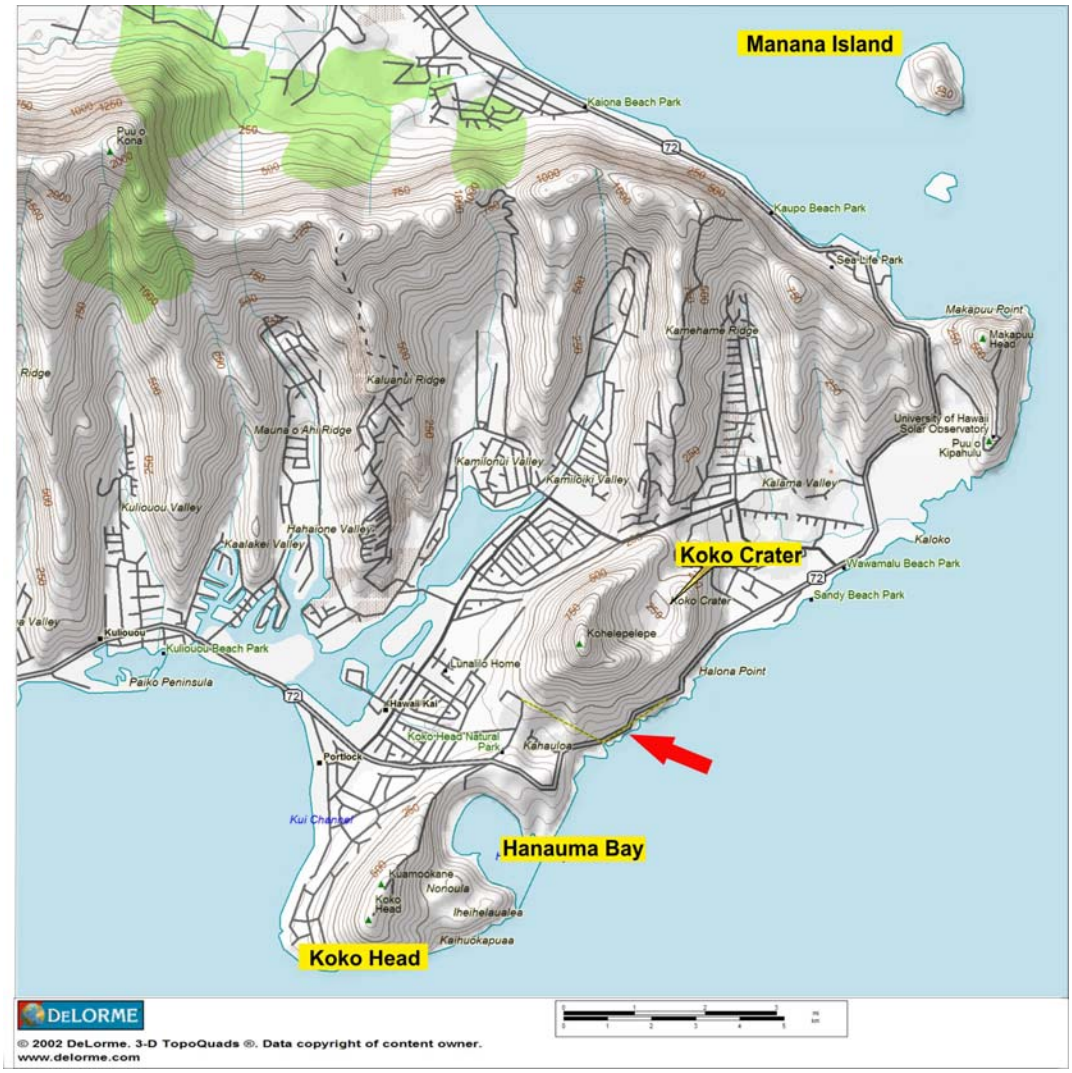

Figure 4. Southeastern shore of Oahu, Hawaii.

The tuff rings and tuff cones comprising this peninsula were constructed from eruptions of the Koko Rift, a NE-SW trending fissure that extends from Manana Island to about 3 km past Koko Head (about 12 km total length). Arrow indicates the location of the study area.

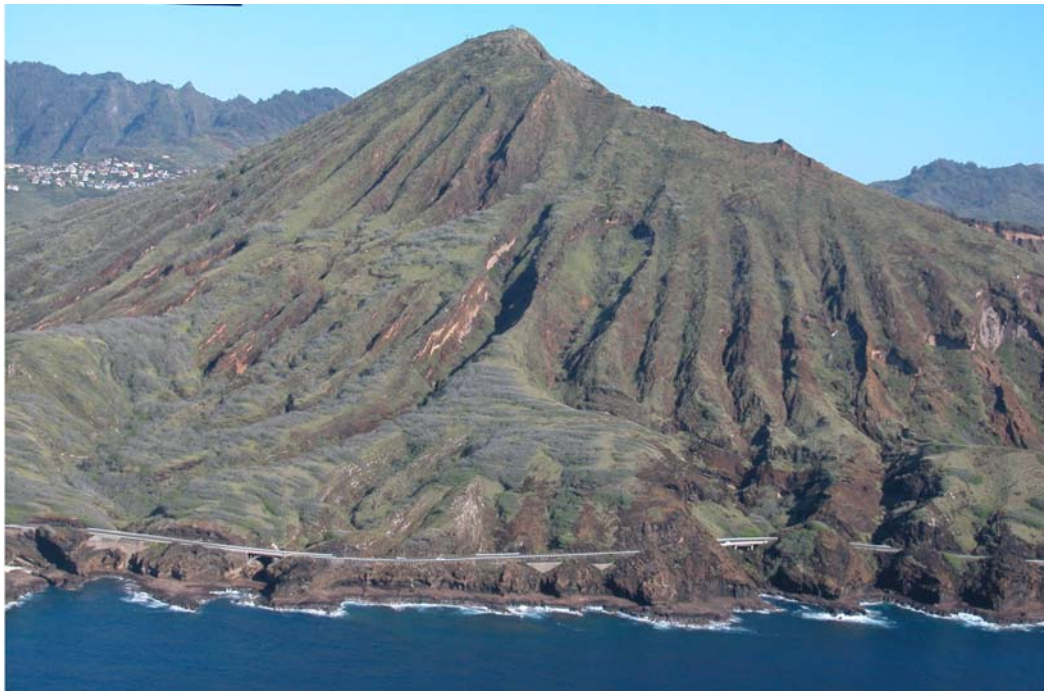

Figure 5. Koko Crater.

The topographic peak of the cone occurs on its southwestern side due to the piling of ash by trade winds. Steep valleys and sharp ridges indicate the extent of flank erosion. View is towards the northwest.

Koko Crater tuffs can be divided into three units. The basal unit consists of an explosion breccia and 1 to 2 m of lapilli fall (Wohletz and Sheridan, 1983). The breccia is clast-supported, largely composed of angular fragments of Koolau basalt with little intervening, fine-grained material. The lapilli-fall beds are 20 to 60 cm thick and display poorly developed normal grading. Above this unit lie 3 to 5 m of thinly bedded and massive planar pyroclastic surge deposits that exhibit varying degrees of palagonitization and an abundance of coral reef fragments (Wohletz and Sheridan, 1983; Grant and Heiken, 1985).

The upper unit comprises the majority of the cone and is composed of poorly stratified massive lapilli tuffs which dip 20 to 30˚ away from the crater (Grant and Heiken, 1985). Much of this has been extensively altered to palagonite, an alteration product that results from the prolonged interaction of fresh basaltic glass with water at low temperatures (Hay and Iijima,

1968; Fisher and Schmincke, 1984). Palagonitization of fresh glass involves a substantial gain in H_2O (about 900 percent) and variable losses of Si, Al, Na, K, and generally Ca (either as oxides or ions). A substantial portion of these species is subsequently precipitated as opal, calcite, montmorillonite, and/or zeolite cements which consolidate the tuffs (Hay and Iijima, 1968; Fisher and Schmincke, 1984). Zeolites and calcite most commonly cement the palagonite tuffs at Koko Crater and constitute between 15 and 30 percent of those rocks (Hay and Iijima, 1968). Koko Crater is vertically zoned with respect to the abundance of palagonite. The largest amounts of altered tuff occur in the lower interior portions of the cone while the remainder of the tuff is largely unaltered and commonly associated with opal-cemented lapilli tuffs that are olive-gray and friable to moderately well indurated (Hay and Iijima, 1968).

2.4. Local geology: field area

The study area is located along a portion of the southeastern (seaward) base of Koko Crater where cross-sections of the incisional structures are clearly exposed in a series of seacliffs and easily accessible owing to an adjacent wave-cut platform that varies in width from approximately 5-20 m (Figure 6).

Figure 6. Field area, SE Koko Crater

The field area is located at the southeastern base of Koko Crater. Cross-sections of the incisional structures are well-exposed in the seacliffs here, and access is granted by a wave-cut platform intervening between the cliffs and the ocean.

The flank deposits at this location are composed of phreatomagmatic ash and lapilli and can be divided into two units (Figure 7). Unit 1, the lower of the two, corresponds to the basal breccia and lapilli-fall unit described above. It is dominantly composed of poorly sorted, massive to crudely-bedded lapilli tuff ejected directly from the Koko Crater vent(s). Lenses and

poorly developed beds of basalt fragments derived from older Koolau flows are sporadically distributed. Tabular, laterally continuous beds of lapilli fall that display repetitive patterns of normal grading are observed as well. Characteristics of unit 1 are illustrated in Figure 8.

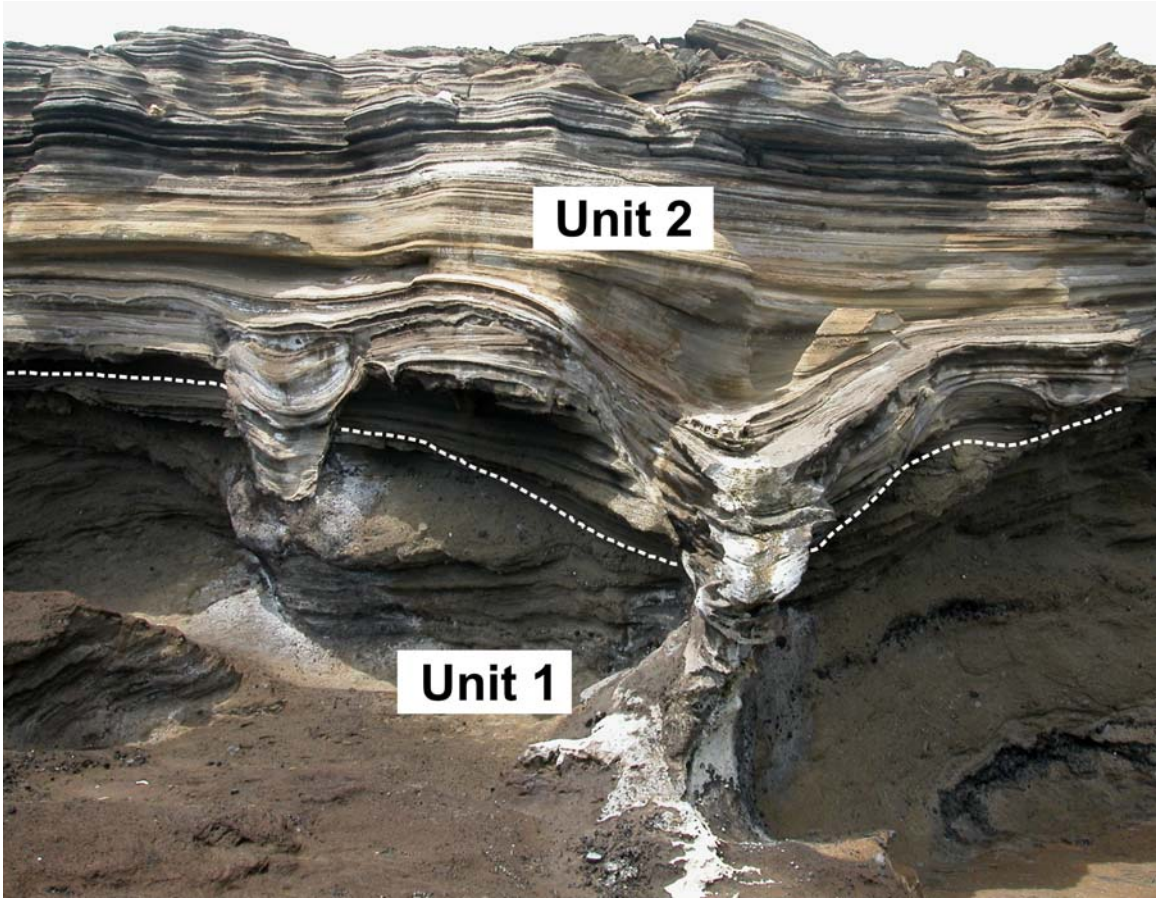

Figure 7. The two units comprising the lower southeastern flank deposits at Koko Crater.

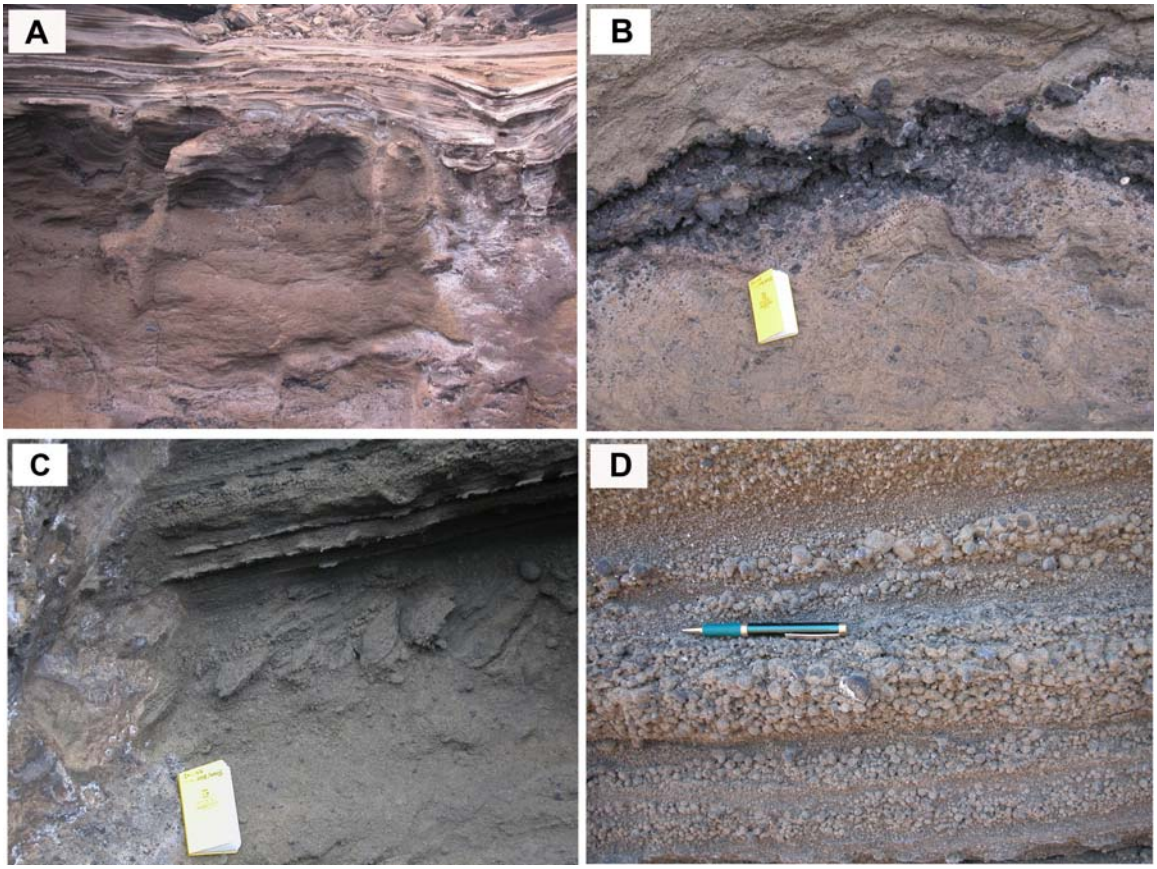

Figure 8. Characteristics of unit 1 tephra deposits.

(A) Unit 1 deposits constitute the lower 2/3 of this photograph (photo spans about 4 m). The tuffs are dominantly massive with little internal structure. (B) Lenses and poorly developed beds of basalt fragments have accumulated from explosions through older lava flows from the Koolau Range. Some clasts exceed 10 cm in length. (C) Unit 1 is largely massive, but is locally capped by (generally) crude and discontinuous bedding. (D) Plane parallel beds of lapilli fall are normally-graded with abundant accretionary and armored lapilli (cored with basalt fragments).

In striking contrast to unit 1, unit 2 comprises well-bedded and laminated sequences of intercalated pyroclastic surge and airfall deposits that contain abundant coral reef fragments. Directional data obtained from dunes and cross-beds contained within these sequences suggest that the deposits originated at Hanauma Bay, a neighboring tuff ring that lies approximately 2 km to the southwest along the Koko rift (Fisher, 1977) (Figure 4). C^{14} dating of the coral reef fragments signifies that the tephra was deposited in the Holocene, approximately 35,000 years ago (Gramlich et al., 1971).

Incisional structures have been eroded into both units in this area. While some of the larger structures extend into unit 1, initiation of incision is consistently confined to unit 2. Beds of vesiculated ash, soft-sediment deformation structures, abundant accretionary lapilli, bedding sags, and characteristically steep margins of the incisional structures indicate that the ash and lapilli of both units were wet and cohesive upon deposition. These characteristics have significant implications for the erosional mechanisms proposed below.

3. Hydrovolcanic processes and products

3.1. Introduction

Hydrovolcanism (phreatomagmatism) results from the interaction between magma and external water. Water sources include groundwater and surface water in marine, lacustrine, lagoonal, littoral, and subglacial environments (Sheridan and Wohletz, 1983; White and Houghton, 2000). Since water is so prominent near the surface of Earth, hydrovolcanic eruptions are common, particularly during the opening phases of an eruption. Hydrovolcanism dominates the eruptive products of small monogenetic volcanoes (tuff cones, tuff rings, and maars), where it is typically of the "Surtseyan" type (Thorarinsson et al., 1964; Sheridan and Wohletz, 1983; Kokelaar, 1986; White 1991; Vespermann and Schmincke, 2000; Cole et al., 2001). Hydrovolcanism is also common on many stratovolcanoes and caldera volcanoes (Sheridan and Wohletz, 1983.) Magmas of any composition may be involved in hydrovolcanic processes, from basaltic (e.g. Surtsey volcano, Iceland; Thorarinsson et al., 1964) to more silicic compositions (e.g. Sugarloaf Mountain, Arizona, USA; Sheridan and Updike, 1971).

The expansion of external (non-juvenile) steam is the dominant mechanism that drives hydrovolcanic explosions, though juvenile steam expansion can contribute (Fisher and Schmincke, 1984). Confining pressure and temperature conditions at the magma/water interface largely control the formation and subsequent behavior of steam (or supercritical fluid). The critical pressure for water is the threshold value which limits the liquid/vapor phase transition. For pure water, this value is 21.74 MPa (Zimanowski, 1998), which is equivalent to approximately 216 bars and water depth of about 2 km (Fisher and Schmincke, 1984). The corresponding equilibrium (boiling) temperature under such pressure is 647 K (Wohletz, 1986).

For saline water, equilibrium pressure and temperature values increase in response to the presence of dissolved solids. "Superheated" water remains in a liquid state above its boiling point (for any given pressure) and will "flash" to steam in response to a number of different possible disturbances, such as a sudden reduction in confining pressure or the passage of a seismic wave (Wohletz, 1986). Explosive hydrovolcanic eruptions ensue when large quantities of external water flash to steam.

The Molten Fuel-Coolant Interaction (MFCI) model, based on experiments and theory, is the principal basis used to model the effects of magma-water interaction (Peckover et at., 1973; Colgate and Sigurgeirsson, 1973; Wohletz and McQueen, 1981; Zimanowski et al., 1997). While the effects of scaling between experiments and real volcanic settings are still uncertain, it is believed that most sustained hydrovolcanic explosions are the natural equivalent of MFCIs (Wohletz, 2003; Zimanowski and Büttner, 2003).

3.2. Hydrovolcanic eruption processes

Hydrovolcanism is powered by the thermal and kinetic energy produced by the intimate mixing of water and magma. Rapid vaporization and expansion of large volumes of water, resulting from the flux of thermal energy from magma to water, are essentially the primary mechanisms that drive hydrovolcanic eruptions (Sheridan and Wohletz, 1983; Zimanowski, 1998). Eruptions can be explosive or non-explosive depending on the water/magma mass ratio (maximum explosivity of basaltic magmas is achieved with mass ratios between 0.1 and 0.3, Sheridan and Wohletz, 1983), the stability of the water/magma contact, and the pressure/temperature conditions of the system (Figure 9).

The initial contact between rising magma and external ground or surface water results in the immediate transfer of heat across the interface. Vapor films are established as a consequence of boiling and the coalescence of many small bubbles. Vapor films create a two-phase (liquid-gas-liquid) system by physically separating the magma and water; the vapor phase acts as a buffer by reducing (but not preventing) the transfer of thermal energy across the contact.

The presence of stable (i.e. undisturbed) vapor films creates density contrasts between the magma and water which ultimately cause water entrapped by magma to buoyantly rise to the surface; the ascent promotes boiling, and as a result steam will separate and rise from the system incrementally in relatively small volumes while the films are stable. While the expanding vapor may result in an eruption, the activity will likely be non-explosive, typically phreatic.

Explosive eruptions, in contrast, result when vapor films simultaneously collapse and large quantities of water (intimately mixed with magma) flash to steam (Figure 9). Film collapse is promoted by the passage of shock waves through the interface that are strong enough to cause destabilization or by various fluid instabilities in the film (Wohletz, 1986; Schmincke, 2004). The films collapse in a domino effect, but breakdown is envisaged as simultaneous because, once initiated, all films collapse in a few nanoseconds (Zimanowski, 1998). Disrupting shock waves are produced when a material is forced to expand faster than the speed of sound. They can be generated by volcano-seismic events or thermal fracturing. The latter mechanism arises in environments where temperature contrasts are high, such as magma/wall rock contacts. Thermal stresses imparted on the wall rock can cause rapid expansion and fracturing, and rock failure releases shock waves that can consequently trigger the destabilization of the vapor films.

Disintegration of the vapor films brings the magma and water into direct contact, producing a liquid-liquid (single phase) state at the interface. In the absence of vapor films, the

transfer of heat from magma to water increases by 1-2 orders of magnitude (Fiedler et al., 1980). The rapid and intense flux of thermal energy causes the water to become superheated. This state is accompanied by thermal expansion of the water and, consequently, pressurization of the system. The melt becomes quenched and fragmented in response to (1) thermal stresses as rapid cooling is accompanied by contraction, and (2) mechanical stresses imparted by pressurization of superheated water. These and other fragmentation mechanisms are discussed in the next section in greater detail.

Superheated water vaporizes within milliseconds (Zimanowski, 1998) in response to any of a number of possible disturbances, such as the passage of a moderate-to-high frequency seismic wave or a sudden reduction in system pressure. In the absence of external triggers, spontaneous vaporization will occur when superheating reaches some maximum temperature (Wohletz, 1986). The volume increase accompanying this rapid phase transition accelerates the expansion of overlying magma, causing fragmentation. Steam finally decouples the system, driving the eruption by expanding and transporting pyroclasts out of the vent. Thus thermal energy is ultimately converted into kinetic (mechanical) energy.

Collectively, these explosive mechanisms operate almost instantaneously. Under direct magma/water contact conditions (i.e. following vapor film destabilization), substantial heat transfer in a short time period overloads the system with thermal energy such that non-juvenile water flashes to steam and the system consequently explodes within a few milliseconds (Zimanowski, 1998; Schmincke, 2004). The process of rapid heat transfer is periodic, however, and so explosive eruptions are characterized by discrete, pulsating blasts separated by millisecond or shorter intervals (Sheridan and Wohletz, 1983).

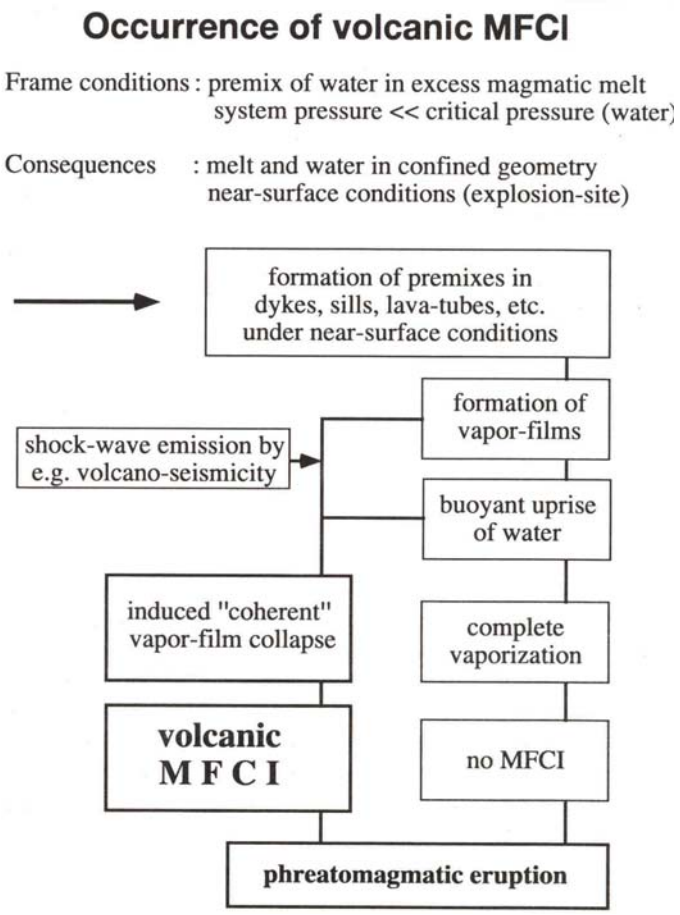

Figure 9. Processes causing explosive and non-explosive hydrovolcanic eruptions.

MFCI = Molten Fuel Coolant Interactions wherein hot melts interact with water; hydrovolcanic explosions may be referred to as volcanic MFCI (after Zimanowski, 1998).

Hydrovolcanic explosions can be prolonged, self-sustaining events due to the establishment of a positive feedback system which begins with the collapse of the vapor films at the pre-mix interface. The rapid transfer of thermal energy from magma to water ultimately fragments the melt; this enlarges the surface area of the interface, bringing more water into direct contact with magma (Wohletz, 2003). Heat flux increases and progressively larger volumes of water become superheated and vaporized, causing further fragmentation and growth of the contact area. In this way, previously uninvolved parts of the system become disrupted.

Experimental modeling of hydrovolcanic explosions using both magma and their analogs (Wohletz and McQueen, 1981; Wohletz and Sheridan, 1981; 1982; Sheridan and Wohletz, 1983; Zimanowski et al., 1997a; 1997b; Zimanowski, 1998) has demonstrated that the degree of explosivity (i.e. the efficient conversion of thermal to kinetic energy) is strongly dependent on the water/magma mass ratio, the geometric area of the pre-explosive interface, and the confining pressure of the system. The intensity of explosions increases with (1) increasing contact area, which allows for a greater overall transfer of thermal energy and (2) decreasing confining pressure, wherein the transition from liquid to vapor and the subsequent expansion of steam are minimally inhibited. For basaltic magmas, maximum explosivity is achieved with water/magma mass ratios between 0.1 and 0.3 (Sheridan and Wohletz, 1983). Very high ratios (which can result, for example, when lava flows into the ocean) will not generally produce an explosion because the system temperature is too low and thermal energy transferred from the lava to the surrounding water will not be sufficient to cause explosive vaporization. Explosions may ensue, however, if some water becomes trapped beneath a lava flow or if lava and water come together in an enclosed space such a lava tube, dike, or sill (Schmincke, 2004).

Further experiments show that explosivity is drastically reduced (or even prevented) when vesicles are present in the magma at certain concentrations (Zimanowski, 1998). Exsolved gas bubbles may have the ability to stabilize the vapor films that form upon initial magma/water contact, either by providing mechanical support or by absorbing the shock waves that would otherwise promote film collapse. Stabilization of the bounding vapor phase prevents the intimate mixing of the two liquids and inhibits heat flux across the contact such that the system does not become overloaded with thermal energy.

3.2.1. Mechanisms of magma fragmentation during hydrovolcanic explosions

Hydrovolcanic tephra is generated by both explosive and non-explosive mechanisms. Because fragmentation of the melt increases the magma/water contact area, the following methods of pyroclast formation all contribute to the positive feedback system that enables self-sustaining eruptions.

Granulation is the primary mechanism of fragmentation in non-explosive hydrovolcanic activity (Fisher and Schmincke, 1984; Kokelaar, 1986). The exposure of magma to extreme cooling rates (following contact with water) causes the transition of the magma to a supercooled liquid and then to a glass. Chilling is accompanied by a rapid and substantial volume decrease, causing pronounced strain accumulations in a short period of time. Fracturing (i.e. failure) occurs when strain build-up exceeds the mechanical strength of the melt (Fisher and Schmincke, 1984; Zimanowski, 1998). Granulation is a brittle fragmentation mechanism that operates after the melt has cooled and solidified.

Fragmentation also occurs following direct contact with magma, when water becomes superheated and pressurized as a consequence of thermal expansion. Because the water/melt system is mechanically coupled under direct contact conditions (Zimanowski, 1998), pressurization of the water imparts high levels of stress directly to the melt; magma will disintegrate (fragment) when stresses exceed its mechanical strength. Once cracks form, pressurized water intrudes and causes the cracks to propagate, thereby inducing fragmentation.

Pyroclasts can also be generated by fragmentation of the melt surface, i.e. detachment of magma fragments at the melt/water interface. This process is facilitated by Landau or Taylor instabilities that can develop in the vapor films. Landau instabilities (Shepherd and Sturtevant, 1982; Sturtevant and Frost, 1984) form during vapor film establishment in response to surface

roughness created by the formation of bubbles and the evaporation of steam. The pore pressures of expanding gas cause surface instabilities and the creation of waves at the interface. The number and amplitude of the waves is dependent on the density contrast, surface tensions, and viscosities of the two fluids (Zimanowski, 1998). When wave amplitudes grow to a certain threshold, the strength of the magma is exceeded and fragments detach from the surface. Taylor instabilities (Corradini, 1981), in contrast, form in response to film thickness oscillations promoted by collapse of the vapor films. The resulting distortion of the interface generates surface waves which also promote magma fragmentation with excessive amplitude growth. According to Wohletz (1986), Landau instabilities may best fit experimental observations of fuel-coolant interactions (FCIs).

Rapid vaporization of large quantities of water (i.e. "flashing" of water to steam) is an explosive mechanism of pyroclast formation. The liquid/vapor phase transition is accompanied by expansion and, therefore, pronounced volume increases. Explosive expansion releases shock waves into the surrounding system. The conversion of thermal energy to kinetic energy occurs as the expanding steam quickly accelerates the surrounding melt; mechanical energy is then utilized for the work of further (fine) magma fragmentation, crater excavation, and ejecta dispersal (Wohletz, 1986).

3.2.2. Surtseyan eruption processes

Hydrovolcanic eruptions result from the interaction of magma and water at (theoretically) any location in the conduit. In the specific case where external water accesses the top of the vent, either by direct flooding or seeping through walls of an accumulating tephra ring, Surtseyan-type eruptions commonly result (Kokelaar, 1983). This particular style of

hydrovolcanic activity was recognized and named after the early eruptive stages of Surtsey Volcano, Vestmann Islands, Iceland in November 1963. Similar activity has been displayed (and well documented) at other localities, e.g. Capelinhos and Taal volcanoes (Machado et al., 1962; Moore et al., 1966; Waters and Fisher, 1971, Kokelaar, 1986; Cole et al., 2001).

Surtseyan eruptions comprise three types of activity: pulsating explosions of "tephra-finger" or "cock's tail" jets, phases of continuous uprush wherein large sustained (up to 10 km) vertical eruption columns are produced, and (commonly) magmatic activity that produces lava flows and scoria (by way of fire fountaining) whenever water is denied access to the vent (Thorarinsson et al., 1964).

Surtseyan eruptions commonly begin with the intermittent, explosive, ballistic ejection of black jets of tephra. These explosions propel bombs and finer tephra several hundred meters into the air, and can be separated by several seconds, with smaller explosions occurring in between (Thorarinsson et al., 1964). The frequency of jetting reflects the rate of supply of magma into the vent and/or the time for sufficient heat transfer to the water to occur. When discrete explosions occur so frequently that individual events can no longer be distinguished, phases of continuous uprush activity ensue (Figure 10). Continuous uprush is characterized by the production of columns of tephra and steam that can reach altitudes of several kilometers and persist for several hours (Thorarinsson et al., 1964). Base surges (which are "wet," low temperature (mean T below 100˚C), low-concentration pyroclastic density currents) are also common occurrences during such phases of Surtseyan eruptions (Figure 11). These largely result from (1) the inclined ejection of steam and tephra and (2) partial column collapse, particularly at the margins where air resistance is greatest (Waters and Fisher, 1971).

Figure 10. Eruptive phase of Surtsey Volcano, Iceland in 1963

A convective vertical eruption column (left) and tephra-finger jets (right) illustrate intense explosive activity. Relatively tephra-free columns of steam rise (and collapse) at the margins. Jets illustrate density separation of tephra and condensed steam (from Thorarinsson, 1964).

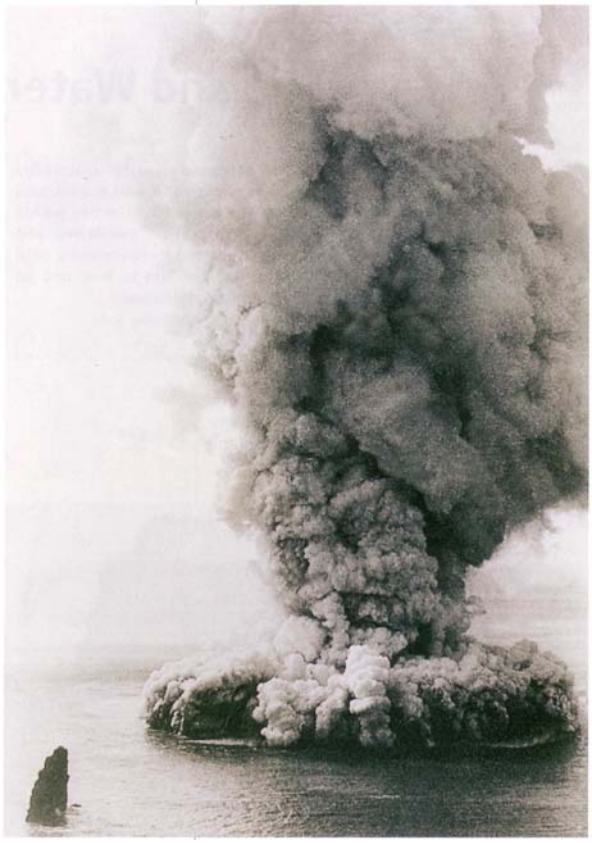

Figure 11. Base surges, Capelinhos volcano, Azores

Base surge flows ("wet" low–concentration pyroclastic density currents) originating from a sustained eruption column, Capelinhos volcano, Azores, 1957 (from Waters and Fisher, 1971).

When water is denied access to the vent, or when the rate of magma flux greatly exceeds the flow of water into the vent, a new eruptive phase commences that is characterized by purely magmatic activity. Fire fountaining, Strombolian eruptions, and lava flows result during this drier phase (Walker and Croasdale, 1972). As the volume of water accessing the vent commonly fluctuates throughout the duration of an eruption, it is common to find hydroclasts and scoria interbedded in the same deposit.

According to Kokelaar (1983), Surtseyan activity results when external water gains access to the top of the vent, which is filled with a poorly-sorted mixture of tephra, glass fragments, and water during an eruption (Figure 12). A geometrically simple magma/water

interface does not exist; ascending magma instead encounters a slurry of basaltic clasts and water that is probably partially mobilized by the rise of steam from greater depths in the conduit. Upon contact, liquid water and clastic deposits become incorporated in the magma, and steam consequently forms and entrains tephra as it rapidly expands, producing the characteristic tephra jets. These jets are often observed spreading in various directions upon ejection from the vent (Figure 10) as a result of eruption through the mobile slurry. Continuous uprush activity is a consequence of the same mechanism fuelled by a higher rate of magma supply. When the relative input of external water is decreased, the water already entrapped in the system becomes heated towards its boiling temperature. Higher temperatures provide more thermal energy for the conversion to kinetic energy; therefore, stronger explosions result when water is temporarily blocked from the vent entrance.

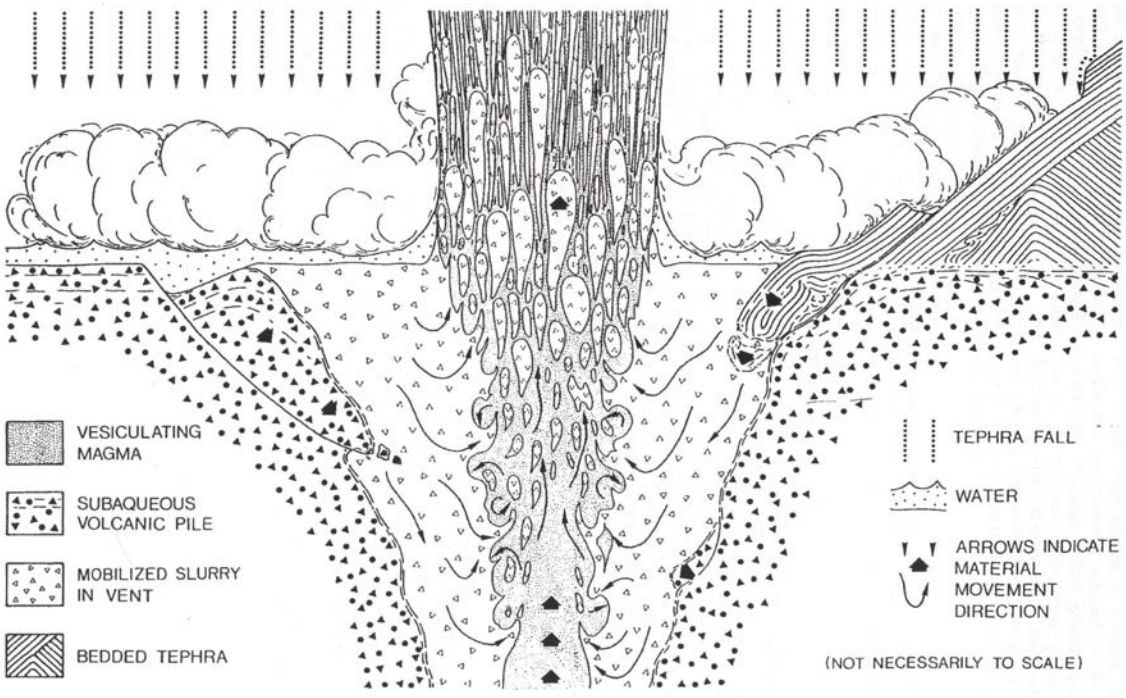

Figure 12. Mechanisms of discrete tephra-jetting and/or continuous uprush activity in Surtseyan-type volcanic eruptions.

Ascending magma in the conduit encounters a mixture of tephra and water. This slurry is constantly replenished by the inward slumping and fallback of tephra, and by flooding of the top of the vent by surface water (after Kokelaar, 1983).

3.3. Products of explosive hydrovolcanic eruptions

Explosive hydrovolcanic eruptions typically produce heterogeneous mixtures of juvenile particles, wall fragments and grains, liquid water, steam, and magmatic gas. Deposits generally share the following characteristics: (1) vesicle-poor to non-vesicular juvenile clasts (Heiken, 1972; Lorenz, 1987); (2) fine grained (ash and fine lapilli sized) clasts that display poor to very poor sorting (Walker and Croasdale, 1972; Fisher and Schmincke, 1984) due to intense fragmentation and rapid emplacement (3) high concentrations of non-juvenile lithic fragments (>90% in many maar deposits) derived from the fragmentation and excavation of country rocks and surrounding unconsolidated deposits (Fisher and Schmincke, 1984); (4) indications of "wetness," such as armored and/or accretionary lapilli, the plastering of (cohesive) ash, and soft sediment deformation (slump structures, bomb sags) (Walker and Croasdale, 1972); (5) syn-eruptive/eruption-fed debris flows, due to the high water content of the ejected material (Leat and Thompson, 1988).

Individually, hydrovolcanic pyroclasts are normally equant to subequant and bounded by blocky, angular fracture surfaces (Fisher and Schmincke, 1984; Walker and Croasdale, 1972; Heiken, 1972), but a wide variety of morphologies also occurs (Honnorez and Kirst, 1975; Wohletz and Krinsley, 1983; Grant and Heiken, 1985). These characteristics, along with the absence of achneliths ("fluidal" fragments of solidified lava spray) and spatter, indicate that pyroclast formation occurs in cooled (quenched) glass that is fragmented prior to expulsion from the vent. Clast morphology is therefore dominantly controlled by stresses in the chilled magma, in contrast to purely magmatic (basaltic) eruptions wherein molten droplets of magma are ejected from the vent and the resulting shape is dominantly dependent on surface tension and bursting of vesicles (Heiken, 1972).

Hydrovolcanic vitric clasts are characteristically poorly vesicular. This is because quenching of magma by external water is accompanied by a drastic decrease in temperature and, therefore, increase in viscosity, which inhibits volatile exsolution (Fisher and Schmincke, 1984), and also because it may take place prior to exsolution of magmatic volatiles under relatively high confining pressures (Heiken, 1972; Heiken and Wohletz, 1985). Juvenile clasts can be vesiculated, however, if magma/water interaction occurs at shallow confining pressures and/or at high partial pressures of the magmatic volatiles. Of course, the degree of vesicle development also depends on the volatile content of the magma. At Surtsey (1963-1964), fall deposits were dominated by vesicular ash (with spherical and irregularly shaped vesicles) while surge deposits largely comprised poorly vesicular, angular hyaloclastites with curviplanar breakage surfaces (Heiken and Wohletz, 1985). Figure 13 depicts examples of vesicular and non-vesicular basaltic vitric clasts from Koko Crater, Oahu, Hawaii that were also emplaced (respectively) by fallout and surge processes.

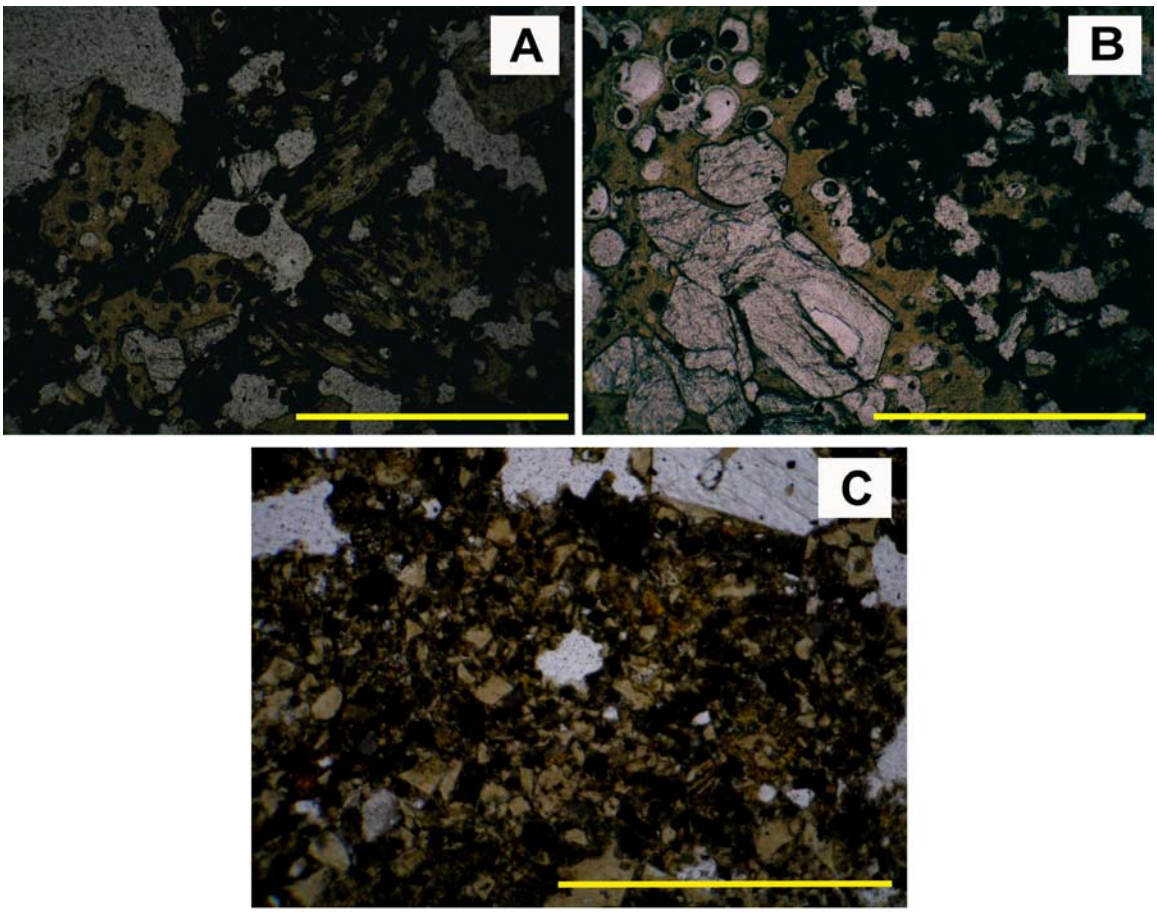

Figure 13. Vitric clasts from basal flank deposits at SE Koko Crater, Oahu, Hawaii.

Yellow bars span 1 mm. (A,B) Vesicular clasts erupted from Koko Crater; these samples were collected from deposits emplaced by airfall. Vesicles indicate that magmatic volatiles were actively exsolving prior to (or during) fragmentation and expulsion from the vent. Clast surfaces are largely bounded by fracture surfaces that cut vesicles. (C) Non-vesicular clasts in deposits emplaced by pyroclastic surges originating at Hanauma Bay. Small, blocky nature is indicative of fine fragmentation by highly explosive activity.

Hydrovolcanic tephra emplacement mechanisms include fallout, pyroclastic surges, and debris flows (Walker and Croasdale, 1972; Sheridan and Wohletz, 1983; Leat and Thompson, 1988). Fallout occurs by direct ballistic ejection from the vent, fallout from an eruption column or from a pyroclastic density current. Airfall tuffs are moderately sorted and commonly exhibit plane mantle bedding with little variation in lateral thickness, poorly developed normal or inverse grading, and coarser grains than base-surge deposits, particularly near the source vent (Leys, 1983; Wohletz, 1998).

Pyroclastic surge currents are characterized by low concentrations of solid particles entrained in a turbulent mixture of steam and water (Cas and Wright, 1987). They travel at high velocities and are not initially topographically constrained as a consequence of inflation. Base surges, originating from the basal portions of hydrovolcanic eruption columns (Figure 11), characteristically deposit sequences of well-bedded ash and lapilli in beds less than 1 mm to several cm thick. Common internal bedforms include cross-laminations, ripple laminations, cross-bedded dunes, and planar and massive beds. Soft sediment deformation structures such as convolute beds, slump features, and bedding sags are also prevalent (Moore, 1967; Fisher and Waters, 1970; Wohletz and Sheridan, 1983; Wohletz, 1998). Pyroclastic surges are classified as "wet" if the transport medium is condensing steam (i.e. temperature $\leq 100^{\circ}C$) and "dry" if the transport medium is superheated steam (i.e. temperature $> 100^{\circ}C$). Deposits from wet surges largely comprise thick, massive to planar beds of cohesive tephra. Mudflow deposits, beds of vesiculated tuff, and accretionary lapilli are common. Dry surges, in contrast, characteristically deposit thin sheets of unconsolidated, well-stratified tephra from which steam can readily escape (Sheridan and Wohletz, 1983).

In hydrovolcanic settings, debris flows (discussed further in section 5.4.1) can be generated by direct effusion from the vent, collapse of water-laden tephra jets, partial column collapse (wherein the gas/pyroclast mixture contains abundant condensed water), and by the remobilization of wet tephra deposited at or above the angle of repose (Leat and Thompson, 1988). Debris flow deposits are characteristically massive, very poorly sorted, and variable in lateral thickness.

3.4. Tuff cones and tuff rings

The most common hydrovolcanic landforms are tuff cones and tuff rings. These are monogenetic volcanoes as they are largely constructed by a single eruptive event, which can persist for several years. Because hydrovolcanism is so common, tuff cones and tuff rings are the second most common type of volcanic edifice (scoria cones are the most abundant, Green and Short, 1971).

Tuff rings exhibit low topographic profiles, with thin (less than 50 m) sections of rim beds and gentle slopes that are characteristically less than 15˚. Central craters are wide; when they are depressed below the pre-eruptive ground surface, the edifice is classified as a maar (Ollier, 1967). Tuff cones have similarly wide central craters, but display steep outer slopes (greater than 25˚) and sequences of rim deposits that exceed 100 m in thickness (Wohletz and Sheridan, 1983).

Basal deposits of both tuff rings and tuff cones are commonly explosion breccias (or finer deposits) composed of angular fragments of country rock supported in an ash/lapilli matrix. Breccias represent pre-existing surficial material at the vent that is shattered during the initial explosions (Wohletz and Sheridan, 1983). In tuff rings, the overlying apron of tephra is fine-grained and thinly bedded. Traction current, massive, and planar bedforms indicate that emplacement is dominantly by highly inflated pyroclastic (base) surges; intercalated beds of ash- and lapilli-fall are also common. Tuff cones largely comprise thick units of weakly bedded or massive tephra largely deposited from steam-laden (wet) surges and fallout (White, 1991). Lapilli- and/or ash-fall beds are more abundant than in tuff rings. Additionally, tephra are relatively coarser and commonly hydrothermally altered to palagonite (Wholetz and Sheridan, 1983; Heiken and Wohletz, 1985).

The morphological and compositional differences between tuff rings and tuff cones (illustrated in Figure 14) are attributed to a wide variety of factors. Fundamental among these factors is variation in the energy of eruption, which in turn affects both the eruption temperature and subsequent depositional processes. Eruption temperature determines the state of erupted water (and, consequently, the pyroclast transport medium) and grain sizes of ejected tephra as the degree of fragmentation is largely determined by the efficient conversion of thermal to mechanical energy. Depositional processes, namely pyroclastic surge and fallout, are influenced by several features in addition to eruption energy, including depositional setting (shallow submarine, lacustrine, etc.), competence of country rocks, level and lithology of aquifers, and properties and behavior of magma (Sohn, 1996). These factors subsequently influence explosion depth, conduit geometry, mode of magma-water interaction, and magnitude of explosion (Sohn, 1996).

Steeper slopes of tuff cones are attributed to greater cohesion of the tephra; additionally, tuff cones contain larger volumes of palagonitized tephra (Sheridan and Wohletz, 1983). These characteristics indicate cool (below 100˚C), wet emplacement where the majority of erupted water was condensed (or condensing). Combined with coarser grain sizes, which reflect less intense fragmentation, it is apparent that less energetic eruptions are involved in the construction of tuff cones as compared to tuff rings.

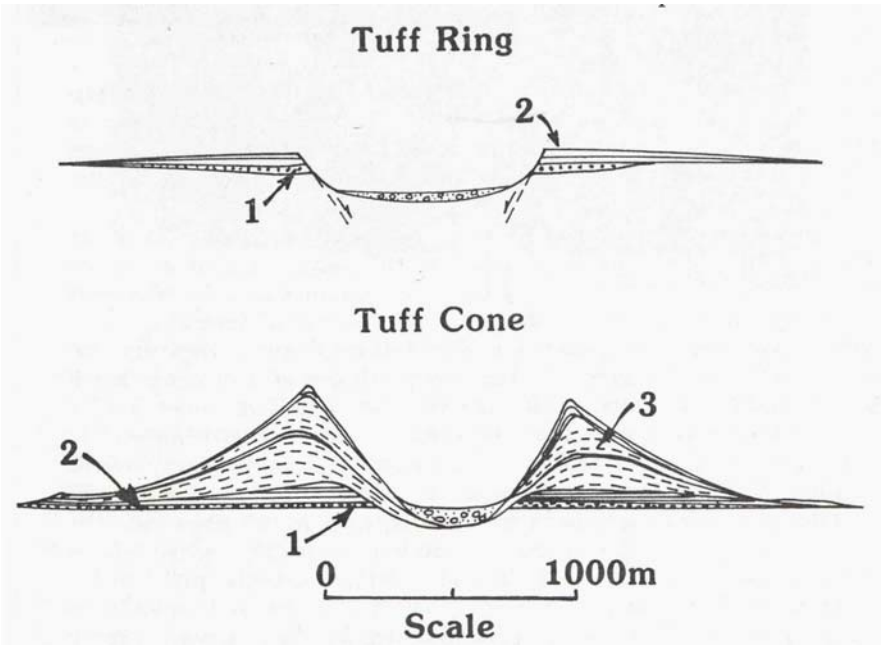

Figure 14. Tuff rings and tuff cones

Cross-sections illustrating the morphological and compositional differences between ideal tuff rings and tuff cones. Deposit types include: (1) explosion breccia, (2) thinly bedded deposits, and (3) massive, thickly bedded deposits (after Wohletz and Sheridan, 1983).

4. The origin, evolution, and characteristics of rill and gully networks on steep hillslopes

4.1. Introduction to rills and gullies

Erosion of hillslopes occurs mostly by some combination of raindrop impact, overland flow/sheetwash, movement of water through subsurface pipes, and mass movements (Knighton, 1998). The initiation and characteristics (continuous or discontinuous, permanent or ephemeral) of rills and gullies on hillslopes are mainly functions of the erodibility and hydraulic properties of the hillslope material. Factors that affect these properties include soil mineralogy (particularly clay content), porosity, permeability, infiltration capacity, cohesion, water content, shear strength, and the presence of vegetation.

Rills and gullies are generated by essentially the same mechanisms (Bennett et al., 2000), which include surface flow, piping, and mass movement (i.e. shallow landsliding). The concentration of surface flow, also referred to as overland flow, is often the primary initial cause of incision. Overland flow on hillslopes is largely controlled by the infiltration capacity of the hillslope material. Infiltration is the process by which water penetrates the surface horizon and percolates downward. It is influenced by a variety of factors, including type and intensity of precipitation, soil porosity, soil moisture content, vegetation, cultivation, cracks, slope, exposure to freezing, presence of swelling clays, degree of surface compaction, and development of a surface crust (Selby, 1993). These last two variables are mostly influenced by impacting raindrops, which can collapse pores and/or dislodge and splash fines into void spaces. The ultimate effect of raindrop impact is formation of a thin crust, or seal, which reduces infiltration while enhancing ponding and surface runoff.

When infiltration is minimal or impossible (due to low infiltration capacities or ground saturation), impacting water is forced to flow along the surface rather than penetrate it. Overland flow exists in two varieties. Classic Horton overland flow (Horton, 1945) is actually infiltration-excess overland flow, generated when rainfall intensities simply exceed the infiltration capacities of the hillslope material. This usually happens during short-lived, high intensity storms. In such circumstances, flow is manifested as a sheet of water that progressively increases in thickness towards the base of the slope. Infiltration-excess overland flow is rare in nature but can occur on frozen soils and large areas of bare rock. Overland flow on hillslopes is more commonly saturation-excess flow, generated during prolonged, low-intensity rainfall events that slowly saturate the soil. When rain falls on saturated areas into which water cannot infiltrate, overland flow results as a mixture of return flow and direct runoff (Selby, 1993). Return flow comprises subsurface water which returns to the surface after moving through subsurface drainage paths such as micropipes and tunnels (Selby, 1993).

Overland flow can be erosive without forming rills or gullies. Thin, relatively uniform flow removes particles from the surface with no concentration of erosion. Fluctuations in flow thickness, however, may cause depressions to be eroded at a much higher rate, initiating small channels (Carson and Kirkby, 1972). The presence of desiccation cracks promotes concentration of surface flow (in addition to pipe flow, discussed below) and therefore strongly influences rill network development. Desiccation cracking most commonly occurs on the surfaces of clay-rich soils with high shrink-swell capacities, but some cracking occurs on all cohesive soils (Bryan, 2000). Micro-topography and macro-scale surface roughness also influence the nature of overland flow. Irregularities on the surface promote the formation of concentrated flowlines ("threads") that converge and diverge around obstructions such as pebbles and plant stems; such

surface roughness creates frictional resistance to flow and therefore promotes turbulence (Selby, 1994).

Vegetation strongly influences the erodibility of a hillslope. Rill and gully erosion is most prominent on hillslopes with little or no vegetative cover. Vegetation decreases the likelihood of water erosion by: 1) shielding the surface from direct raindrop impact, thereby preventing dislodgement of material and/or rainsplash transport; 2) increasing soil strength and porosity through the binding effects of roots; 3) decreasing runoff velocity and, therefore, the ability of water to cut through and entrain sediment; 4) insulating soil against diurnal temperature fluctuations which otherwise may cause cracking and/or frost heaving; 5) promoting soil compaction; and 6) drying out topsoil through processes of transpiration (Selby, 1993; Carey et al., 2001). Organic-rich topsoil is very permeable under a healthy vegetative cover, promoting more infiltration and less overland flow. The influence of vegetation on hillslope stability is exemplified at Mount St. Helens. Prior to the eruption of May 18, 1980, infiltration capacities of the forested areas surrounding the vent exceeded rainfall intensities and snowmelt. The eruption removed much of the forest vegetation and deposited a blanket of fine-grained tephra over the permeable topsoil. Consequently, infiltration capacities were substantially lowered and frequently exceeded, and overland flow (predominantly in the form of rill wash) immediately began to erode the tephra into the Toutle River (Collins and Dunne, 1986).

High infiltration rates and capacities reduce the amount of overland flow that a hillslope is subjected to, but also alter the physical properties of a soil mass (mostly by reducing internal strength). This consequently results in periodic failure of the material in mass movements. Mass movements promote the initiation of rills and/or gullies by providing 1) unconsolidated material

that is prone to erosion and 2) surface scars that serve as topographic depressions, which encourage concentration of overland flow.

Pipes are subsurface drainage paths that form by the erosional enlargement of void spaces. They resemble macropores but tend to be erosionally enlarged and show a high degree of connectivity in the downslope direction. Pipes exist in many different environments, from arid to humid temperate and humid tropical (Dunne, 1980; Laity and Malin, 1985; Jones, 1990; Parker, Sr. et al., 1990). Dimensions range from 0.02 m to over 1 m in diameter and from a few meters to over a kilometer in length. Flow velocities through pipes have been estimated at values similar to that of overland flow, typically ranging between 0.015-0.3 m/s (Selby, 1994). Depending on pipe dimensions, slope, and soil erodibility, however, velocities can be up to an order of magnitude more rapid (Selby, 1993).

Pipes will only form when subsurface material is weak enough to be eroded by (usually) low-velocity flows but strong enough to support walls and a roof surrounding the central void. Pipes are particularly common in smectite-rich soils because desiccation cracking provides easy access to the subsurface. Surface water can rapidly infiltrate a crack and travel laterally in layers of highly permeable material. If this lateral seepage is fast enough, soil particles can be moved and pipe erosion will commence.

Because it promotes subsurface flow, piping commonly contributes to rill and gully development. Roof collapse and surficial emergence of water as return flow are both factors favoring surface channel development. The steep scarps and steep walls characteristic of gullies may be directly related to pipe development and collapse (Parker, Sr., et al., 1990; Knighton, 1998).

4.2. Rheology of rill and gully-forming flows

A flowing fluid on and beneath the surface is crucial to rill and gully formation. Reynolds number (R_e) and Froude number (Fr) are quantitative measures that describe flow behavior. R_e is an index of turbulence and can be calculated using the relationship $R_e = \rho dv/\mu$, where ρ, d, v, and μ are fluid density, depth, velocity, and viscosity (respectively). R_e values less than 500 denote laminar flow while those values greater than 2000 are indicative of turbulent flow behavior; the range 500-2000 is a transition (Selby, 1994; Boggs, 1995; Prothero and Schwab, 1996). Unconfined fluids moving across open surfaces (e.g. thin surface runoff) have R_e values below this range and therefore exhibit laminar flow (Prothero and Schwab, 1996).

The Froude number (Fr) describes flow state in terms of the ratio between flow velocity (inertial forces) and the force of gravity; $Fr = v/\sqrt{(gd)}$, where g represents acceleration due to gravity. When Fr is less than 1.0, the flow is described as tranquil, streaming, or sub-critical; values greater than 1.0 denote rapid, shooting, or super-critical flow (Selby, 1994; Bryan, 2000). Both, however, are types of turbulent flow. In general, scouring of a hillslope will occur when a flow exhibits turbulence, so both parameters (R_e and Fr) are useful in predicting erosive capabilities.

4.3. Origin, evolution and characteristics of rills

4.3.1. Origin of rills

Baur (1952) defined rill erosion as the "removal of soil by running water with the formation of shallow channels that can be smoothed out completely by cultivation." Because rill formation is not confined to agricultural soils, this definition is not sufficient for general

purposes. A more appropriate, though simplistic, definition of rill erosion is "the removal of soil by concentrated sheet flow" (Maidment, 1993).

Concentration of overland flow, often induced on natural hillslopes by microtopography or vegetation, is major factor in rill development (Bryan, 2000). According to Savat and De Ploey (1982), competence of the flow is mainly a function of slope and Froude number (Fr). Fr values greater than 1 denote supercritical flow; flow instability features accompanying this state cause localized increases in bed shear stress, which in turn enhance the erosive capabilities of a flow. Savat and De Ploey (1982) state that critical Froude numbers for the onset of channel (specifically, rill) erosion vary between 2.0 and 3.0. Reynolds number (R_e) is likewise important as it is a measure of the conditions necessary for turbulent flow. The probability of turbulence, and thus rilling, increases with slope angle. An increase in slope is accompanied by a decrease in topsoil shear strength and an increase in flow velocity and the magnitude of the gravitational force component parallel to the slope. If density, depth, and viscosity of the water remain unchanged, an increase in velocity could solely cause an increase in R_e. Thus the erosive capability of overland flow increases, and particles are entrained and transported more readily.

Merritt (1984) and Knighton (1998) describe four separate stages in rill formation that ultimately reflect changes in flow state. These are: sheetflow (unconcentrated overland flow), flowline development (overland flow with concentrated flow paths), micro-rills without headcuts, and micro-rills with headcuts. In laboratory experiments Reynolds number and sediment yield progressively increase from one stage to the next, with rill incision taking place when the flow makes the transition from laminar to turbulent ($R_e > 2000$).

4.3.2. Evolution of rills

Rills can rapidly extend upslope with the development and migration of headcuts while becoming larger and deeper downstream due to channel erosion (Selby, 1994). Commonly, rills develop parallel or elongated dendritic drainage networks (Higgins et al., 1990). Horton (1945) described parallel networks as representing the initial stages of development, with dendritic patterns evolving subsequently through cross-grading and the disintegration of rill walls. According to Schumm et al. (1987), the most common mode of network development is probably the "extension" mode, wherein individual rills that preferentially grow in size and sustain flow throughout a rainfall event persist as permanent, or master, rills into which other ephemeral (tributary) channels eventually drain. In the former scenario, virtually all rills in the drainage network form simultaneously; this is not the case in the latter model as tributary rills form subsequent to the establishment of the master rills. In premature stages of network development, model rills are assumed to be regularly spaced along a hillslope (Favis-Mortlock et al., 2000). This is not necessarily a realistic scenario, however, as initial incision seems to be controlled by spatially variable factors such as material type and the distribution of surface irregularities.

4.3.3. Characteristics of rills

Rills are small channels with (typically) v-shaped cross-sectional profiles and flaring sides that occur most frequently on non-vegetated slopes steeper than 2-3˚ (Savat and DePloey, 1982; Rauws, 1987). Rill width and depth range from a few centimeters to a few tens of centimeters. This relatively small size is likely due to the short duration of most surface flows

responsible for rill incision, in addition to the increasing compactness (and hence decreasing erodibility) of soil with depth (Carson and Kirkby, 1972).

Most rills are transient erosional features, destroyed naturally between rainy seasons or individual rainfall events. They can also be destroyed during the course of a single storm if the rill walls collapse, the bed and/or walls liquefy, or splash on interrill areas introduces quantities of material that exceed the transporting capacity of the channel. Obliteration of rills is also often the result of infilling. Freeze-thaw, frost wedging, and frost heaving processes deform soil and break up the surface, filling rills in-situ. Similarly, disturbance of the surface by animals can cause material to move into rills and repeated wetting/drying of the soil surface produces tension cracks in the uppermost (1-5 mm) soil layers, promoting failure of dried soil which travels downslope and can fill pre-existing rills and other surface depressions. In all such cases, the fill typically exhibits a high infiltration capacity; runoff will therefore decrease and new rills will preferentially form elsewhere (Carson and Kirkby, 1972). Because successive flows produce rills in consistently different positions, rill erosion contributes to the overall (usually even) lowering of hillslopes. Despite the relatively small channel size and ephemeral nature, rilling is a major form of erosion on hillslopes with little to no vegetation, contributing 50-90% of total sediment removal (Knighton, 1998).

4.4. Origin, development, and characteristics of gullies

4.4.1. Origin of gullies

Commencement of gully erosion is almost always due to the concentration of surface runoff flowing at a velocity sufficient to detach and transport particles (Carey et al., 2001).

Incision by surface flow (storm runoff and/or snow meltwater) is most common where breaks occur in the vegetative cover of the hillslope. Variations in environmental conditions are typically responsible for either an increase in flood runoff or a decreased capacity of water courses to carry flood runoff. Climate change, deforestation, excessive burning of vegetation, faulting, overgrazing on agricultural soils, local changes in slope, and extreme storms are all examples of environmental changes that promote gully erosion (Selby, 1993). Climate change is the most important, however, as variations in rainfall intensity and/or frequency are usually involved and vegetation can subsequently be affected.

4.4.2. Development of gullies

Gullies commonly grow by upslope migration (Knighton, 1998). The steep, near-vertical, or even overhanging scarps suggest that erosional extension originates at the base of the headcut. This may result from waterfall action and subsequent backsplash, given that surface runoff gains energy (and therefore erosive potential) as it plunges over the gully head. Upslope scarp migration can also, however, result from sapping, wherein particles are entrained and removed from the base of the headcut (either individually or in bulk) by the emergence of subsurface water from a permeable medium and/or by saturation and reduction of the strength of the soil (Higgins et al., 1990). The seepage erosion involved in this process causes undermining and weakening of the scarp so that it collapses, at which point surface wash removes the debris. Generally, seepage erosion is probably important only in non-cohesive materials (or materials with low cohesion due to weathering) as it entails the entrainment of material by water flowing through and emerging from a permeable medium (Knighton, 1998).

The role of return flow in the sapping process emphasizes the role of piping in gully formation and morphology. The characteristic steep scarps of most gullies may form and migrate from the development of pipes and the subsurface flow convergence they promote (and eventually release). Additionally, the steep walls may be attributed to roof collapse. Some gullies, particularly those in arid regions and semi-arid badlands, are thought to form almost exclusively from pipe development and subsequent collapse (Selby, 1993).

In general, gully development involves waterfall erosion or sapping at the head, channel erosion of the bed, and collapse or slumping of the banks which causes progressive widening of the gully sides. As with rilling, gully erosion rates increase with slope angle. Where slope decreases, zones of deposition (fans) form in the lower portions of the channels.

4.4.3. Characteristics of gullies

Gullies are steep-sided watercourses which transport ephemeral flows during heavy or extended rainfall events. Compared to rills, gullies are relatively large. Gully dimensions (width and depth) usually exceed 0.3 m, while rill dimensions range from a few cm to a few tens of cm (Brice, 1966; Selby, 1993). Gullies typically form in loess, volcanic (pyroclastic) ejecta, gravels, alluvium, colluvium, semi-consolidated sands, and debris from mass movements (Selby, 1993). These materials exhibit low degrees of consolidation and are therefore weak and highly erodible.

Morphologically, gullies are characterized by steep scarps (headcuts) and steep walls (Blong, 1970; Selby, 1994; Carey et al., 2001). U-shaped cross-sectional profiles are typical, but irregular and asymmetric cross-sections are also common (Figure 15). Additionally, rectangular profiles can form when the slope of the gully floor is only a few degrees and ephemeral stream flow can easily erode the base of the walls. This undercutting action causes the walls to remain

steep (Figure 15). Gullies generally exhibit low width-to-depth ratios, having widths greater than about 0.3 m and depths greater than about 0.6 m (Brice, 1966). Gully depth is often limited by the depth to the underlying rock; therefore, gullies are usually less than 2 m deep although depths of 10-15 m can be achieved on deep alluvial and colluvial soils (Carey et al., 2001).

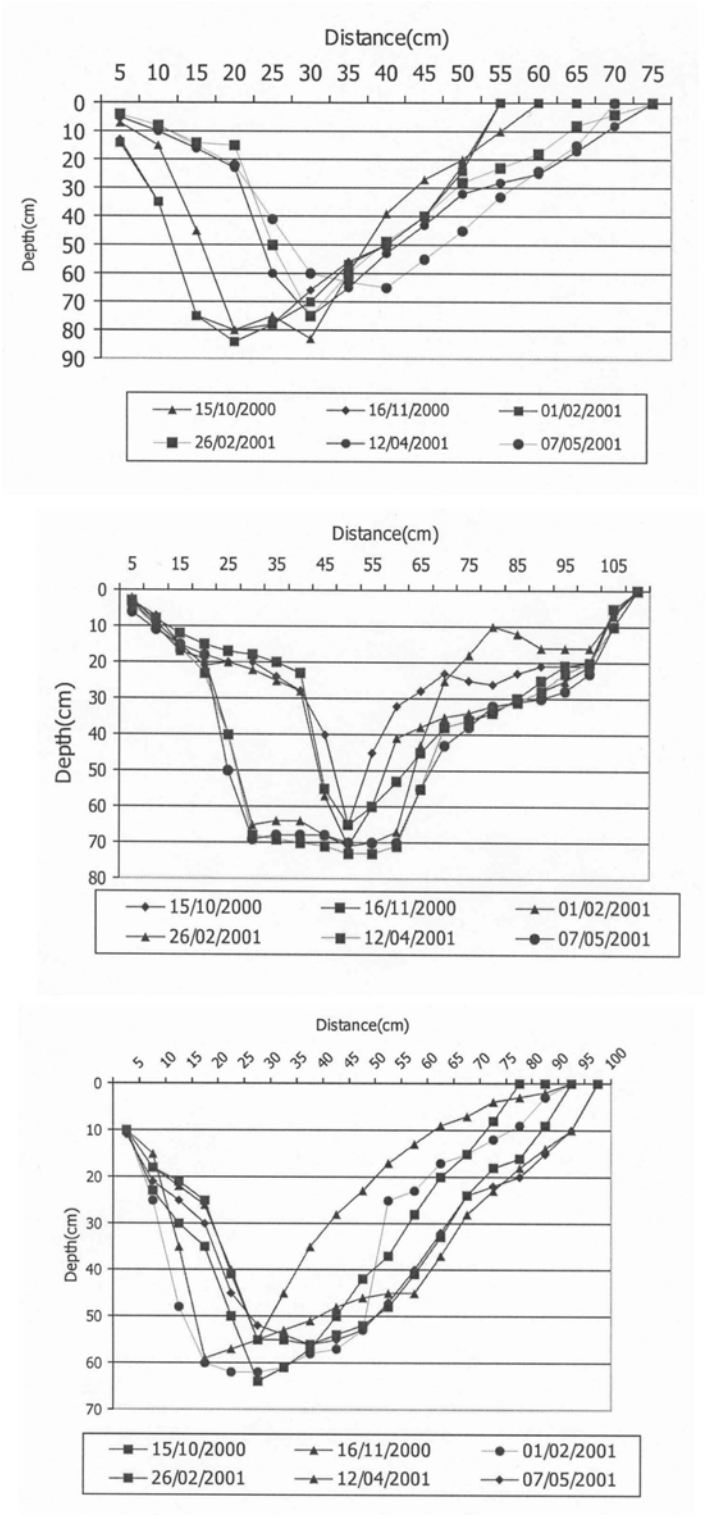

Figure 15. Plots illustrating variations in cross-sectional profiles of gullies.

Nejad and Rezazadeh (2002) recorded progressive changes in the profiles of 3 gullies (each represented by a separate plot) following 43 rainfall events in the loess hilly area of Gorgan, Iran; the 6 dates on each plot represent those events that caused measurable changes in gully morphology. Profiles are typically asymmetric; U-shaped, v-shaped, and rectangular profiles are all represented.

4.5. Relationships between rills and gullies

Morphological and behavioral similarities suggest that the genesis of gullies from rills is a common occurrence. Gullies frequently head in the tracks of pre-existing rills. Both share the formational processes of overland flow and piping. Both characteristically extend upslope by scarp migration, and both increase in width and depth downslope as runoff and catchment area increase.

Gullies can develop directly from permanent rills simply through erosional enlargement of a rill structure by prolonged overland flow. The destruction of rill divides also promotes such a transition. Divides between rills can be destroyed by (1) undercutting and/or saturation of rill walls, which reduces material strength and promotes bank collapse, and (2) erosion of interrill areas through rainsplash and overland flow. Savat and De Ploey (1982) state that while rills may deepen and transform into gullies, vertical development seems to be a self-limiting process and entrenchment does not exceed a few decimeters.

Some morphological differences between rills and gullies, however, imply that they may differ in their genesis. Rills commonly display v-shaped cross-sectional profiles while gullies exhibit U-shaped cross-sectional profiles (with flat bottoms and steep sides). Observations of rills suggest that erosional enlargement by overland flow simply produces larger valleys that retain the characteristic v-shaped rill profile (Higgins et al., 1990). Conclusions may therefore be drawn that some gullies may never have been rills; while overland flow develops and enlarges rills, sapping and migration of headcuts are the chief processes in gully development.

5. Debris Flows

5.1. Introduction to debris flows

Gravity-driven mass flows of rock fragments and water are common processes at volcanoes. "Lahar" is a term that is often used to describe a spectrum of such wet mass flow processes that originate at a volcano, either syn-eruptively or post-eruptively. The term has also recently been more narrowly defined to refer to two rheological categories of wet mass flow, namely hyperconcentrated (flood) flow (HFF) and debris flow, whose generation and behavior are largely controlled by the relative proportions of sediment and water (Pierson and Costa, 1987; Smith and Lowe, 1991). According to Beverage and Culbertson (1964), hyperconcentrated (flood) flows contain solids concentrations of 40-80% by weight, while debris flows comprise at least 80% solids by weight. The resulting sediment/water ratio for each flow type has significant implications for flow behavior, particle transport mechanisms, and mode of sediment deposition (Figure 16).

Most voluminous lahars are associated with stratovolcanoes, and hence are mostly of intermediate to silicic composition, but flows of much smaller volumes have been observed during basaltic phreatomagmatic eruptions of Surtseyan type (Lorenz, 1974; Fisher and Schmincke, 1984).

5.2. Rheology, transport and deposition

Debris flows are defined as non-Newtonian flows of sediment and water that contain at least 80% solids by weight (about 60% by volume) (Beverage and Culbertson, 1964) and reflect a relatively uniform mixture of solid and liquid phases in vertical profiles. They exhibit yield

strength (or resistance to flow) derived from grain collisions and cohesion between silt- and/or clay-sized particles (Smith and Lowe, 1991). Debris flows that contain greater than approximately 3-5% clay-sized particles in the matrix are termed "clay-rich" or "cohesive." These can travel great distances from the source (more than 100 km) with little or no change in rheology (Vallance and Scott, 1997). Flows containing less than 3-5% clay are classified as "granular" or "non-cohesive" (Pierson, 1998). "Mudflow" typically refers to cohesive debris flows.

Hyperconcentrated (flood) flows are non-Newtonian fluid-solid mixtures possessing little strength (Smith and Lowe, 1991), with solids concentrations between 40-80% by weight (20-60% by volume; Beverage and Culbertson, 1964), and water contents greater than that of debris flows. They can possess some fluvial characteristics such as localized turbulence but transport very high sediment loads, and thus are generally more erosive than debris flows (Vallance and Scott, 1997; Vallance, 2000).

5.2.1. Flow behavior

As a consequence of high sediment concentrations and high bulk densities, debris flows behave as Bingham plastic fluids that do not flow until the yield strength of the material is exceeded. Once the yield strength has been exceeded, flow can occur on slopes as shallow as 1-2° (Costa, 1984). Debris flows generally travel downslope in a laminar fashion with a consistency that resembles wet concrete; turbulent behavior may locally develop on steep slopes (Enos, 1977). They are typically channeled into pre-existing drainageways (Smith, 1986), but may also build their own channels as levees form along the flow margins.

At volume concentrations of about 20-30% solids, particle interactions will dominate the support mechanisms and transport processes of any flow (Fisher and Schmincke, 1984). Debris flows contain at least 60% solids by volume (Beverage and Culbertson, 1964), and flow behavior is largely controlled by grain collisions and cohesion between clay- and silt-size particles (depending on clay content). Matrix strength is commonly sufficient to transport boulders within the body of the flow or at the surface. In hyperconcentrated flows, where water content is higher and solids comprise 20-60% by volume (Beverage and Culbertson, 1964), clast support is by some combination of grain interactions, buoyancy, and fluid turbulence (Figure 16).

Waves or surges are common within the body of a debris flow or hyperconcentrated flow and result from a temporary constriction that causes the flow to pond above the channel bottom and then drain away (Fisher and Schmincke, 1984).

Flow transformations (Figure 17) are common in lahar events and usually reflect a change in rheologic behavior from laminar to turbulent or turbulent to laminar (Fisher, 1983). Transformations often result from downstream bulking or dilution of a flow (Smith and Lowe, 1991). Bulking involves the erosion and subsequent incorporation of sediment, which can result in a significant increase in flow volume and internal strength. Bulking following erosion and collapse of channel banks is a particularly common process. Dilution occurs either with the addition of water or a decrease in sediment concentration by deposition of (usually) the largest or densest particles (Figure 17). Dilution begins at the flow front and migrates back through trailing portions of the lahar (Vallance 2000). A lahar may experience several flow transformations during a single event (Fisher, 1983). Deposition from a debris flow occurs mostly by en-masse freezing as velocity and/or slope decreases, causing the applied shear stress to fall below the critical yield strength of the material. When the flow stops, water separates

from the granular material by percolation or evaporation and the flow consolidates and solidifies at the rate at which pore fluid drains out (Fisher and Schmincke, 1984; Pierson and Costa, 1987). Deposition from hyperconcentrated flows occurs by episodic deposition of material settling out of suspension separately (Smith and Lowe, 1991).

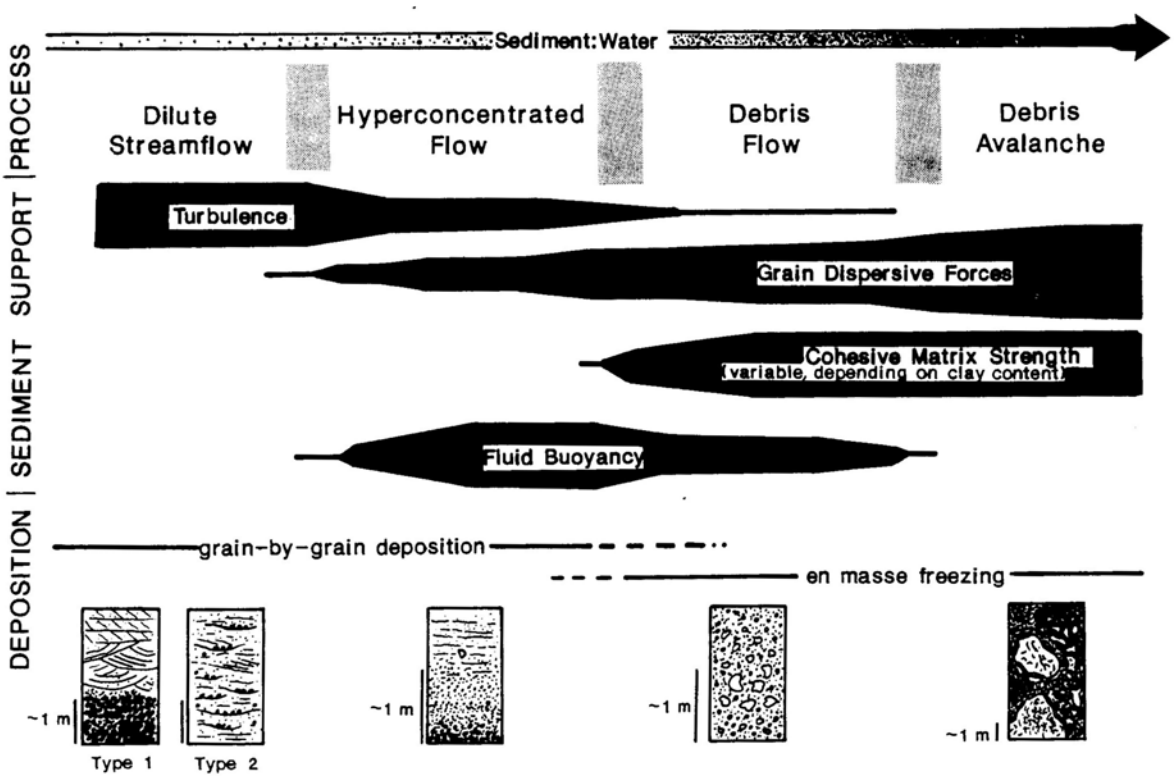

Figure 16. Sediment flow classification

Classification of wet gravity-driven sediment flows based on sediment support, depositional mechanisms and sediment/water ratio (after Smith and Lowe, 1991).

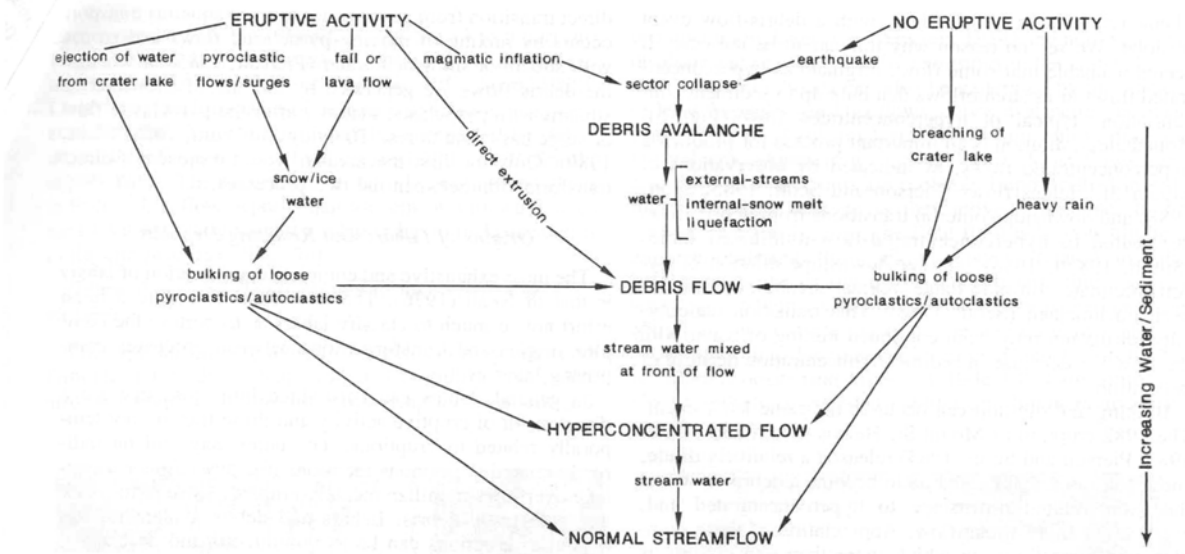

Figure 17. Flow transformations

Flow diagram illustrating some possible flow transformations that may take place during lahar events generated by different mechanisms (after Smith and Lowe, 1991).

5.3. Lahar deposits

Thicknesses of lahar units can vary from a few centimeters to several meters. A typical thickness is < 5 m, but some lahar deposits are greater than 200 m thick. Deposits are thinnest on steep slopes but become thicker in valley bottoms and topographically low-lying areas (Fisher and Schmincke, 1984). While thickness tends to be relatively constant on shallow slopes, it can locally vary depending on the configuration of underlying topography. Surfaces of lahar deposits are extremely flat on the large scale but likewise can be locally undulating due to irregular underlying topography. Surface hummocks may also be locally developed (e.g. Vallance and Scott, 1997).

Debris flow deposits are generally thick, matrix-supported, massive to crudely stratified, and extremely poorly sorted (Waldron, 1967; Manville et al., 1998). Massive deposits are usually attributed to en masse deposition (Johnson, 1970; Fisher and Schmincke, 1984). Debris

flows that are rich in water are more likely to develop crude stratification. Individual clasts are usually subangular to angular, and vesicles may occur in the matrix if the flow was cohesive.

Hyperconcentrated flow deposits can also be massive, but are more typically weakly stratified. Low-angle cross-bed sets, ripple laminations, and scour structures may also be present (Smith and Lowe, 1991). The lower sediment/water ratio of these flows compared to debris flows is reflected in the occurrence of these structures, reflecting better sorting within the flow, fluid turbulence, and deposition from traction currents. Vesicles may also be present in clay-rich matrices but are less prominent than in debris flow deposits. Individual beds can be ungraded, normally graded, or reversely graded. Smith (1986) suggests that hyperconcentrated flows are turbulent enough to allow differential settling of particles and the subsequent development of graded beds. The presence, absence, and nature of grading are related to the relative concentration of solids and fluids. In flows with lower solids concentrations, such as hyperconcentrated flows, normal grading is more likely to develop due to low internal strength and the inability of the flow to support large, dense particles as velocity decreases (Fisher and Schmincke, 1984). Reverse grading may develop in various ways. Middleton (1970) suggests one possible mechanism in which smaller clasts in a high solids concentration flow are sifted downward between larger clasts during movement, thereby preventing the larger ones from settling. Generally, however, reverse grading is attributed to dispersive pressure at the boundary layer of a flow (Schmincke, 1967; Sallenger, 1979; Lowe, 1982). Because such pressure is virtually ineffective in cohesive sediment (Lowe, 1982), reverse grading is most commonly restricted to the basal portion of a debris flow deposit with low clay content (i.e. non-cohesive).

5.4. Initiation of lahars

The generation of lahars requires (1) unconsolidated debris, (2) steep slopes and substantial relief at the source, (3) a triggering mechanism, and (4) an adequate water source (Vallance, 2000). Most lahars begin by gravitational failure on steep slopes (> 15 - 20˚) due to a rapid influx of large amounts of water (Costa, 1984). The presence of water promotes failure of material by lubricating individual grains and increasing pore pressure between grains, weakening the material by reducing internal friction and shear strength. Potential water sources include rainfall runoff, rapidly melted snow and ice, lake water, pore water and hydrothermal water. Enhanced runoff is particularly favored on steep volcanic slopes because they are commonly mantled by poorly sorted pyroclastic debris (with reduced infiltration) and have little or no sediment-stabilizing vegetative cover (e.g. at Irazú Volcano, Costa Rica, Waldron, 1967).

Lahars can be triggered during an eruption or eruptive episode (syn-eruptive) or after an eruption (post-eruptive), including after long periods of quiescence. They may also be less directly related to a particular eruption or eruptive episode, originating on any steep slope covered with volcaniclastic debris, including volcanoes that have long been extinct (e.g. Manville et al., 1998). Syn-eruptive mechanisms of initiation include: rapid melting of snow and glaciers by contact with lava flows/domes and pyroclastic deposits, and from geothermal heating (Waitt et al., 1983; Fairchild, 1987; Major and Newhall, 1989); eruption through and drainage of lakes or water vaults by expulsion, or by failure of confining materials such as rock or ice (Neall, 1976; Nairn et al., 1979; Scott, 1988; Smith and Lowe, 1991; Manville et al., 1998); edifice or flank collapse and the release of pore, ground, or hydrothermal water (Janda et al., 1981; Vallance and Scott, 1997); flow and slumping of wet tephra fed from phreatomagmatic jets and plumes and possibly by direct effusion from a vent (Wohletz and Crowe, 1978; Smith, 1980; Leat and Thompson, 1988; Mueller et al., 2000). Post-eruptive lahars can be triggered by intense

rainfall (Waldron, 1967), lake or water vault outbreaks (Glicken et al., 1989), and by liquefaction, gravitational failure, or seismic disturbance of wet volcaniclastic deposits (Glicken et al., 1989; Sohn and Chough, 1992). Pyroclastic density current deposits may be able to directly initiate a lahar through mechanical mixing and melting of snow and ice, or possibly during transition in transport medium from gas to water (Smith and Lowe, 1991). From studies of lahar deposits at South Fork Toutle River, Mount St. Helens, Fairchild (1987) postulates the formation of a lahar by the application of relatively small shear stresses to the summit snowpack by a laterally-directed pyroclastic surge. In his model of initiation, passage of the hot cloud induces failure of the snowpack at weak boundaries between snow layers. Subsequent creation of slab avalanches disrupts and mobilizes the snowpack, exposing more surface area of the snow to the surge cloud and encouraging rapid melting of snow. A lahar transforms directly from the surge cloud due to the addition of water.

Lahars triggered by edifice- or sector-collapse can originate by several mechanisms, including (1) the shallow intrusion of magma or growth of a lava dome, which promote destabilization of an edifice, (2) magmatic or phreatic eruptions, (3) volcanic or tectonic earthquakes, (4) pre-failure weakening of rock due to prolonged hydrothermal alteration, and (5) deposition of pyroclastic debris above the angle of repose. For dry, unconsolidated (cohesionless) pyroclastic material, the angle of repose is approximately 35˚; that of wet, hydrovolcanic tephra is approximately 24˚-30˚ (Wohletz and Sheridan, 1983). Once this value is attained, further deposition of material on the flanks will cause failure and remobilization of material downslope until stability is again achieved. Failure is manifested either as slumping of sectors of the edifice, or as shedding of upper layers (Leat and Thompson, 1988). The process of hydrothermal alteration increases the probability of lahars triggered by collapse by promoting the

breakdown of framework silicates and the subsequent formation of clay minerals such as kaolinite and smectite. The addition of such clay minerals influences a rock mass by increasing porosity but decreasing permeability, thereby allowing the rock to store large amounts of water. Such hydrothermally altered rock disintegrates and liquefies relatively easily upon deformation. Most collapse-related lahars initially behave as debris avalanches because they have a relatively high sediment/water ratio. Debris avalanches with significant pore and/or hydrothermal water in the rock debris may liquefy during deformation of the material and transform to debris flows (Vallance and Scott, 1997; Vallance, 2000). This flow transformation may also take place by incorporation of surface water during transport (Pierson and Scott, 1985; Smith, 1986). Lahars are often clay-poor because most form from mobilization of the fresh, coarse pyroclastic debris that typifies the surface deposits of the steep proximal slopes (Fisher and Schmincke, 1984). Clay-rich lahars, though rare, may be derived from debris avalanches generated by sector collapses of fluid-saturated, hydrothermally altered edifices (Crandell, 1971; Vallance and Scott, 1997).

5.4.1. Phreatomagmatic eruption-fed lahars

Relatively small-scale debris flow deposits are common in phreatomagmatic pyroclastic sequences, particularly those of Surtseyan origin (Sohn, 1995). They can be generated by direct feeding from subaerial and subaqueous jets and plumes (Leat and Thompson, 1988; Mueller et al., 2000), by direct eruption from a vent (Wohletz and Crowe, 1978; Smith, 1980; Leat and Thompson, 1988), or by failure of wet deposits of fallout and density current tephra (Lorenz, 1974; Leys, 1983; Leat and Thompson, 1988; Sohn and Chough, 1992).

Debris flows produced directly from subaerial and subaqueous tephra jets that collapse due to water ingestion are a primary eruptive phenomenon and are said to be "eruption-fed" by the tephra jets (Mueller et al., 2000). The debris flow deposits described by Mueller et al. (2000), derived from this mechanism, are planar but laterally discontinuous beds of lapilli tuff which contain local abundances of low-angle scours. The occurrence of bomb sags within these units provides supporting evidence of deposition by tephra jetting. At Surtsey volcano, Iceland, Lorenz (1974) describes "mud flow" deposits derived from the gravitational failure of wet, poorly-sorted vesiculated ash deposited on the steep inner and outer slopes of Surtur I crater. Such phreatomagmatic lahars, generated from the remobilization of beds of wet tephra, may be primary or secondary eruptive features depending on whether slumping of tephra occurs syn- or post-eruptively.

5.5. Erosive capabilities of lahars

Erosion by lahars occurs primarily through undercutting of banks, and to a lesser extent through clast-by-clast (piecemeal) erosion of channel beds (Waldron, 1967; Brantley and Waitt, 1988). The undercutting of banks and valley walls in turn creates unstable slopes prone to subsequent gravitational failure. Relatively fragile deposits (such as tephra layers) preserved and undisturbed at the base of debris flow deposits suggests that piecemeal erosion is more significant in the more water-rich hyperconcentrated flows (Vallance, 2000). Bulking (described above) exemplifies the erosive capabilities of some debris flows as it is facilitated by the detachment and incorporation of sediment at the flow boundary (Scott, 1988).

The waxing flow front and peak stages of a lahar are most erosive, but the erosive capabilities of lahars in general are greatest where the occurrence of turbulent behavior is most

probable. Turbulence creates localized increases in bed shear stress (Bryan, 2000), and is most likely to occur on steep slopes where flow velocities are highest. Shear stresses imparted on underlying beds locally enable overriding lahars to readily erode poorly consolidated deposits such as alluvial deposits or tephra layers (e.g. Janda et al., 1981; Lowe at al., 1986). Water-rich, hyperconcentrated flow phases are generally more erosive than sediment-rich debris flow phases, perhaps due to the greater degree of turbulence (Vallance, 2000).

6. Description and interpretation of "U-shaped channels" at SE Koko Crater

6.1. Introduction

The incisional structures previously described as "U-shaped channels" by Fisher (1977) occur in the basal flank deposits at SE Koko Crater. Cross-sections of the incisional structures are well exposed in the cliff faces at the base of this tuff cone. Intervening between the cliffs and the shoreline is a wave-cut platform that extends approximately 200 m in length and varies in width from about 5-20 m; this platform provides very easy access to cross-sectional exposures of the structures and, moreover, exposes plan views of the channel networks. Descriptions of gullies from 26 different localities along a short stretch of the shoreline (Figure 2) are presented below. Characteristics of the incised and infilling tephra are also described, and interpretation of formation mechanisms of the structures is presented.

6.2. Rills at SE Koko Crater

Rills are very common in the pyroclastic density current (PDC) and fallout deposits (and their reworked equivalents) that mantle Koko Crater's lower SE flanks. Rills are defined here as channel-like incisional structures less than 15 cm wide and deep. At Koko Crater they typically display V-shaped cross-sectional profiles (Figure 18), but U-shaped profiles also occur. In plan view, the rills are sinuous and commonly bifurcating (Figure 34).

An interesting observation is that rill incision is always correlated with units of underlying vesiculated ash deposits, i.e. rill incision occurs only on the upper surfaces of these beds. Rill sets are common along single stratigraphic horizons, with each rill typically laterally separated by less than 30 cm (Figure 18). Such sets occur frequently throughout the successions.

The rills at Koko Crater are cut to approximately the same depth (less than 15 cm) and do not extend below the vesiculated ash layers into the next underlying bed.

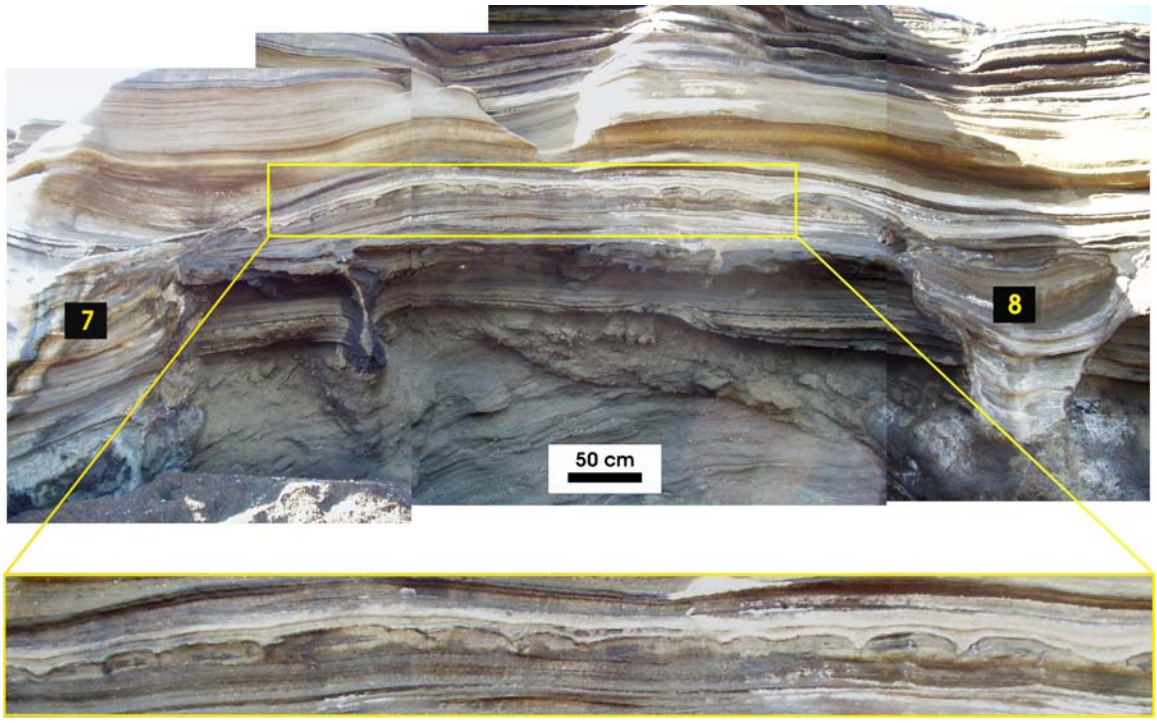

Figure 18. Rills incised into a bed of vesiculated ash

The vesiculated ash bed here is laterally continuous between gullies 7 and 8. Rill structures are less than 15 cm wide and deep and typically display broad V-shaped cross-sectional profiles. Gullies 7 and 8 both originate in the same ash unit as the rills.

6.3. Gully morphology

Larger (>15cm wide) incisional structures also occur at SE Koko Crater and are here termed gullies. The gullies also originate completely within the Hanuama Bay succession, although unlike the rills many gullies cut into the underlying Koko Crater deposits. They display pronounced variation in width, depth, marginal slope angles, and cross-sectional profiles. Dimensions and cross-sectional profiles are particularly variable (Table 1, Figure 19). Gullies range from approximately 0.3 to 5 m in width and 0.3 to 3 m in depth. Gully 25 is a complex

composite structure which far exceeds these average dimensions. A detailed stratigraphic column through gully 25 is presented in figure 28.

Figure 19 illustrates the cross-sectional morphologies of gullies and demonstrates that few display a simple "U-shape." Gullies exhibit symmetrical and asymmetrical U-shaped, V-shaped, and rectangular profiles. Some basal profiles display combinations of these forms, e.g. V-shaped or rectangular basal portions sometimes widen upwards into more rounded U-profiles (Figure 20). Different profile forms occur within the primary margins of those gullies that have experienced multiple cut-and-fill episodes (Figure 21A).

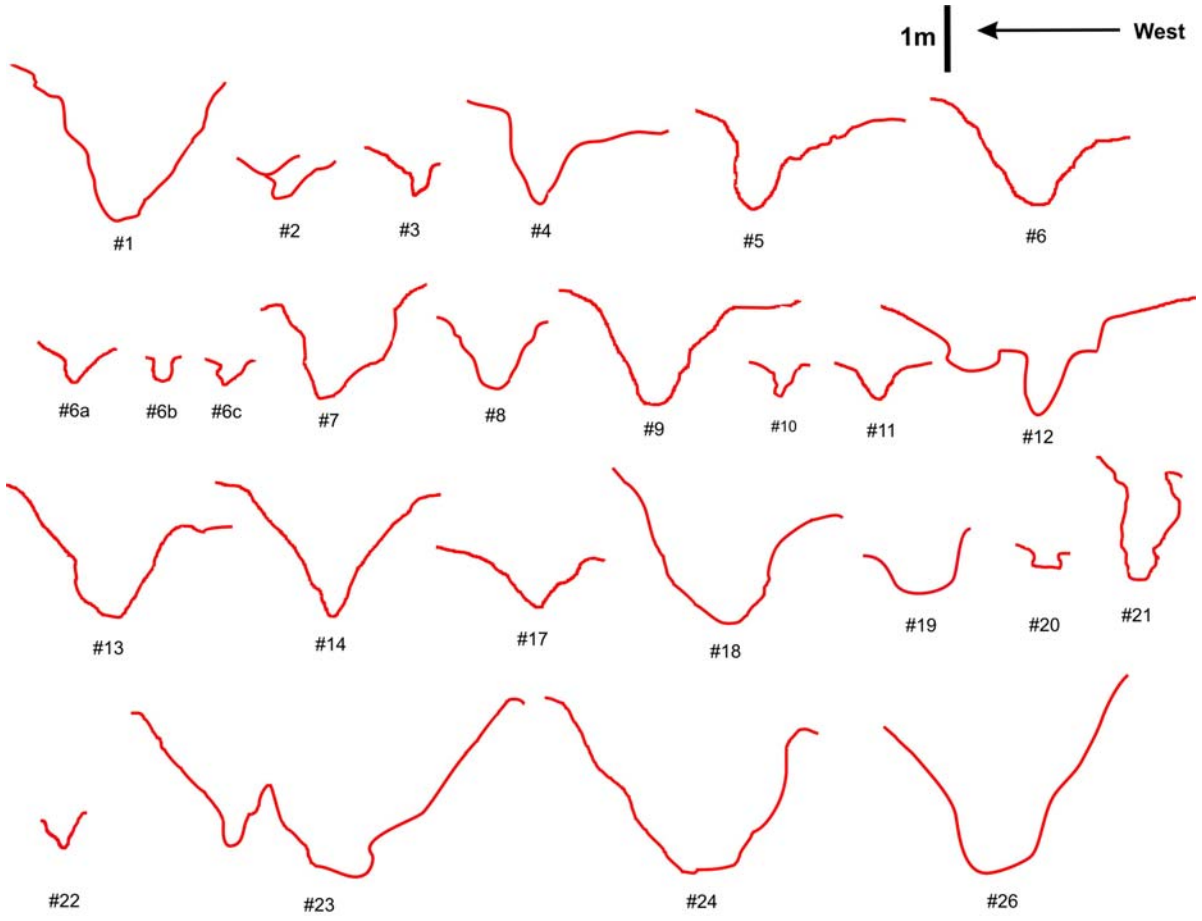

Figure 19. Cross-section basal profiles of gullies in SE Koko Crater tephra (viewed along or close to longitudinal axes)

Secondary gullies created as a consequence of multiple cut-and-fill episodes are not included here. Cross-sections for gullies 15, 16, and 25 are not illustrated; 15 and 16 are exposed only on the foreshore platform and 25 is a large, complex structure which does not exhibit a simple profile such as these.

Gully cross-section margins are typically steeper than 50 degrees, with the upper margins frequently 90 degrees or greater. Gully walls are often disrupted and irregular, contributing to common asymmetric profiles. Longitudinal axial trends (mostly ranging between 315 and 360˚, Table 1) are approximate values measured at the point of gully exposure in the cliff face. The axial trends of the cliff and foreshore components of the same gully are sometimes different. In addition, fills may display several gully-cutting episodes, each with different axial trends (Figure 21).

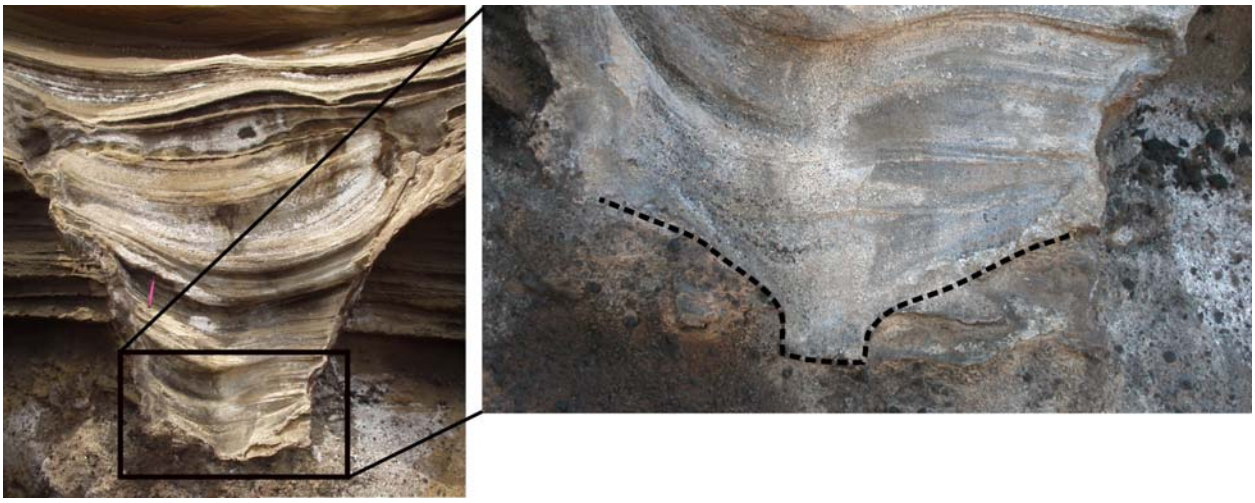

Figure 20. Combination of cross-sectional profile forms displayed in gully 8
A rectangular basal "rill" is modified upwards into a rounder U-shape

Table 1. Physical characteristics of gullies at SE Koko Crater.

Gully Number	Location	Orientation	Marginal Slope (˚)	Maximum Depth (m)	Maximum Width (m)
1	21˚16.644'N, 157˚41.010'W	6	40-90	2.5	3.5
2	21˚16.643'N, 157˚41.015'W	357	19-32 (top) 55 (basal)	0.33 (upper portion) 0.6 (lower portion)	0.91 (upper portion) 1.22 (lower portion)
3	~ 2 m east of gully #1	342	70 (NE margin) ~ 90 (SW margin)	0.7	1.3
4	21˚16.650'N, 157˚41.011'W	342	45	1.3	2.5
5	~ 3.5 m east of gully #4	342	> 90	1.3	2.5

6	~ 1 m east of gully #5	354	50-60	1.3	2.5
6a	21˚16.649'N, 157˚40.996'W	310	45 (NE margin) ~ 85 (SW margin)	0.5	1.15
6b	21˚16.649'N, 157˚40.997'W	324	~ 90	0.3	0.4
6c	21˚16.651'N, 157˚40.999'W	282	45 (NE margin) ~ 85 (SW margin)	0.51	0.33
7	21˚16.649'N, 157˚40.998'W	305	60-70	2	1.5
8	21˚16.653'N, 157˚40.989'W	320	55	2	1.24
9	21˚16.652'N, 157˚40.987'W	307	~ 55	1.68	2
10	~ 1 m east of gully #9	321	57 (NE margin) ~ 90 (SW margin)	0.4	0.3
11	~ 1.5 m east of gully #10	324	50	0.6	0.7
12	21˚16.666'N, 157˚40.987'W	324	72	2.2	3.7
13	21˚16.668'N, 157˚40.983'W	330	82 (top) 66 (base)	2.2	2.3
14	21˚16.659'N, 157˚40.978'W	319	62	2.2	0.61
15	21˚16.657'N, 157˚40.975'W	134	n/a	n/a	2
16	21˚16.657'N, 157˚40.970'W	135	n/a	n/a	n/a
17	21˚16.659'N, 157˚40.967'W	355 (cliff) 152 (foreshore)	45-50	0.8	1.6
18	21˚16.670'N, 157˚40.977'W	320	75 (NE margin) 81 (SW margin)	2.21	2.3
19	< 1 m east of gully #18	340	67 (top) 47 (base)	0.9	1.3
20	< 1 m east of gully #19	320	~ 95 (NE margin) 69 (SW margin)	0.71	0.33
21	21˚16.663'N, 157˚40.967'W	315 (top) 350 (base)	~ 90	1.52	0.41
22	< 1 m east of gully #21	315	58	0.56	0.46
23	21˚16.673'N, 157˚40.957'W	326	46 (top) 60-65 (base)	2.2	5
24	21˚16.674'N, 157˚40.955'W	330	56 (NE margin) 43 (SW margin)	2.8	3.3
25	~ 4 m east of gully #24	331	n/a	~ 8	~ 5
26	n/a	n/a	60 (NE margin) 54 (SW margin)	3	3.5

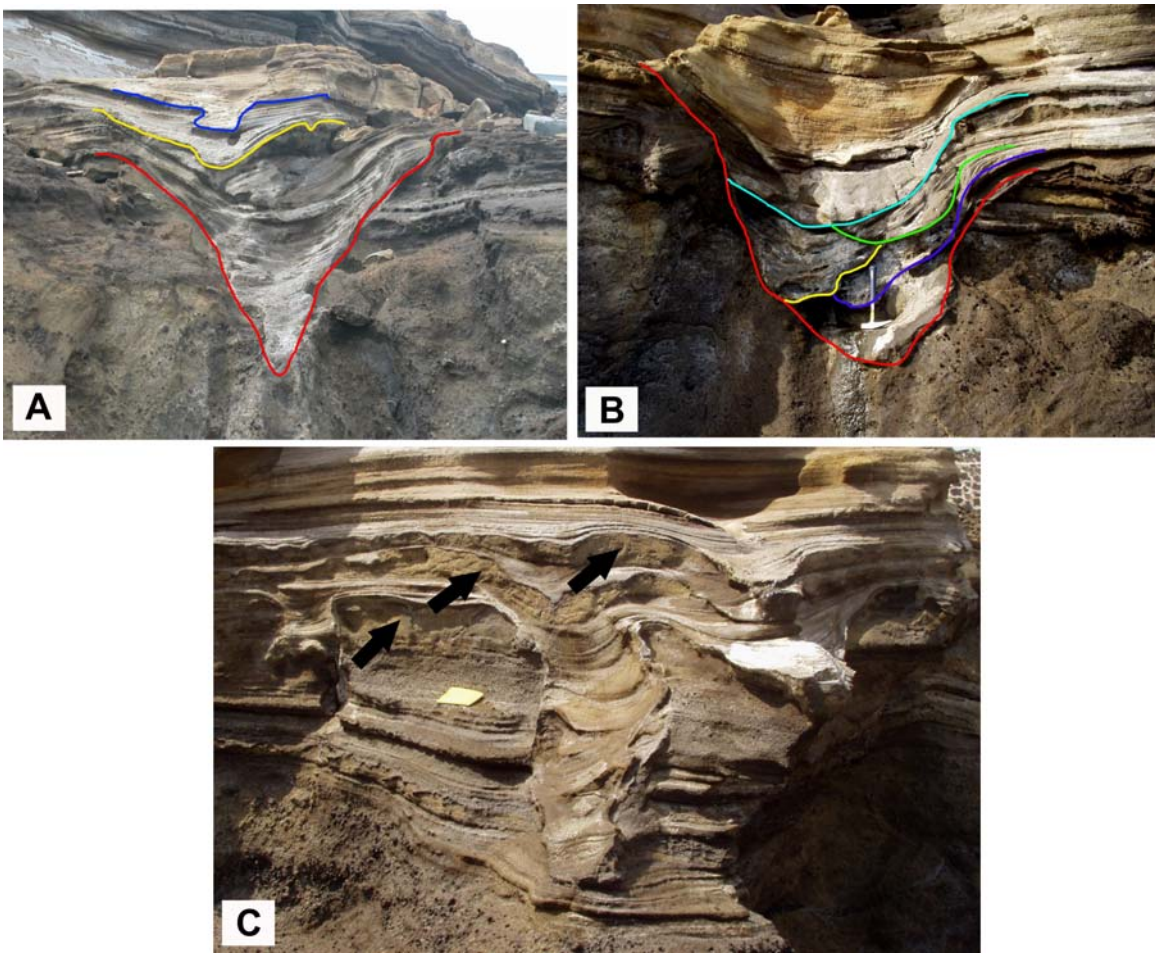

Figure 21. Gullies that record multiple episodes of cut-and-fill

(A) Stacked secondary channels in gully 14; each erosional event has produced a separate structure with a morphologically distinct cross-section. V-shaped (red line), U-shaped (yellow line), and rectangular (blue line) profiles are represented within the primary structure as a result. (B) Gully 18; cross-cutting relationships between U-shaped secondary channels. The initial gully is traced in red. (C) Cut-and-fill is always initiated in vesiculated ash layers (black arrows).

6.4. Description of Gully-Fill Facies

A variety of facies infill the gully structures (Table 2). Each facies has been assigned a code which denotes grain size and internal structure with the following letters: A = ash, L = lapilli, f = fine, c = coarse, m = massive, b = bedded, v = vesiculated. Well-bedded ash and fine-grained lapilli tuffs (Lf_b), fine vesiculated ash (Af_v), massive, poorly sorted vesiculated lapilli (Lm_v), and chaotically slumped tephra (Lf_m, massive fine-grained lapilli and Lc_m, massive

coarse-grained lapilli) comprise the 5 gully fill facies. The well-bedded tuffs (Lf_b) comprise the vast majority of fill material. Representative examples of these various facies are depicted in Figure 22 and described below. Photomicrographs of each facies are presented in Appendix A.

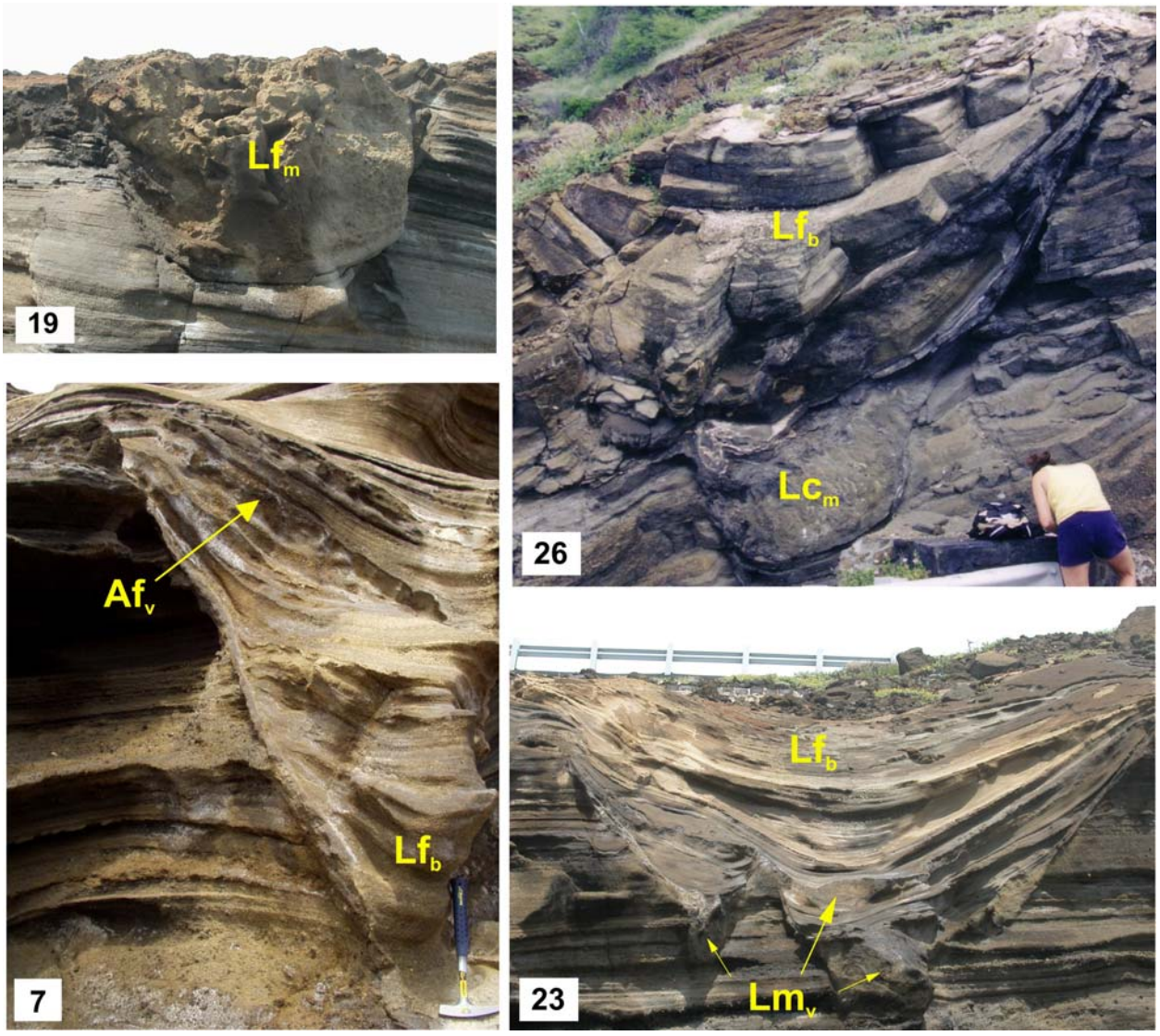

Figure 22. Representative examples of gully-fill facies

Gully number is indicated at the lower left corner of each photograph. See Figure 24 for closer views of Lm_v facies in gully 23; refer to Table 2 and the body of the text for descriptions and interpretations of each facies.

Table 2. Summary of gully-fill facies

Facies Code	Brief Description	Interpretation
Lf_b	Thin, evenly bedded and laminated lapilli tuff; moderately to well-sorted; millimeter to centimeter thick beds; accretionary lapilli intercalated	deposition from pyroclastic surges
Af_v	Fine vesiculated ash; tuff vesicles < 1 – 5 mm diameter; massive and evenly bedded; maximum bed thickness ~ 10 cm; unconformable upper contacts; rare coral fragments	deposition of wet ash (cosurge fallout)
Lm_v	Massive, poorly sorted lapilli tuff; glassy ash matrix with tuff vesicles; scoria fragments and blocky intraclasts; highly variable bed thickness, 5 cm-0.8 m (maximum)	debris flow deposits, derived from the syn-eruptive failure of vesiculated tuff beds
Lf_m	Massive lapilli tuff; chaotic; moderate sorting; abundant coral reef and scoria fragments in glassy matrix; very similar to uppermost Lf_b material (at highest stratigraphic levels only)	slumped Hanauma Bay and Koko Crater tephra
Lc_m	Massive lapilli tuff; accretionary lapilli, armored lapilli, and blocks in glassy matrix; armored lapilli up to 1 cm diameter	slumped Koko Crater tephra

6.4.1. Lf_b lithofacies

With few exceptions, gullies are largely infilled with well-bedded (and laminated) ash and lapilli tuffs (Lf_b facies). This material dominantly comprises a matrix of light brown, angular, sub-millimeter-sized glassy fragments with sporadic augite crystals and coral reef fragments. Accretionary lapilli are abundant. Individual beds are various shades of gray and light brown with thicknesses ranging from less than 1 cm (laminae) to approximately 4 cm. Parallel bedding is usually displayed (Figure 23). Individual beds commonly parallel the gully margins (Figure 24), with thinning common towards the upper margins. Beds also occasionally buttress against the margins at steep angles (Figure 25).

Figure 23. Parallel bedding in the Lf_b lithofacies

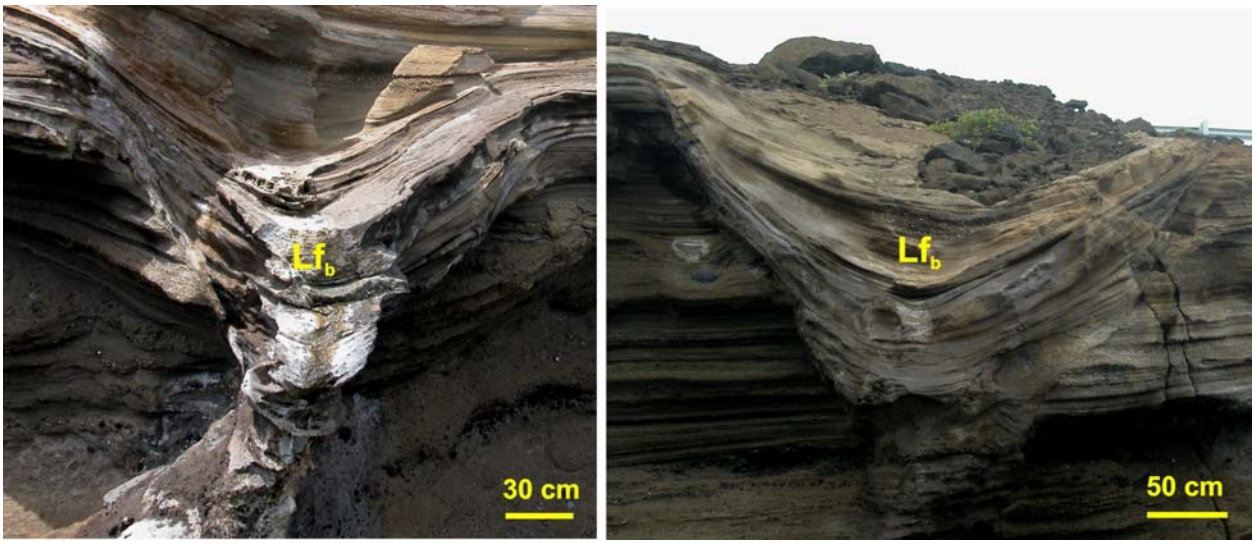

Figure 24. Bedding in the Lf_b lithofacies

Where the Lf_b facies comprises the bulk of gully fill, as in gully 9 (left) and 24 (right), bedding commonly parallels the concavity of gully margins.

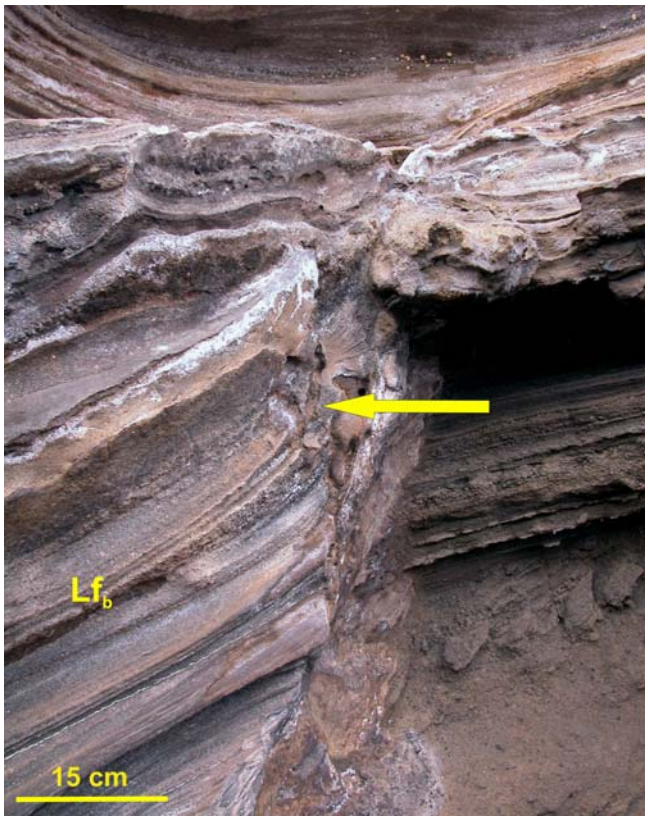

Figure 25. Steep buttressing of Lf_b beds against the margins of gully 7

6.4.2. Af_v and Lm_v lithofacies

Af_v and Lm_v units are commonly intercalated in the successions of stratified lapilli tuffs that comprise the bulk of the fill material and therefore constitute only a small portion of the total fill (Figure 26, 27, 28). Unlike Lf_b material, individual units display irregular upper boundaries that are frequently disrupted by rill incision and bed thicknesses that are more laterally variable, reaching a maximum at the central gully axis.

Af_v and Lm_v deposits occur in both extra and intra-gully settings and play a substantial role in the channel formation mechanisms proposed below. Therefore, detailed discussions of these facies are reserved for subsequent sections in which their description and interpretation are presented in conjunction with their influences on rill and gully development.

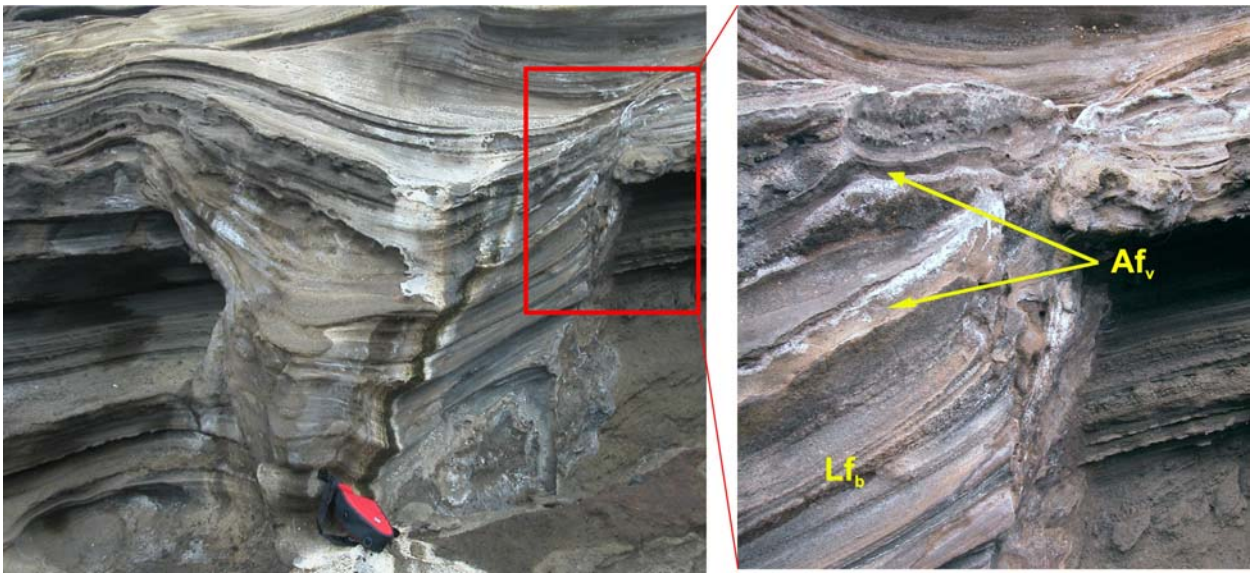

Figure 26. Intercalated Af_v and Lf_b lithofacies in gully 7

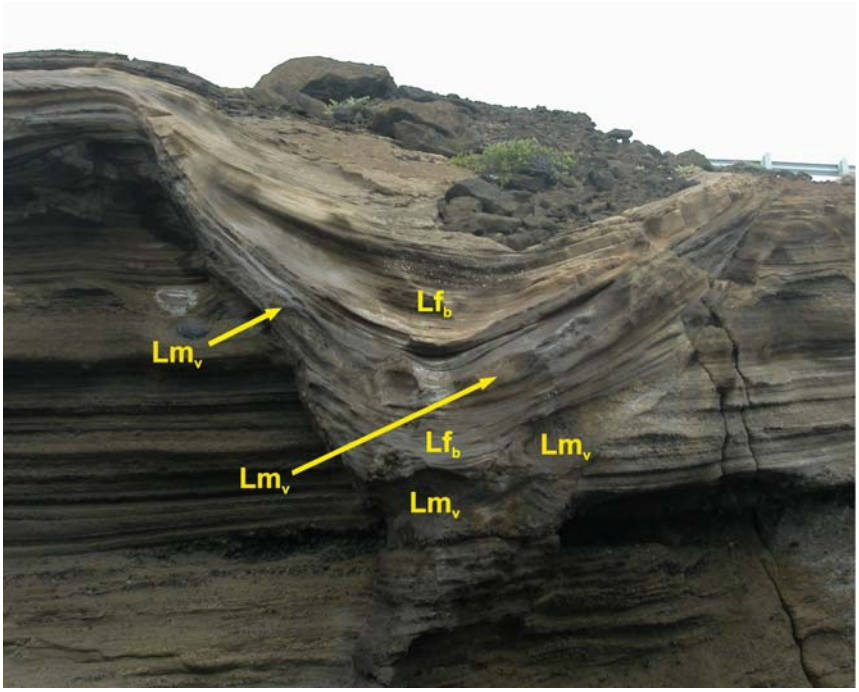

Figure 27. Intercalated Lm_v and Lf_b lithofacies in gully 24

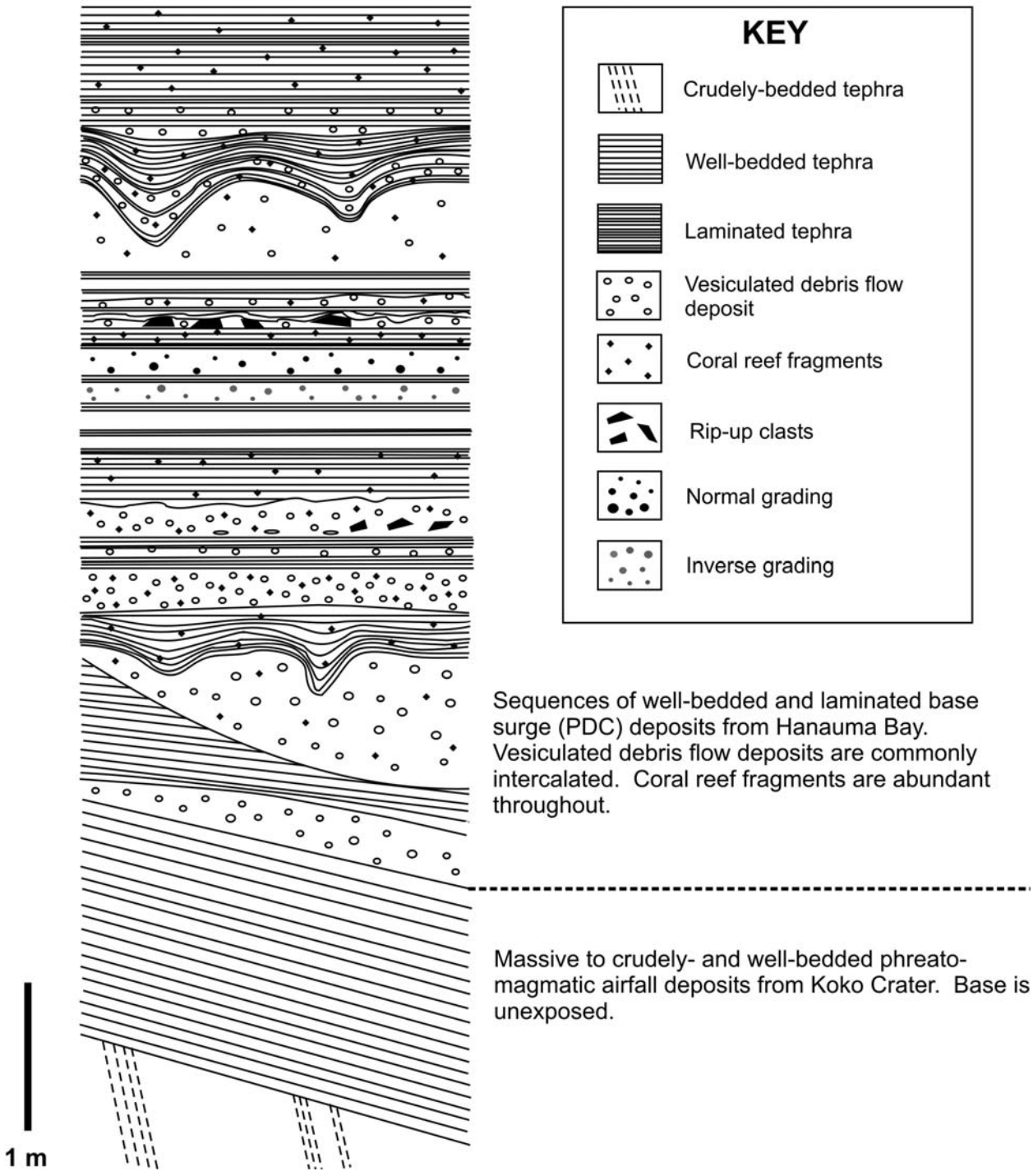

Figure 28. Stratigraphic section through gully 25

Vesiculated debris flow deposits (Lm_v lithofacies) are repeatedly intercalated with well-stratified pyroclastic density current (surge) deposits (Lf_b lithofacies). Lm_v units frequently display lateral variation in thickness; upper surfaces are commonly disrupted by minor channel incision.

6.4.3. Lf_m and Lc_m lithofacies

Lf_m and Lc_m units (Figure 22) comprise much larger portions of the total gully fill than the Af_v and Lm_v lithofacies. They are both poorly sorted and completely lack any internal stratification; the lack of vesicles mainly distinguishes these facies from the Lm_v lithofacies. Their origins are deduced from compositional similarities with (directly) outlying tephra.

Except for the lack of internal stratification, the Lf_m lithofacies is nearly identical to the uppermost units of the Lf_b lithofacies. Both facies are light brown, extremely rich in coral fragments, and represent the last phases of surge or co-fallout deposition. Lf_m material completely infills only gully 19. This gully is stratigraphically higher than almost all the rest (Figure 2B) and is not covered by further successions of surge deposits.

Accretionary lapilli are common in the Hanauma Bay surge and fallout ash deposits. Large (>1cm) armored lapilli, however, are present only in the underlying sequences of fallout (and their resedimented equivalent) deposits which originate from Koko Crater. The Lc_m facies, represented as fill material only in the basal portion of gully 26 (Figure 22), contains abundant armored lapilli. Grading and internal stratification are absent in these deposits.

6.4.4. Multiple cut-and-fill episodes

Fill material in several gullies record multiple cut-and-fill events. Each erosional episode creates a new cross-sectional profile, such that several different profile morphologies can consequently be represented in a single gully (Figure 21). Stratigraphic analyses reveal that most episodes of erosion are at the same stratigraphic levels as units of vesiculated ash.

A definable basal layer accompanies some primary gullies and later cuts. Beds of gullies 1, 6b, 7, 18, and 26 are lined with a layer of gray, well-sorted, ash. The thickness of this layer varies but does not exceed 4 cm. Petrographically, this material is similar to Af_v and Lf_b tephra.

6.5. Vesiculated tuffs (Af_v) and slope incision

Light brown to gray beds of vesiculated ash (Af_v) are commonly interbedded with the stratified lapilli tuffs (Lf_b) (Figure 26). They are easily identifiable by the presence of vesicles and lack of internal stratification. Vesicles are usually spherical and less than 2 mm in diameter while larger vesicles deviate from the spherical form and are mostly elongated.

Vesiculated tuffs are dominantly composed of fine ash, which largely consists of light brown, angular, (usually) non-vesicular glass fragments less than 0.5 mm in size. Minor augite crystals and occasional coral fragments are included in the matrix (Figure 29). The augite phenocrysts display euhedral crystal forms despite pronounced fracturing and physical deformation.

Vesiculated ash layers vary in thickness from laminae to beds approximately 10 cm thick and can pinch out or be laterally extensive. In the latter case, they are frequently continuous into the gullies where they commonly thicken. Upper contacts are commonly disrupted by rill incision while the lower contacts are planar and conformable with underlying beds (Figure 18).

Incision of both rills and gullies always originates at the upper bedding planes of (in-situ or remobilized) vesiculated tuff units (Figure 18). Vesiculated tuff layers are common within the sequences of mantling and infilling PDC and fallout deposits from the Hanauma Bay craters. Rill and gully structures therefore originate at many stratigraphic levels. The association of rills

and gullies with this facies suggests a direct relationship between the emplacement of the vesiculated tuffs and rill incision (section 6.7.2.).

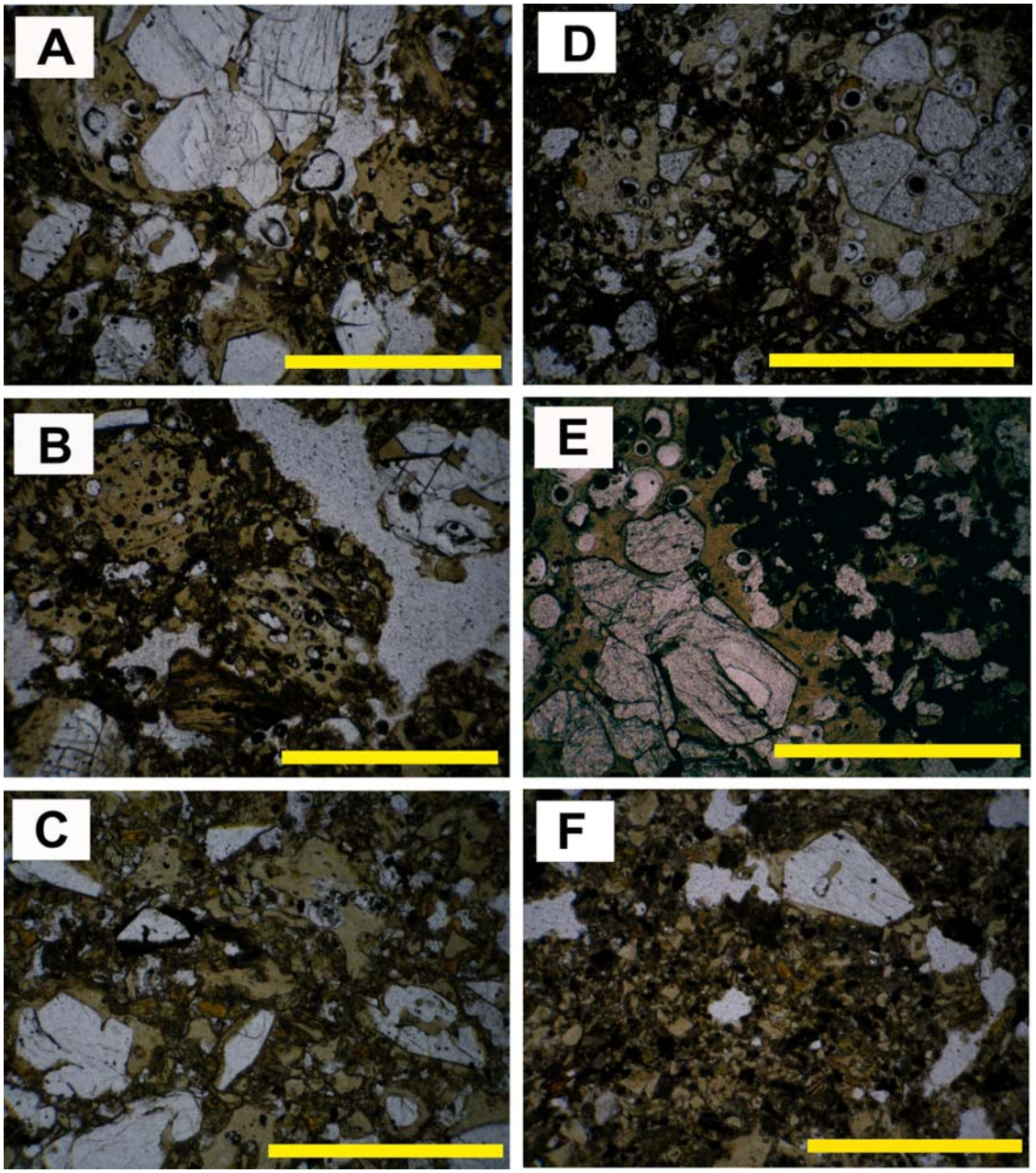

Figure 29. Photomicrographs of Af_v lithofacies, Lm_v lithofacies, and primary Koko Crater tephra.

Yellow bars are all 1 mm in length. (A) and (B) Debris flow deposits (Lm_v facies) from gully 25; (C) Debris flow deposit (Lm_v facies) from gully 23; (D) and (E) Primary (extra-gully) Koko Crater tephra from locations 1 and 22, respectively; (F) In-situ vesiculated tuff (Af_v facies) from gully 5. All share the same bulk composition. Glass fragments in (F) are fine and mostly non-vesicular; (D) and (E) do not contain coral fragments. Analysis of these samples indicates that debris flow deposits are combinations of primary Koko Crater tephra and in-situ vesiculated tuffs.

6.6. Lm_v facies and incision

Thick, massive, poorly sorted vesiculated deposits are observed both inside and outside the margins of many gullies, particularly the largest ones. These deposits occur (1) as a thick (up to 0.5 m) basal unit intervening between the outlying tephra and the gully interior or (2) intercalated with stratified gully fill (Figures 27, 28, 30). Upper and lower contacts are sharp and usually conformable. Upper contacts are occasionally eroded by small gullies less than 30 cm wide and deep (Figure 28).

Vesicles in these deposits vary in both shape and size. Some are spherical and less than 1 mm in diameter; others are deformed and greater than 1 cm in length. The largest vesicles are elongated and similarly orientated, particularly when they flatten at the bases of individual units. Vesicles also flatten (and curve) around some large blocks present in the matrix (Figure 31A). Rip-up clasts of bedded lapilli tuff (with internal stratification still preserved) are also commonly observed in the matrix (Figure 31B).

Componentry resemblances between these deposits and the vesiculated tuffs (Af_v facies) are apparent. Light brown vesicular glass dominates the composition of the Lm_v matrix, with euhedral to subhedral broken augite (and olivine?) crystals comprising the vast majority of phenocrysts. Coral reef and crystalline basalt fragments are also occasionally present. In contrast with the vesiculated tuffs, however, individual grains in the Lm_v facies are much larger, with some glass and crystal fragments reaching over 0.5 mm in size. Glass fragments are angular, conspicuously fractured, and generally comprise a much greater percentage of the matrix (Figure 29).

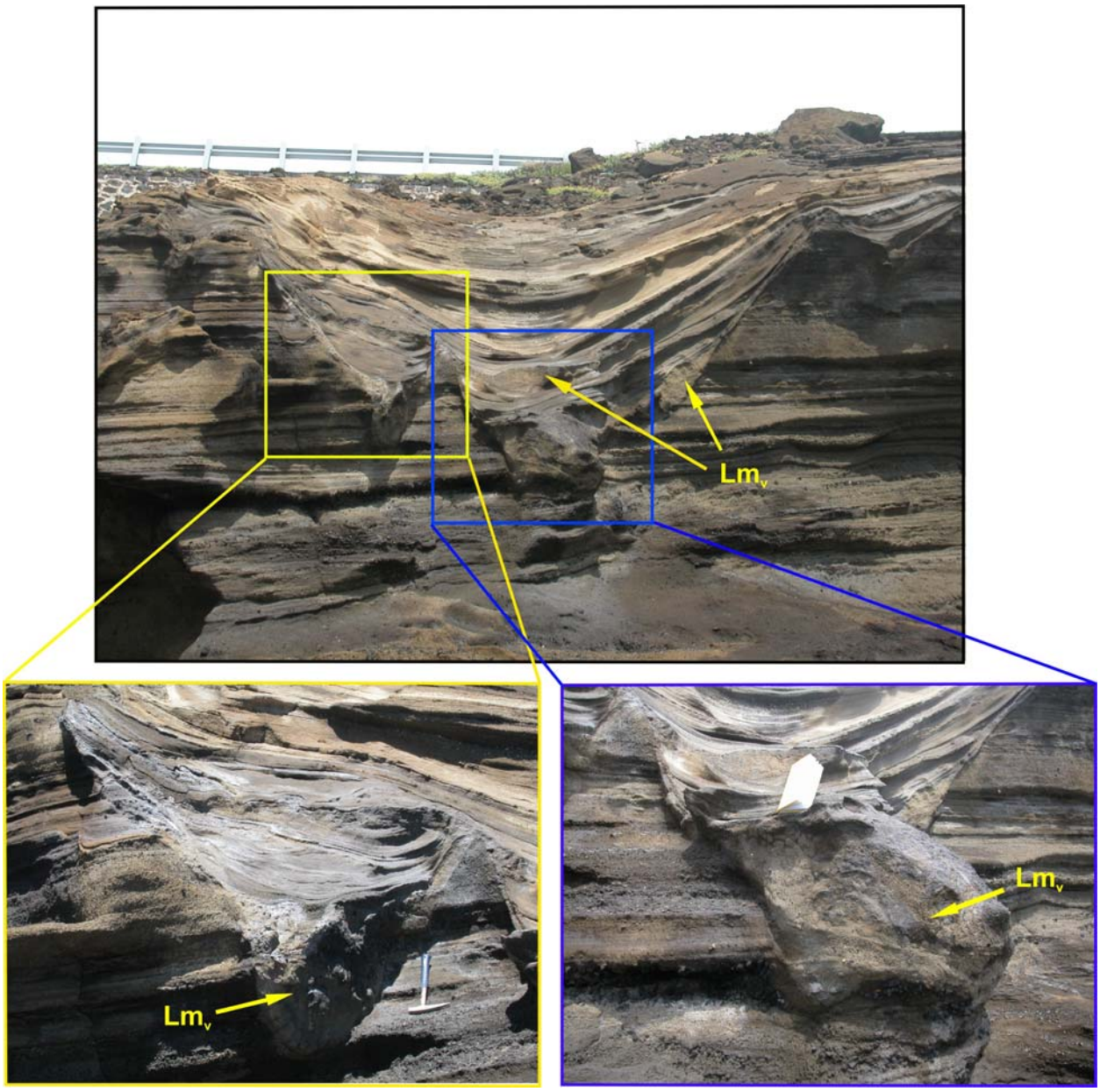

Figure 30. Lm$_v$ deposits of variable thickness comprising the basal unit of gully 23.

Additional Lm$_v$ units are intercalated within the other gully fill material. Maximum gully width is approximately 5 m.

6.7. Interpretation of gully-fill facies

6.7.1. Lf_b lithofacies

The internal stratification, accretionary lapilli, and (rare) bedforms present in the Lf_b facies, in addition to petrologic similarities with outlying tephra, indicate that this lithofacies originates from deposition by pyroclastic surges (low-concentration PDCs) and co-deposited fallout. Low-angle cross-bedding and low-amplitude waveforms are rare but, together with the sharp truncation of beds against the northeastern margins of the gullies, indicate a PDC flow direction from the south-east, i.e. perpendicular to the longitudinal axes of the gullies).

6.7.2. Af_v and Lm_v lithofacies

The presence of vesicles in the Af_v lithofacies and the fact that Af_v layers are common within the sequences of mantling and infilling PDC and fallout deposits from the Hanauma Bay craters suggests that the Af_v facies represents vesiculated tuff emplaced by rapid deposition from pyroclastic surges (Lorenz, 1974).

The Lm_v deposits are interpreted as debris flow deposits. This interpretation is based on (1) the poorly sorted nature of the material, (2) pronounced variations in deposit thickness, (3) massive nature, (4) the presence of flat, elongated vesicles at the bases of individual units (a consequence of shearing) and curved, flattened vesicles around some large blocks within the matrix, both of which indicate deposition by flow (Figure 31A), (5) the presence of stratified rip-up clasts that have obviously been derived from underlying beds of lapilli tuff (Figure 31B), and (6) the presence of intraclasts that lack surrounding sag features, indicating they were

incorporated prior to or during flow and also demonstrate the internal strength of the material (Figure 31C).

6.7.3. Lf_m and Lc_m lithofacies

The compositional similarities between the Lf_m and Lf_b lithofacies suggest that the Lf_m facies is the reworked (slumped) equivalent of PDC deposits. Because Lf_m deposits only occur in one gully (gully 19) that is stratigraphically higher than almost all the rest and is not covered by subsequent successions of PDC deposits, it is concluded that this facies originated during emplacement of the last pulses of pyroclastic surges from Hanauma Bay.

The presence of armored lapilli in the Lc_m lithofacies is indicative of primary Koko Crater tephra as armored lapilli is absent in the Hanauma Bay surge and fallout ash deposits. The lack of bedding, grading, or sorting further suggests that this material has been reworked as a debris flow deposit. It is concluded that the Lc_m facies is primary Koko Crater tephra that, like the Lf_m facies, slumped down the flank of Koko Crater.

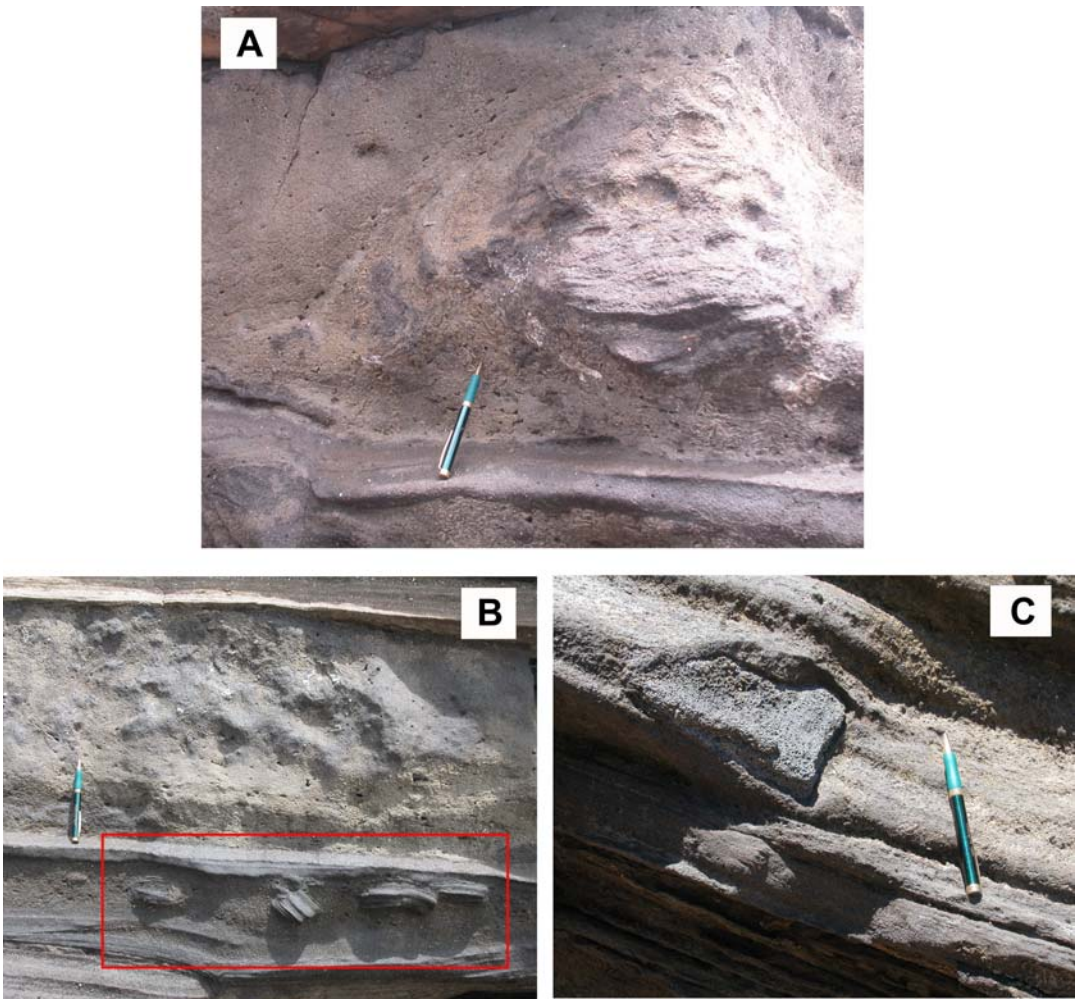

Figure 31. Characteristics of the Lm_v lithofacies

The Lm_v facies is interpreted as deposits of syn-eruptive ("hot") debris flows. This is based on several characteristics, including (A) flat, curved vesicles around obstacles, indicating flowage; (B) rip-up clasts derived from the underlying bed of stratified tephra; (C) the absence of bedding sags and deformed vesicles around blocky intraclasts. This block was incorporated prior to (or during) displacement and illustrates the internal strength of the debris flow.

6.8. Discussion and interpretation of rills and gullies at SE Koko Crater

The gullies described above have been previously interpreted as "surge-eroded" by Fisher (1977). In this earlier model of formation, surge currents initially flow northeasterly from crater(s) at Hanauma Bay, up the steep sides of Koko Crater and laterally across its lower flanks. Pre-existing drainage paths eventually cause (1) the current direction to shift to southeasterly

(downslope and parallel to present longitudinal gully axes) and (2) surges to concentrate into the topographic depressions, thus enhancing their erosional effects. Pyroclastic density current deposits (surge deposits) and associated fallout does provide the bulk of gully fill material, but field observations in this study indicate that they did not give rise to incision. Evidence of substrate erosion, such as entrained rip-up clasts or truncation of underlying bedding/lamination are absent in the PDC deposits, unlike in other facies such as Lm_v (Figures 30 and 31B). Internal bedforms (low-angle cross-beds and waves in particular) indicate that the dominant direction of current flow was northeasterly (perpendicular to long gully axes).

Surface flow, piping, and mass movement are the primary mechanisms by which rill and gully networks are generated on steep hillslopes (Knighton, 1998). Field observations suggest that all three processes were active at Koko Crater and collectively created the rill and gully networks. However, there are a number of factors specific to wet phreatomagmatic eruptions and their deposits that strongly influenced rill and gully development at SE Koko Crater.

6.8.1. Factors affecting rill and gully incision at SE Koko Crater

The lower southeastern flanks of Koko Crater are constructed from sequences of primary and reworked phreatomagmatic fall and surge deposits. Being fine-grained, cohesive, and emplaced on an active volcanic slope, the tephra inherently had many characteristics that promote the formation of rill and gully networks in the absence of erosion by pyroclastic or mass flows. These include low infiltration capacities, a tendency towards desiccation cracking and piping, association with erupted water and steam, the presence of surface irregularities such as blocks and bomb sags, and the lack of a stabilizing vegetative cover.

The degree of vegetation on a slope has considerable effects on the stability and, ultimately, erodibility of the constituent slope material. A healthy, extensive vegetative cover decreases the likelihood of water erosion because vegetation diverts direct raindrop impact (preventing soil or sediment dislodgement), decreases runoff velocity, increases material strength and porosity, promotes soil compaction, and keeps the uppermost layers dry through processes of transpiration (Selby, 1993). At Koko Crater, a protective vegetative cover was clearly absent at the time of extensive tephra emplacement, thus increasing the susceptibility of the tephra to erosion by surface runoff.

The initiation of rill and gully networks on any hillslope is largely a function of the hydraulic properties of the slope material, particularly infiltration capacity. Where infiltration capacities are low, the vertical seepage of water into the subsurface is minimal (or prohibited) and impacting water is transported along the surface as overland flow. Fine-grained (ash-sized) pyroclastic deposits that display high levels of cohesion characteristically have low infiltration capacities. Decreased infiltration is accompanied by increases in both the volume of water transported as surface flow (as opposed to throughflow) and the flow velocity. At higher velocities, the ability of surface flow to incise and entrain sediment increases as well.

Overland flow can be erosive without forming rills or gullies if the flow is thin and relatively uniform. The concentration of surface flow creates variations in flow thickness, which may cause depressions to be eroded at a much higher rate (Carson and Kirkby, 1972). Micro-topography and macro-scale surface roughness play crucial roles in channel initiation by influencing the formation and subsequent convergence of flowlines from unconcentrated surface flow. Desiccation cracks, blocks (outsized clasts), and bomb sags are all prevalent types of

surface irregularities in a phreatomagmatic environment that increase roughness and therefore encourage the concentration of runoff.

Desiccation cracks have been observed on some exposed tuff surfaces at Koko Crater (Figure 32). Given the fine-grained, cohesive nature of the material (especially the wet vesiculated ash), desiccation cracking was presumably a common occurrence. In addition to creating topographic depressions into which surface flow concentrates, desiccation cracks also provide access to the subsurface and therefore promote pipe development (discussed below). Bomb sags are also observed in the PDC deposits and likewise provide depressions and, therefore, potential sites of surface flow concentration.

Piping may have also been a common and active process at Koko Crater. Figure 33 illustrates a bulbous-shaped structure in a bed of vesiculated ash; it has a circular cross-section unlike any of the aforementioned rills or gullies and is interpreted as a remnant pipe structure. The occurrence of this feature in a vesiculated tuff bed is not surprising because pipes will only form when subsurface material is weak enough to be eroded by (usually) low-velocity flows but strong enough to support walls and a roof surrounding the central void of the drainage path. The cohesive nature of the vesiculated ash makes it naturally conducive to pipe formation for two reasons: (1) Wet, sticky ash is sufficiently competent to support a hollowed pipe structure. The cohesive strength of the vesiculated ash is reflected in the steepness of the rill and gully margins. Following the 1980 eruption of Mount St. Helens, Collins and Dunne (1986) reported near-vertical rill margins in silty (ash and fine-lapilli) tephra and convex, gently-sloping margins in sandy (lapilli) tephra. (2) Cohesion makes the fine-grained tephra prone to desiccation cracking. Pipes are commonly found in conjunction with desiccation cracks because such tensional

fractures provide easy access to the subsurface. Once surface water infiltrates a crack, lateral seepage erosion can commence.

Steep walls and U-shaped cross-sectional profiles are morphologically characteristic of gullies in general. Some gullies, particularly those in arid regions and semi-arid badlands, are thought to form exclusively from pipe development and subsequent roof collapse (Selby, 1993). The likelihood of piping at Koko Crater, combined with consistently steep gully margins and U-profiles, suggests that gully morphology is probably (at least in some instances) a consequence of this process. It is important to note that piping is an erosive mechanism that exploits the subsurface, thereby initiating gully formation without the precursory effects of surface flow and rilling. While most Koko Crater gullies appear to be modified enlargements of rills, the evidence for piping implies that some may have formed independent of earlier rills.

Figure 32. Desiccation cracks on an exposed tuff surface at SE Koko Crater
Such cracks promote piping and the concentration of surface flow, both of which encourage rill initiation.

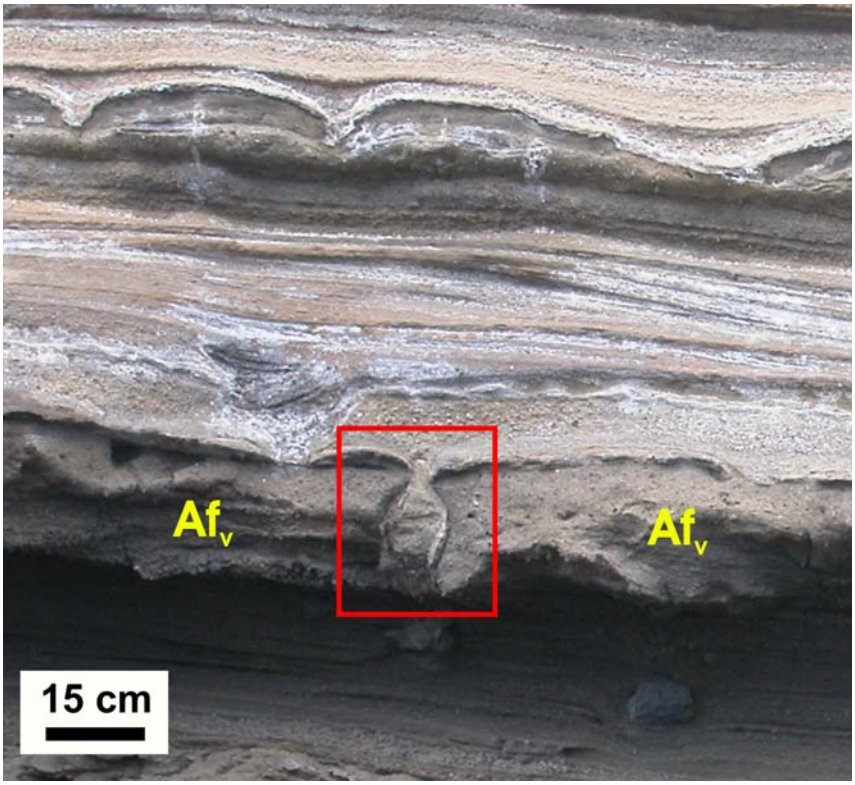

Figure 33. Pipe structure in a bed of vesiculated ash at SE Koko Crater
This structure is located between gullies 7 and 8.

6.8.2. Development and evolution of rill networks at SE Koko Crater

As discussed above there is a correlation between the emplacement of vesiculated tuffs and initial rill (and subsequent gully) incision, demonstrated by the fact that rill incision always occurs on the upper surface of vesiculated tuff beds. Vesiculated tuffs typically form from the rapid deposition of hot, wet ash (Lorenz, 1974; Rosi, 1992) by fallout or pyroclastic density currents. The correlation of rills with vesiculated ash and the lack of obvious water-escape structures imply that erosive runoff was mostly derived from the release and condensation of associated steam-rich plumes. Both steam and any rain-fed incision were enhanced in these very fine-grained cohesive deposits as a result of lowered infiltration rates.

The amount of time necessary for rills to be established on the vesiculated ash deposits has not been constrained as it is complicated by quantitatively unknown factors, but could have been of the order of a few minutes to days. All rills that have not undergone erosional enlargement into gullies are infilled solely with subsequent PDC and fallout deposits. Preservation of the rill structures indicates that the deposition of this material occurred shortly after incision because rills are inherently transient features that are obliterated with time due to continued erosion of the surface. The formation of desiccation cracks would have greatly augmented the probability of rill erosion by providing depressions into which condensing steam could concentrate. Desiccation cracks would only form if the depositional time lapse was sufficient to allow the uppermost few millimeters of ash to begin to dry out. The presence of desiccation cracks is not a prerequisite for rill incision, however, as condensing steam would concentrate in response to inherent surface roughness. Thus the amount of time required for rills to be destroyed or desiccation cracks to appear is unknown; the amount of time in which initial rill networks developed is also largely unknown but presumed to be brief, culminating prior to deposition of the next overlying bed of PDC deposits.

The occurrence of multiple closely-spaced rills of similar size and cross-sectional form in the same stratigraphic horizon is an indication of concurrent formation. Furthermore, the sinuosity and downslope convergence of rill structures (as observed in plan view in Figure 34) is suggestive of dendritic network development, wherein the convergence and bifurcation of rills eventually creates a drainage system characterized by relatively few master rills fed by numerous tributaries.

If rills were initially arranged in a dendritic network pattern, and most gullies developed from the enlargement of rills, then similar networking patterns should be observed among the

gullies. Some gullies do exhibit sinuosity and bifurcation. Figure 34 shows an example of such behavior in two neighboring gullies longitudinally exposed on the wave-cut terrace adjacent to the shoreline. In the absence of such direct observation, sinuous behavior is also indicated by variations in axial trend within a single gully between the cliff component and the shore component (i.e. the downslope direction); gully 17 is one such example (Table 1). Similar patterns have been observed in vesiculated tuffs at Surtsey, Iceland and are interpreted by Lorenz (1974) as "mudflow channels" that develop on slopes greater than 20 degrees by erosion from water-rich Surtseyan jets (Figure 42). Direct erosion from water-rich jets is not considered likely in the Koko examples due to the distance between Koko Crater and the source vents at Hanauma Bay.

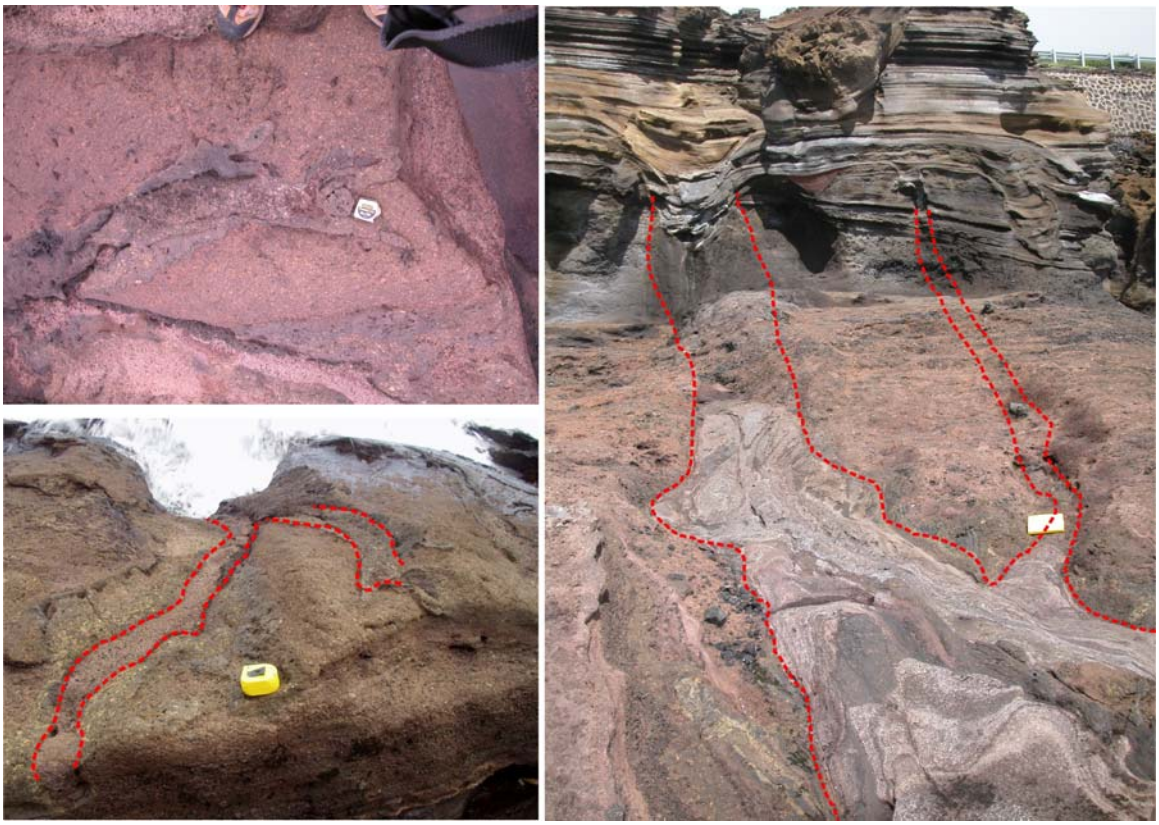

Figure 34. Sinuous, bifurcating behavior of rills (left) and gullies (right) on the foreshore platform at SE Koko Crater

Such behavior is reflective of typical water-eroded drainage network development.

6.8.3. Debris flows and gully incision at SE Koko Crater

In a phreatomagmatic environment, debris flows can be "syn-eruptively" generated by (1) the failure of wet fine-grained tephra deposited on steep slopes (Leat and Thompson, 1988; Sohn and Chough, 1992), (2) the expulsion of a vent-filling slurry of tephra and water (Kokelaar, 1986; Leat and Thompson, 1988) and (3) the collapse of water-laden tephra jets (Mueller et al., 2000; Leat and Thompson, 1988). At Koko Crater, the debris flow deposits are vesiculated and petrographically similar to vesiculated tuffs; both are dominantly composed of basaltic glass and microphenocrysts of augite, with very minor olivine crystals and coral fragments. Tuff vesicles imply "hot, wet" conditions in the host material. Failure of the vesiculated ash deposits shortly after deposition accounts for the compositional similarities and the vesiculated nature of the debris flow deposits (reflecting the entrapment of steam). It is therefore concluded that the debris flows are the syn-eruptive, remobilized counterparts of the vesiculated tuffs.

In contrast with in-situ vesiculated tuffs, glass in the debris flow deposits is largely vesicular and grain sizes are much larger. Dimensions of glass clasts and glass vesicularity are actually similar to those of the vitriclasts in the primary Koko Crater tephra (which likewise shares the same overall lithology, with the exception of coral fragments). These observations suggest that the debris flows were initially derived from the failure of vesiculated tuffs, but some flows subsequently incorporated Koko Crater tephra as erosion proceeded into the underlying units of crudely stratified airfall deposits. Gullies in which debris flows deposits comprise the basal unit, such as gully 23, are obviously incised into these fall deposits (Figures 29 and 30).

Debris flows characteristically follow pre-existing topographic depressions. The occurrence of debris flow deposits as the basal unit of several gullies indicates that the debris flows provided the final episode of (significant) bed modification to previously established

drainage paths. The occurrence of debris flow deposits as intercalated fill material further suggests that present gully morphologies are commonly the end results of many episodes of adjustment as each flow event would have considerably modified an existing incisional structure. It also implies that vesiculated tuffs from Hanauma Bay were repeatedly generated. The ability of the debris flows to cause such pronounced modification is a function of their erosive capabilities, evident in the entrainment of rip-up clasts (Figure 31B) and the incorporation of primary Koko Crater tephra. It is concluded that the debris flows derived from vesiculated tuffs were largely responsible for generating most gullies by exploiting, scouring, and enlarging pre-existing rills incised into vesiculated tuff deposits.

6.8.4. Interpretation of cross-sectional morphology

The variability of cross-sectional morphologies of gullies suggests that, while initial (rill) incision is attributed to the concentration of condensed steam (and possibly enhanced rain-generated runoff), a variety of other mechanisms may be responsible for gully development. The V-shaped, U-shaped, and rectangular profiles depicted in Figure 19 are interpreted here as manifestations of rill enlargement by different erosive processes.

V-shaped gullies at Koko Crater are a consequence of the erosional enlargement of the typical V-shaped rills, with little to no modification. This probably occurred during prolonged exposure to concentrated surface flow, which caused deepening and widening of the original structure but maintained the cross-sectional morphology throughout the enlargement process. V-shaped gullies on non-volcanic hillslopes are sometimes attributed to the same mechanism (Higgins et al., 1990). At Koko Crater, the internal strength of the incised deposits (largely due to cohesion) allowed them to be progressively (and steeply) incised without collapsing.

U-shaped profiles largely resulted from enlargement and modification of the original V-shaped rill either by inward slumping/collapse of channel walls or basal scouring during the passage of debris flows. Wall failure causes a progressive widening of the structure and thus accounts for the high width-to-depth ratios of the largest gullies (which are U-shaped). It also introduces tephra into the channel interior that could subsequently be displaced downslope and further scour the channel bed (e.g. Lf_m and Lc_m lithofacies). Debris flows appear to have shaped the largest U-shaped gullies in particular because these deposits intervene between the outlying tephra and the overlying fill material (e.g. gully 23). U-shaped profiles, particularly those with excessively steep margins, could also be due to the development and subsequent roof collapse of pipe structures.

Rectangular profiles are the least common; only three examples are present in the study area. These are (1) gully 20 (Figure 19), (2) the basal portion of gully 8 (Figure 20), and (3) the youngest secondary channel within the primary margins of gully 14 (Figure 21A). In all cases, relatively flat floors are bordered by very steep, near-vertical walls. The northeastern wall of gully 20 is oversteepened, reaching a maximum slope angle of 105 degrees. The production of these rectangular profiles was likely due to progressive undercutting of the walls by surface flow; if rill floors are gently sloping and runoff is likewise shallow, basal portions of the walls will be eroded and the margins consistently undercut, keeping them steep.

7. Discussion: Erosion by pyroclastic density currents (PDCs)

7.1. Introduction to PDCs

Pyroclastic density currents (PDCs) are heterogeneous mixtures of juvenile pyroclasts, lithics, magmatic gases, and (commonly) external water that are mostly generated during explosive volcanic eruptions (Carey, 1991). PDCs have bulk density values greater than the atmosphere into which they are ejected and consequently flow under the influence of gravity. Pyroclastic flows and pyroclastic surges represent the dense and dilute end members respectively. Many PDC deposits have been found, however, that do not strictly belong in either category (e.g. the 1980 lateral blast deposit at Mount St. Helens, which displays proximal flow characteristics and distal surge characteristics), suggesting that PDCs comprise a class of gravity flows represented by various rheological properties, internal energies, and transport and depositional processes (Carey, 1991; Valentine and Fisher, 1993).

PDCs are produced in several different ways (Figure 35), including partial collapse of a sustained Plinian or hydrovolcanic eruption column, prolonged low pyroclastic fountaining (without the development of a vertical column), direct lateral blasting from a vent in response to decompression of a magmatic or hydrothermal system, and gravitational collapse of an unstable lava dome or lava-flow front (Fisher, 1979; Moore and Sisson, 1981; Rowley et al., 1981; Carey, 1991; Valentine and Fisher, 1993; Calder et al., 2000; Branney and Kokelaar, 2002; Sparks et al., 2002). On average, PDCs flow at tens of meters per second. Initial velocities, however, can reach hundreds of meters per second (Moore and Sisson, 1981; Carey, 1991). The levels of kinetic energy, thermal energy, and momentum that PDCs are generated with often render them

extremely hazardous. The power of a moving current is largely exemplified by the erosive features left behind on the ground surface.

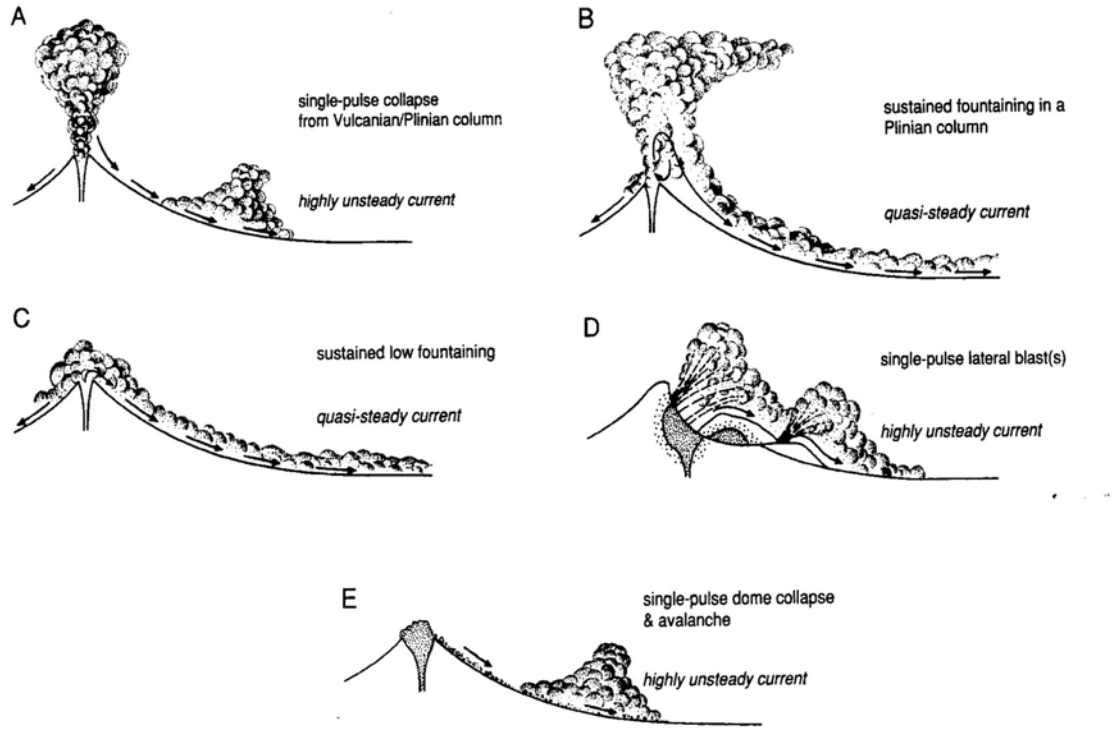

Figure 35. Mechanisms of PDC generation

Mechanisms include (A) short-lived collapse from an eruption column, (B) continuous collapse from a tall, sustained eruption column, (C) low pyroclastic fountaining without vertical eruption column development (i.e. "boil over" eruptions), (D) direct lateral blasting (e.g. in explosive decompression jets), and (E) collapse of an unstable lava dome or lava flow-front (after Branney and Kokelaar, 2002).

7.2. Pyroclastic flows and erosion

Pyroclastic flows are volcanic density currents characterized by high temperatures (up to 1000˚C), high particle concentrations, and (largely) non-turbulent flow behavior. Representing the high-density end member of PDCs, pyroclastic flows are strongly influenced by underlying topography and tend to follow and accumulate in topographic depressions.

Particles in pyroclastic flows are transported by a combination of mechanisms, including particle-particle contact, matrix support, dispersive pressures, buoyancy (especially of low-density pumice clasts), and fluidization (Sparks, 1976; Cas and Wright, 1987; Wilson and Houghton, 2000). Turbulence may or may not contribute. There is evidence that some portions of pyroclastic flows move as relatively dilute currents, and turbulent behavior is promoted when low density dispersions travel at high velocities. If and where present, however, turbulence is not considered a dominant transport mechanism (Wilson and Houghton, 2000; Freundt and Bursik, 1998). Fluidization, in contrast, is believed to play a particularly important role in flow transport (Cas and Wright, 1987). Facilitated by the upward stream of vapors through a bed of cohesionless solids at increasing velocity, fluidization is attained when the drag force exerted across the bed (by the lubricating fluid) equals the buoyant weight of the bed. The inclusion of such fluid thereby enhances flow mobility by providing dynamic support of the grains while reducing friction between the flow and the substrate.

Pyroclastic flows can be divided into a head, body, and tail (Wilson and Walker, 1982). The head is a forerunning region of turbulence, strong vorticity, and intense entrainment of air and/or vegetation (Simpson and Britter, 1979). It commonly displays a cleft-and-lobe structure at the leading edge (especially in high velocity flows), ingesting air primarily through the clefts (Figure 36). The body and tail follow immediately behind the head and are characterized by higher particle concentrations partially transported by fluidization; particle-particle contact, matrix support, and dispersive pressures are more prominent transport mechanisms in these flow components relative to the head region.

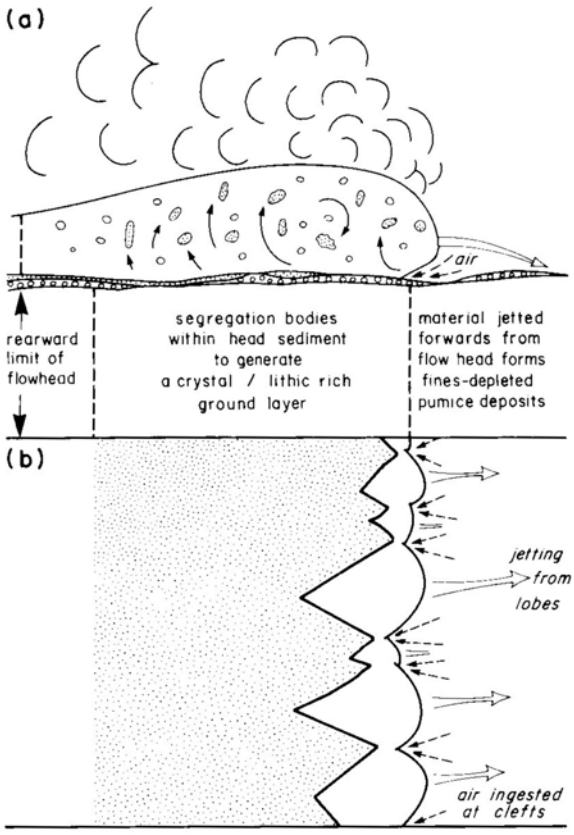

Figure 36. Components of a pyroclastic flow

(A) Cross-section. (B) Plan view. The head is envisaged as a region where particles are dominantly transported by (relatively strong) fluidization and varying degrees of turbulence. It retains a cleft-and-lobe structure at its leading edge, and transport mechanisms are enhanced by the entrainment of air through the clefts. The trailing body and tail are partially mobilized by fluidization; higher particle concentrations encourage other methods of transport such as direct particle contact and dispersive pressures (after Wilson and Walker, 1982).

Sparks and others (1973) present a vertical section through a "standard" pyroclastic flow deposit, or ignimbrite (Figure 37). The flow unit is represented by layer 2. Each unit has a fine-grained basal layer (2a) and a thicker overlying layer (2b). The bulk of the deposit (represented by layer 2b) is poorly sorted. Frequently, it displays normal grading with respect to dense lithic clasts and reverse grading with respect to light pumice clasts. Fluidization is one of the primary mechanisms responsible for this pattern; buoyancy (of pumice clasts in the fluidized matrix) also contributes. This combination of normal and reverse grading is not always diagnostic of

pyroclastic flows as many ignimbrites lack grading altogether while others may show normal grading of both lithics and pumice (Carey, 1991). The concentration of dense lithic clasts in the basal portions of a flow is, however, a common feature and has significant implications for the erosive capabilities of pyroclastic flows because it creates vertical density stratification and a zone of high shear at the base.

Within primary deposits, the presence of this high-shear zone is signified by the common alignment of large clasts parallel to the ground surface and by reverse grading of basal units (layer 2a in Figure 37). Reverse grading is caused by dispersive pressures, wherein particle collisions cause large grains to migrate (upwards) away from the zone of maximum shear (Sparks, 1976; Cas and Wright, 1987). On the ground surface, a variety of erosive features are produced as a consequence of shearing, including the entrainment and removal of erodible material, abrasion of exposed bedrock and boulders (creating smoothed surfaces and striations parallel to flow direction), and the incision of channels or furrows (Rowley et al., 1981; Suzuki-Kamata, 1988; Sparks et al., 1997; Sparks et al., 2002). At Mount St. Helens, Keiffer and Sturtevant (1988) attribute erosional furrows to scouring by longitudinal vortices in the boundary layer of the May 18, 1980 lateral blast. The vortices are established in response to flow instabilities that arise when the flow encounters surface irregularities such as tree stumps and small topographic depressions. Particularly intense shear stresses in the boundary layer are induced by the swirling motion of the vortices, which can bring high-energy fluid (from high velocity zones above the boundary layer) to the ground. Erosion under the vortices consequently appears to have been one order of magnitude larger than what would have been expected in a vortex-free flow of the same (velocity, viscosity, density, and boundary layer thickness) conditions. Some examples of erosion by pyroclastic flows are presented in Figure 38.

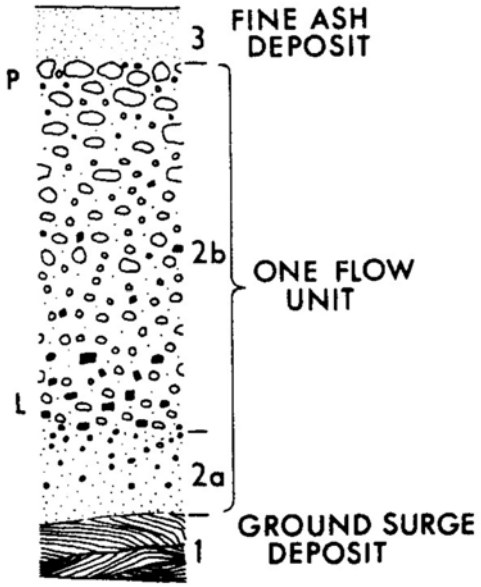

Figure 37. Vertical cross-section through a "standard ignimbrite"

Layer 1 is deposited from the head of the flow (and is absent in most sequences due to poor preservation), layer 2 from the body and tail, and layer 3 from the overriding ash-cloud surge (discussed briefly in the next section). P = pumice clasts, L = lithic clasts (after Sparks et al., 1973)

Erosion by pyroclastic flows therefore occurs largely in the body of the flow as a consequence of shearing (and vortex development in especially powerful flows), but is also possible in the head region as a consequence of fluidization (and variable degrees of turbulence) of more dilute gas-particle mixtures (Cas and Wright, 1987). The entrainment of air and/or vegetation enhances both transport mechanisms because incorporated air (from direct ingestion or combustion of vegetation) is rapidly expanded by high internal flow temperatures.

The erosive capabilities of pyroclastic flows are mainly controlled by the following factors: (1) topography, as erosional features are more commonly produced when currents flow down steep slopes or through constrictions; (2) flow energy; (3) flow thickness, which affects shearing rates; (4) flow composition, especially with regard to the proportions of lithic clasts;

and (5) hardness of the bedrock and availability of loose detritus (i.e. erodibility of the substrate) (Carey, 1991; Sparks et al., 1997; Calder et al., 2000). Bulk density, energy, and volume all increase as flows entrain more lithic clasts. The incorporation of substrate material therefore has significant implications for the scouring capacity of pyroclastic flows as bulking increases erosive potential. Clast durability is also important because clasts that can sustain angularity during transport will serve as more effective erosional tools (Calder et al., 2000).

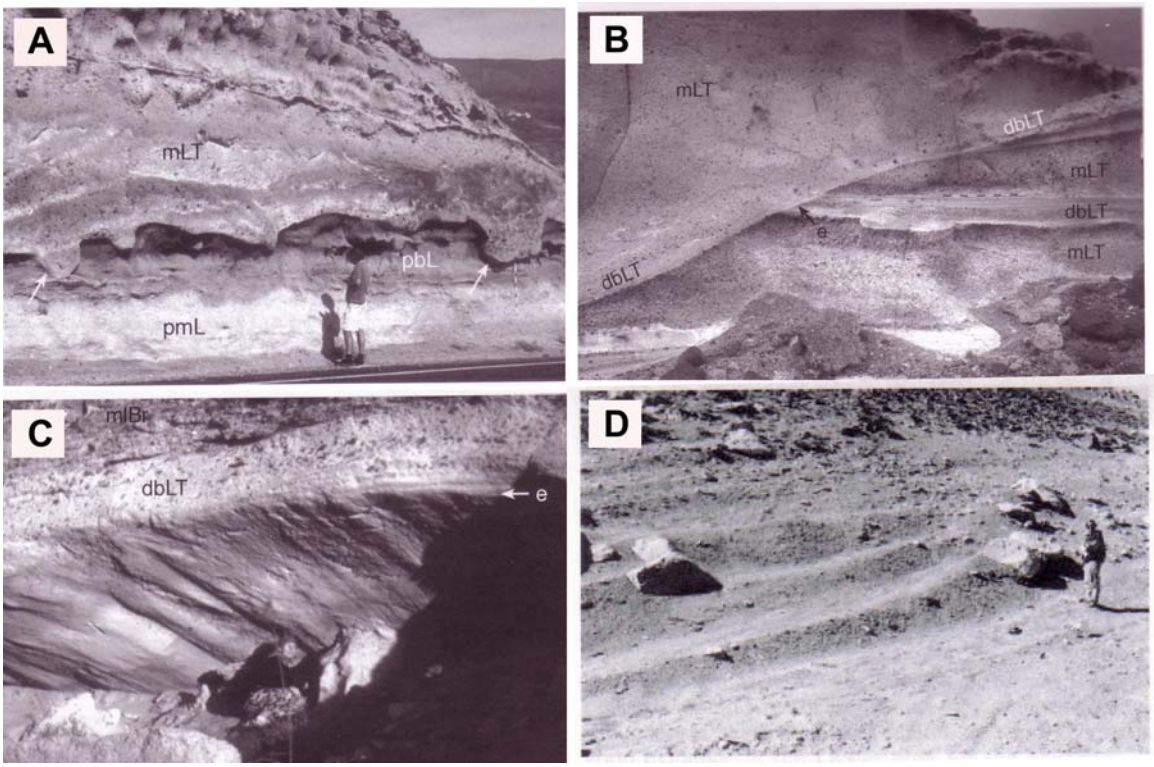

Figure 38. Some erosional features produced by pyroclastic flows.

(A)-(C) from Branney and Kokelaar, 2002; e = erosional surface; mLT = massive lapilli tuff; dbLT = diffuse-bedded lapilli tuff; pmL = pumice lapilli (of Plinian fall origin); mlBr = massive lithic breccia; pbL = parallel-bedded lapilli (Plinian pumice fall). (A) "Gutter casts" at the base of the Arico ignimbrite, SE Tenerife. Inferred current direction is towards the viewer. (B) Truncation of earlier bedded deposits by the emplacement of the Poris ignimbrite at La Caleta, southern Tenerife. Flow direction is from left to right. (C) Casts of erosional furrows, pointing downslope. Current direction is away from the viewer and to the right. (D) Furrows at Lascar Volcano, Chile. Flow direction is from right to left. Erosive capacities of flows were probably enhanced on the lee sides of obstructing blocks (from Sparks et al., 1997).

7.3. Pyroclastic surges and erosion

Pyroclastic surges are relatively low-concentration density currents that, in contrast to pyroclastic flows, largely flow in a turbulent fashion (Moore, 1967; Fisher, 1979). Surges can be two-phase (gas-solid) or three-phase (gas-liquid-solid) dispersions depending on flow temperature; below 100˚C, the system can contain liquid water that is either directly erupted from the vent or derived from steam condensation. Because surges are (initially) fast and highly expanded, they are less topographically constrained than pyroclastic flows. Deposits therefore mantle the pre-existing surface but still tend to thicken in topographic lows. Similar to pyroclastic flows, maximum particle concentrations occur in the basal portions of surge clouds due to segregation and accumulation of large, dense clasts. High lateral shear velocities are consequently developed, which facilitate particle transport by traction and saltation in addition to turbulent suspension of the finer fraction.

Pyroclastic surges can be subdivided into three categories: (1) Base surges are generated from the base of a vertically rising (but partially collapsing) eruption column. They are ground-hugging, turbulent clouds that move outward from the source radially. These have been most commonly associated with hydrovolcanic explosions (Moore, 1967; Waters and Fisher, 1971). (2) Ground surges originate from direct blasts at the vent, partial column collapse, or the ejection of material from the turbulent, fluidized head of a propagating pyroclastic flow (Sparks et al., 1973; Cas and Wright, 1987). Ground surges are associated with pyroclastic flow forming processes but retain the turbulence and low bulk densities characteristic of pyroclastic surges. They precede pyroclastic flows and therefore their deposits are rarely preserved as a result of erosion by the overriding flow (Sparks and Walker, 1973). (3) Ash cloud surges are also directly associated with pyroclastic flows, forming from the convective ash cloud which billows above and behind a pyroclastic flow as fluidization processes elutriate fine ash from the head and body

(Smith, 1960). Only the erosive capabilities of base surges will be discussed here as they are the type of surge emplaced at the Koko Fissure craters.

The transporting medium of base surges is sediment-laden gas traveling at hurricane or greater velocities (Schmincke et al., 1970). Despite relatively low particle concentrations, pyroclastic surges can be powerful and destructive due to high flow velocities and turbulent behavior. Erosive capacities are evident given the presence of (1) broad, shallow scour features either on pre-existing surfaces or at the bases of primary deposit sequences (Wilson and Houghton, 2000; Wohletz, 1998), (2) internal erosional unconformities in bedding sets and bedforms such as dunes, antidunes and chute and pool structures, which suffer stoss-side erosion during progressive construction (Fisher and Waters, 1970; Schmincke et al., 1973; Sigurdsson et al., 1987), and (3) gullies incised into substrate material (Moore, 1967; Fisher, 1977; Leys, 1983). Base surges are also potentially responsible for larger-scale substrate erosion. At Ruapehu Crater Lake, New Zealand, Nairn and others (1979) describe lake margins and pre-existing lava cliffs as being heavily eroded (up to 10 m) by surges generated during an eruption in 1975. Generally, erosion by pyroclastic surges is less effective than by pyroclastic flows due to characteristically lower particle concentrations.

7.3.1. Mechanisms of gully erosion by pyroclastic surges

Different mechanisms have been proposed by which (base) surges erode gullies into the substrate. Wohletz (1988) attributes such erosive capabilities to the establishment of vortices within a turbulent surge current. These vortices spin perpendicular to the flow direction and are created when the surge moves over and/or around topographic obstacles. Constructive meeting

of vortices results in deposition of dunes while destructive meeting (i.e. parting of vortices) causes channel erosion.

An alternative mechanism proposed by Fisher (1977) involves erosion as a function of the physical structure of surge currents and the density contrasts that exist within them due to uneven particle distributions. Photographs of surge-producing eruptions (Waters and Fisher, 1971; Moore, 1967) show surge clouds emanating from their sources in cleft-and-lobe configurations (Figures 11, 39). The lobes are envisaged as separate turbulent cells that join the body of the flow behind the leading front. The concentration of particles is probably greatest in the central, basal portions of each lobe. Gravitationally-induced segregation of light and dense particles during transport and deflation will cause an accumulation of clasts at the bottom of the surge current. Clasts will then migrate towards the central lobe axis where boundary effects are minimized and velocity is greatest. This concentration of particles, coupled with high velocities of the advancing front, facilitates erosion by imparting high shear stresses on the substrate. Gullies incised in this manner are U-shaped because they reflect the lobate morphology of these leading turbulent cells. Widths of the lobes are likely much larger than the resulting incisional structures. It is therefore probable that only the central regions of lobes (where particle concentrations are highest) are erosive.

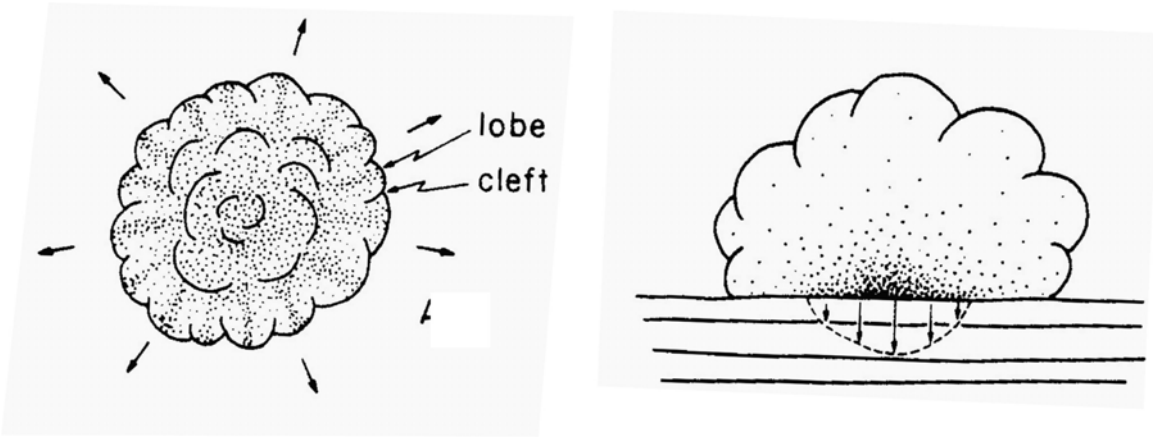

Figure 39. Schematic diagram of a propagating base surge current

(Left) Cleft-and-lobe morphology of the leading edge of a base surge current. (Right) Cross-sectional view through an individual lobe. Particle concentrations reach a maximum in the central, basal region, facilitating erosion of the substrate by the passing current (after Fisher, 1977).

7.4. Origin of the SE Koko Crater gullies

7.4.1. Model by Fisher (1977)

The "U-shaped channels" (gullies) at SE Koko Crater have been largely attributed by Fisher (1977) to erosion by base surge currents. In this model, it is suggested that the gullies formed during the following sequence of events: (1) Small V-shaped fluvial channels develop on the steep outer slopes of the tuff cone; (2) Debris flows, derived from the collapse/slumping of oversteepened walls of the initial "stream channels," slightly modify the pre-existing channels into somewhat more rounded (U-shaped) forms; (3) The subsequent passage of base surges erupted from Hanauma Bay erode and partially or completely reshape the original channels into semi-circular U-shapes. Fisher (1977) suggested that primary gully incision was attributed to the passage of base surges even where mudflow or alluvial deposits do not intervene between the channels and outlying tephra (i.e. in the absence of pre-existing drainage).

According to Fisher (1977), the surge currents responsible for gully development were initially directed towards the northeast upon eruption from the Hanauma Bay craters, sweeping up the steep slopes of Koko Crater and draping deposits across its lower flanks. At higher elevations, the currents became concentrated in pre-existing, southeast-trending drainage paths running down the southeastern face of the cone. Thus the surges experienced a shift in flow direction (from northeast to southeast) in response to this topographic influence and incised channels in the tephra deposited (by the same surges) at the southeastern base of Koko Crater. Erosion is attributed to the cleft-and-lobe geometry of the surge clouds, wherein the highest concentration of particles occurs in the central axial regions of the lobes. The rounded U-profiles of the incised channels consequently reflect this lobate morphology.

7.4.2. Discussion of the Fisher model in light of new research

The erosive capacities of base surges in Fisher's model (1977) are largely contingent upon leading surge cloud morphology as the U-shaped profiles of most gullies are attributed to erosion by frontal lobes. Base surges are known to display cleft-and-lobe morphology as they propagate directly from the base of a phreatomagmatic eruption column (e.g. Waters and Fisher, 1971). According to Fisher (1977), however, the surges responsible for gully erosion at SE Koko Crater did not travel directly from Hanauma Bay to the lowermost flanks of Koko Crater; the surge currents swept up and then down the flanks of the tuff cone (with differing ascending and descending flow directions) before eroding the basal flank deposits. The survival of the cleft-and-lobe morphology, and therefore the ability of the surges to effectively erode the substrate, is therefore theoretical. The new results presented above provide a more concrete explanation of rill and gully formation at SE Koko Crater as they are based on present

stratigraphic relationships and the physical characteristics of rills, gullies, and the deposits of the lowermost flanks.

Among the most significant observations are the initial incision of all rills and gullies into cohesive layers of vesiculated tuff and the common occurrence of vesiculated debris flow deposits as the basal unit in most gullies. These debris flow deposits, wherever present, are clearly erosive into underlying deposits. These observations strongly suggest that running water (specifically condensed steam) and syn-eruptive debris flows are the primary agents responsible for erosion at SE Koko Crater, in contrast to the interpretation proposed by Fisher (1977) that the "U-shaped channels" were excavated by the frontal lobes of base surges advancing down the steep flanks of the cone.

7.5. Examples of rills and gullies on tuff rings and tuff cones attributed to erosion by mechanisms other than pyroclastic surges

Incisional structures with rounded, concave U-profiles occur in both volcanic and non-volcanic environments. On non-volcanic slopes, the characteristic U-shape of many gullies is credited to the collapse of pipe structures or incision by water and/or mass movements (Selby, 1993). In volcanic (particularly hydrovolcanic) environments, the incision of morphologically similar features has been attributed by many authors to erosion by base surge currents (e.g. Moore, 1967; Fisher and Waters, 1970; Fisher, 1977; Leys, 1983; Francis, 1993; Bull and Cas, 2000), though this is not always invoked as the primary formation mechanism (e.g. Lorenz, 1974; Leat and Thompson, 1988, Sohn and Chough, 1992).

Some pertinent examples of incisional structures in hydrovolcanic settings that have been eroded by agents other than pyroclastic base surges are as follows: (1) At the Ilchulbong tuff cone, South Korea, Sohn and Chough (1992) describe U-shaped and V-shaped channels (0.3 to 7

m wide and 0.2 to 1.5 m deep) that occur in series along an erosional surface. Channels are filled with thin-bedded tuff, and a unit of slumped debris commonly exists between the outlying and infilling tuff beds (Figure 40). Incision is interpreted to result from stream flows and sediment slumping during periods of volcanic quiescence. Low-energy pyroclastic surges subsequently filled the channels but did not erode them. (2) Leat and Thompson (1988) describe U-shaped gullies in northwest Colorado, USA, that are about 2-4 m deep and 3-7 m wide with steep margins (30˚ to near vertical) and semi-circular bottoms. These gullies are (partially) filled with deposits of syn-eruptive debris flows that are clearly erosional into underlying beds. Gully formation is credited to erosion by these debris flows. Pyroclastic surge and airfall deposits also constitute a portion of the infilling material. The possibility that the gullies were incised (or modified) by surges has not been ruled out, but this is not the preferred interpretation. (3) Gullies mark a (locally) prominent erosion surface separating the Hatepe and Rotongaio ash units of the *ca.* A.D. 186 eruption sequence at Taupo volcano, North Island, New Zealand (Figure 41). The ashes are interpreted as phreatoplinian fall deposits, and the gullies at the intervening contact are described by Wilson and Walker (1985) as being clearly caused by running water in a brief erosion episode preceding the eruption of the Rotongaio ash. The water may have condensed from vapor in the eruption plume or else was ejected (as liquid) directly from the vent. (4) Lorenz (1974) and Leys (1983) describe meandering "mudflow" channels at the Surtsey and Saefell tuff-rings (respectively), Iceland. The channels at the Surtur I crater (Surtsey volcano) occur on the surfaces of vesiculated tuff beds and were eroded by small debris flows of destabilized tephra (Figure 42). (5) Erosional gullies at Hanauma Bay, Oahu, Hawaii, are associated with angular unconformities in sequences of well-bedded tuffs. According to Moberly and Walker (1987), the discordances are due to syn-eruptive tephra slumping and the

gullies were incised by running water (possibly ejected during explosions). (6) U-shaped erosional bases of high concentration, sub-laminar mass flow deposits are observed by White (1996) at Pahvant Butte, Utah, USA. Incision by these mass flows has affected underlying units of well-bedded ash and lapilli. The deposits are thick and (mostly) structureless, comprising a coarse-ash tephra matrix with rotated blocks of bedded tephra and reverse-grading near the margins.

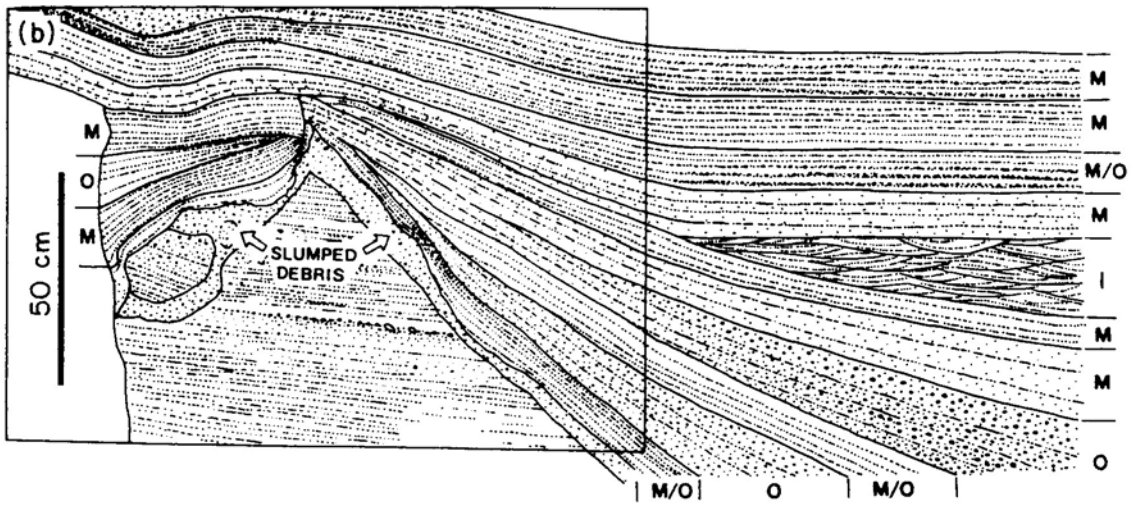

Figure 40. Sketch of the upper portion of a U-shaped channel at the Ilchulbong tuff cone, South Korea.

This structure is filled with thin-bedded tuff and underlain by a unit of "slumped debris." Incision is attributed to stream flows and sediment slumping, with base surges providing only infilling material. M = mantling beds, O = onlapping beds (after Sohn and Chough, 1992).

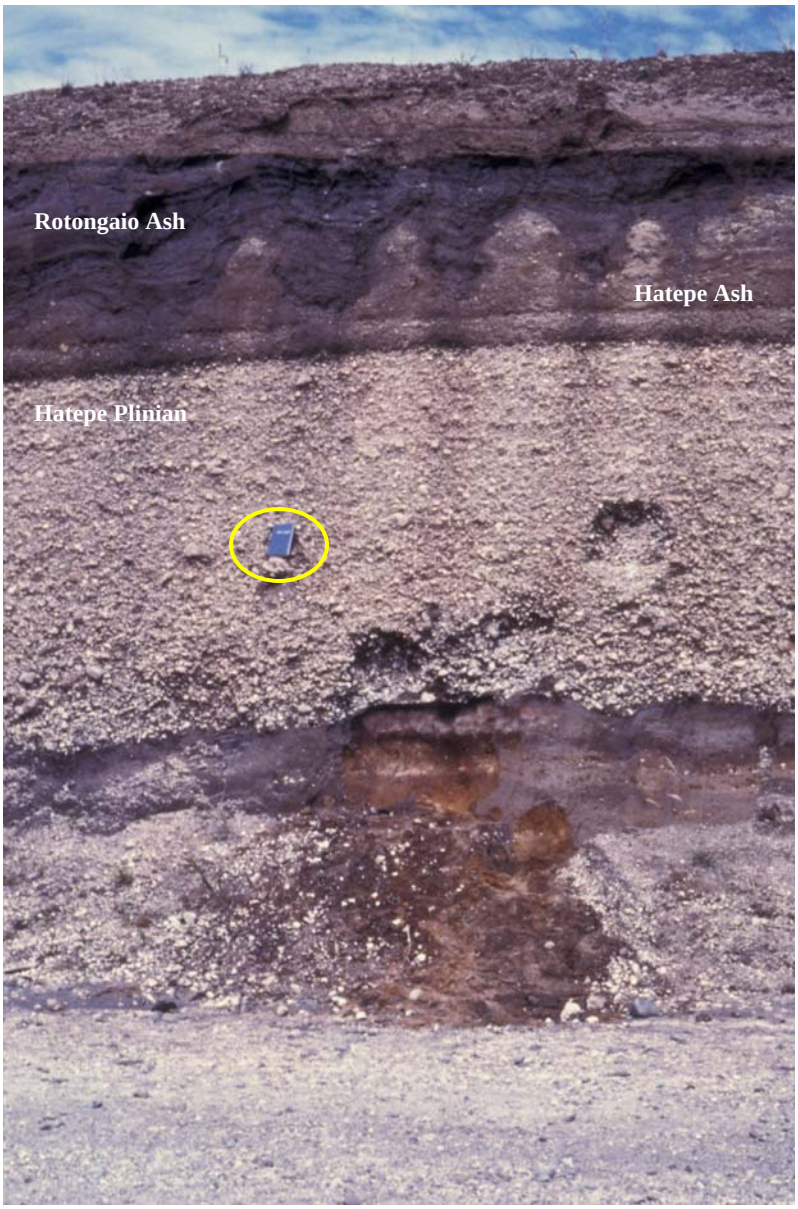

Figure 41. Eruption sequence from the ca. A.D. 186 eruption of Taupo volcano, New Zealand

The Hatepe and Rotongaio ashes are phreatoplinian fall deposits overlying the light-colored Hatepe Plinian deposit in the center of the photograph. The two ash units are separated by a gullied erosional surface. Wilson and Walker (1985) attribute gully erosion to running water that either condensed as rain from a vapor-rich plume or was directly ejected from the vent as liquid. Photograph from Ian Skilling; scale is provided by the encircled notebook in the center.

Figure 42. Bifurcating "mudflow channel" at Surtsey volcano

This channel is incised into a layer of vesiculated tuff by small debris flows of destabilized tephra, Surtsey volcano, Iceland. Flow direction (downslope) is toward the reader. Hammer to the left of the channel provides scale (after Lorenz, 1974)

The ability of pyroclastic surges (particularly base surges) to be powerfully erosive is not disputed here, but surges are clearly not the only erosive agents affecting volcanic slopes. As the literature suggests, running water and debris flows are also effective at eroding the substrate. Additionally, the U-shapes displayed by the incisional structures at Koko Crater should not be considered diagnostic indicators of erosion by surge currents because U-shaped profiles are seemingly characteristic of gullies in many environments, even volcanic settings where surge deposits are completely absent (Walker, 1984).

8. Conclusions

It is concluded that most of the gullies at SE Koko Crater are enlarged rills that were initially incised by condensed steam and/or enhanced rain-fed runoff and enlarged by debris flows generated from slumped vesiculated ash deposits. The rills comprised a network which developed locally into deeper gullies during steam and rain-fed runoff, and also by significant erosion during the emplacement of hot vesiculated debris flows derived from gravitational failure and remobilization of vesiculated ash that incorporated clasts and clots of underlying tephra. The primary erosive agents are therefore considered to be condensed steam and syn-eruptive debris flows rather than base surge currents. More specifically, gullies were generated from rills by combinations of three mechanisms: 1) increased runoff due to lower infiltration in fine-grained cohesive surface layers, 2) progressive failure of rill walls, and 3) scouring of rills, smaller gullies and "planar" surfaces by debris flows. Piping was likely partially responsible for gully formation as well. Pipe erosion exploits the subsurface and can create gullies in the absence of precursory rills.

Rills largely represent immature stages of gully development. The genetic relationship between rills and gullies is illustrated by (1) the association of all incisional structures with only vesiculated facies (in-situ or re-mobilized), (2) the occurrence of both rills and gullies in the same stratigraphic horizon, suggesting that some rills were simply preferentially exploited by subsequent erosive agents, (3) the evidence for bifurcating network development in both rills and gullies, and (4) the presence of basal cross-sections that display combinations of different shapes. This is exemplified in gully 8 (Figure 20). The rectangular basal notch is 10 cm wide, consistent with the average rill size. Although box-shaped rills are rarely observed elsewhere at Koko Crater, Collins and Dunne (1986) reported original rectangular cross-sections in all rills incised

in Mount St. Helens tephra. The preservation of this rill structure is significant because it represents a rare phenomenon; most original rill structures have apparently been completely modified during enlargement. The gullies obviously represent the final products of multiple erosional and depositional episodes. Consistently irregular margins of the gullies at Koko Crater illustrate that the transition from rill to gully was usually accompanied by periodic marginal instability and failure.

Figure 43 depicts a model summarizing the formation of the rill and gully network at SE Koko Crater. Wet fallout and PDC (surge) deposits from Hanauma Bay drape the steep flanks of southeast Koko Crater, and are incised by rills of syn-eruptive condensed steam (and enhanced rain-fed runoff). Coalescence of these ash-bearing rills and slope failure of these deposits generated debris flows of hot (vesiculated) ash. Erosion of the substrate by these flows enlarged the initial rills into gullies, with additional modification provided by periodic marginal failure, continued surface flow, and probably pipe formation. Later phreatomagmatic deposits (fallout and low concentration PDCs) from Hanauma Bay mantled this area and largely filled the gully structures, but did not erode the substrate.

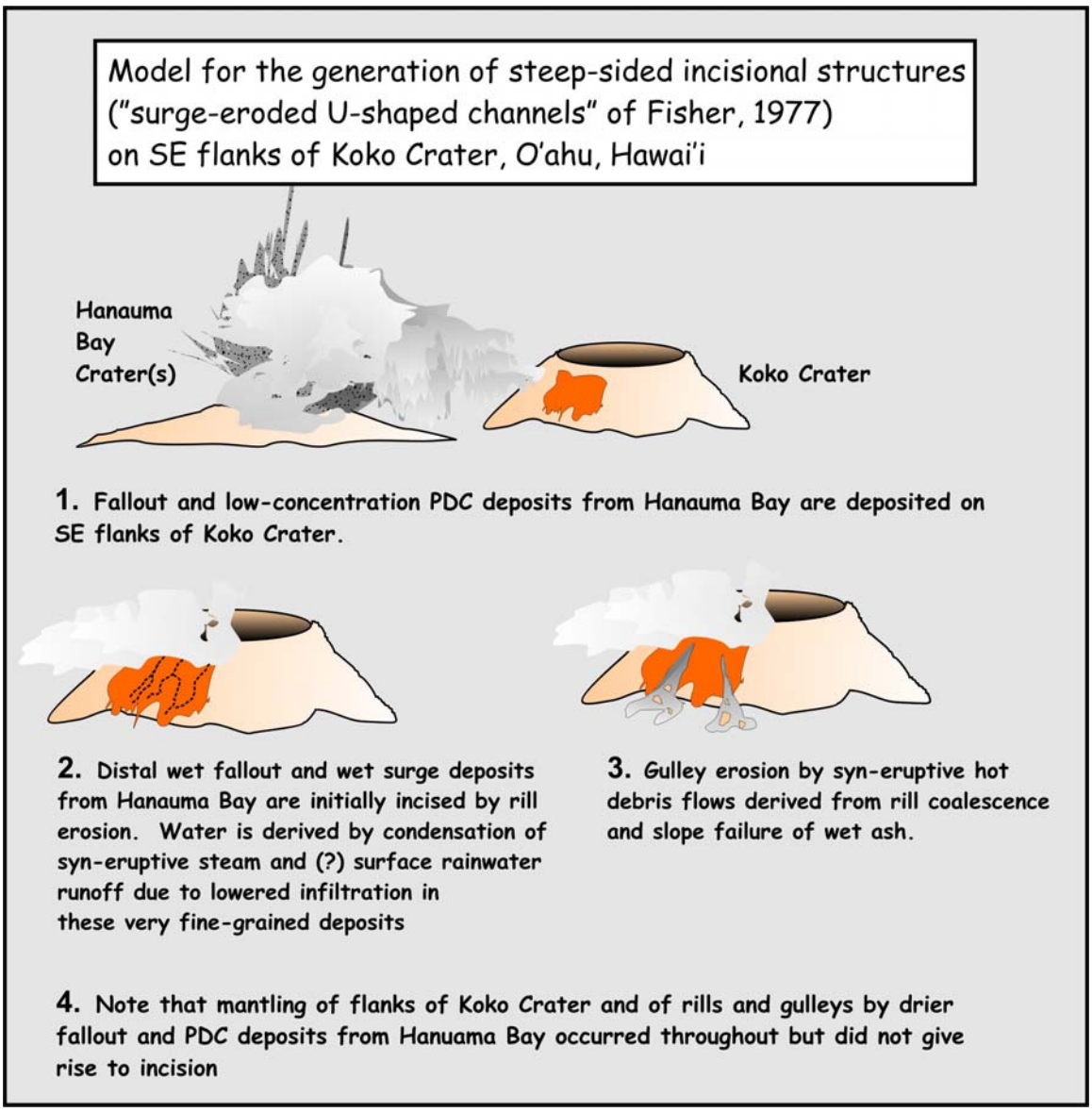

Figure 43. Model summary: Generation of "U-shaped channels" at Koko Crater

APPENDIX A

Photomicrographs of Gully-Fill Facies

Photomicrographs of samples from each gully-fill facies are presented below. Sample numbers are provided beneath each photograph; "KC#" refers to "Koko channel #" and depicts the gully number (see Figure 2) from which each sample is derived. Each photograph was taken in plane polarized light with a low-power (4X magnification) objective lens. The yellow bars superimposed on each photograph are all 1 mm in length.

Detailed descriptions and interpretations of each facies are available in sections 6.4, 6.5, 6.6, and 6.7.

Lm_v lithofacies

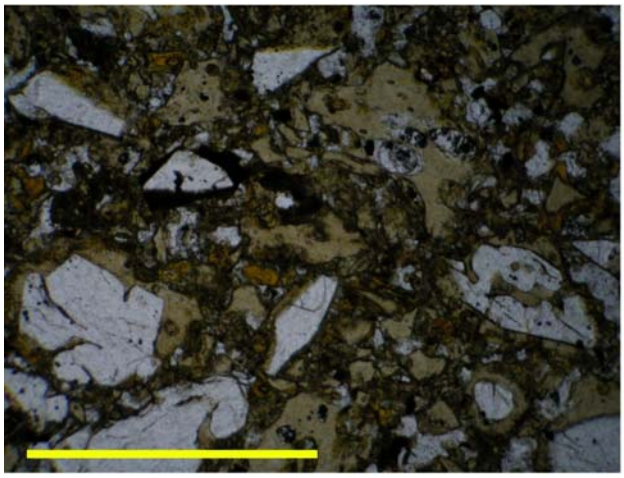

KC23-1

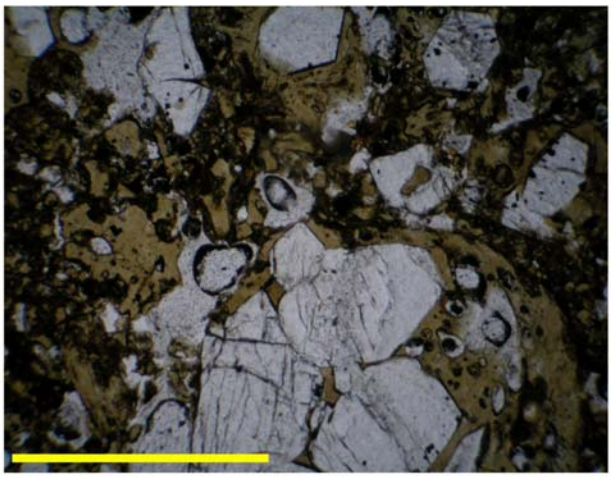

KC25-6A

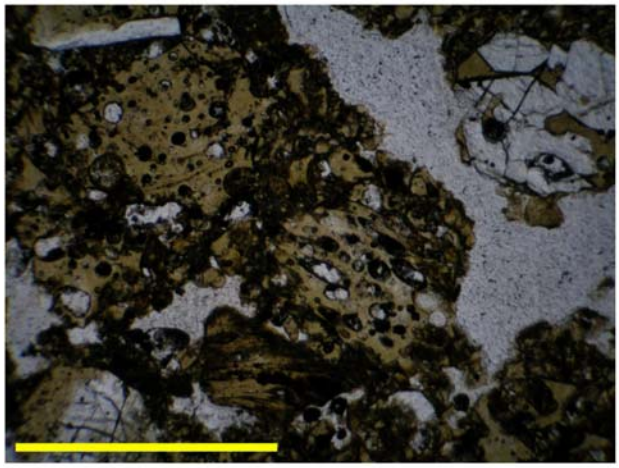

KC25-6B

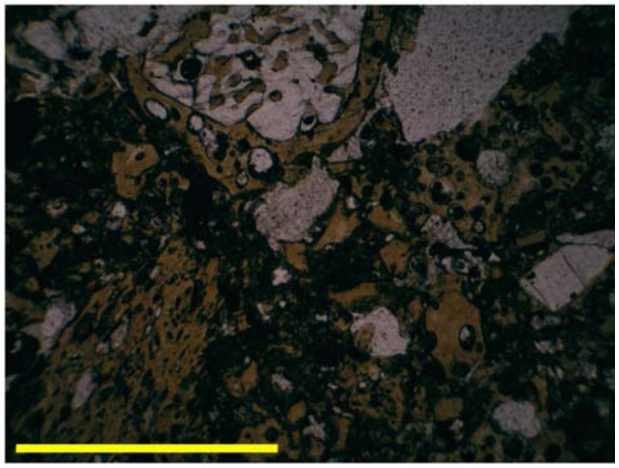

KC25-6C

Lf_b lithofacies

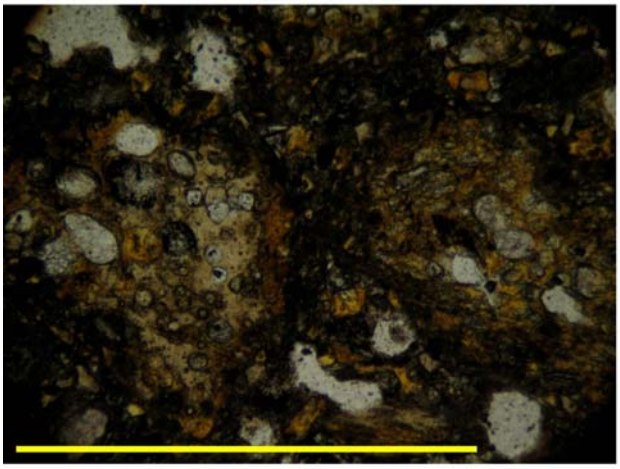

KC1-4A

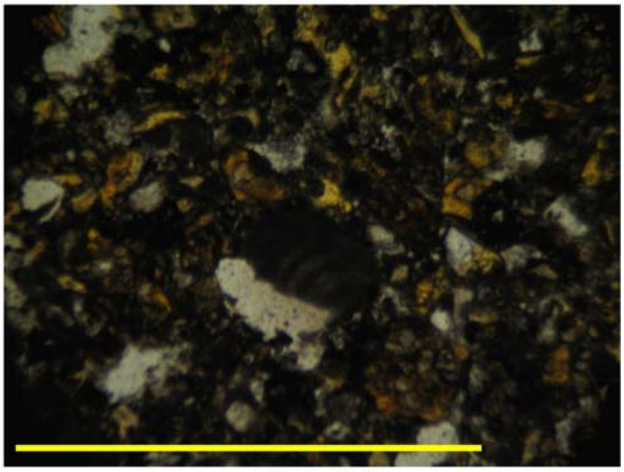

KC1-4B

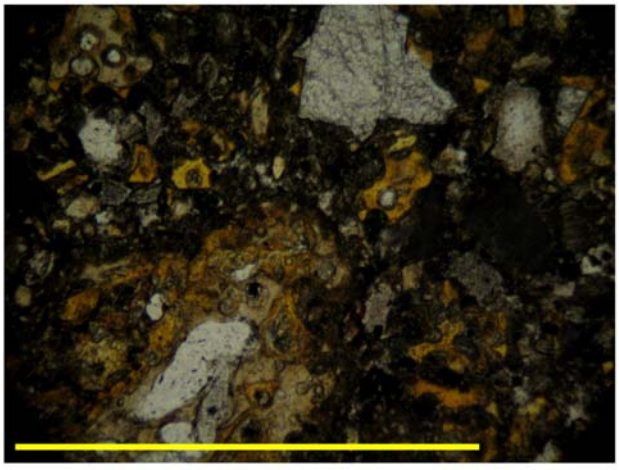

KC1-4C

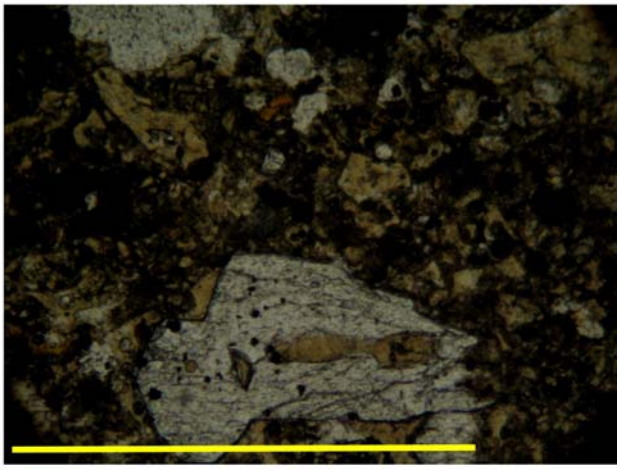

KC7-2A

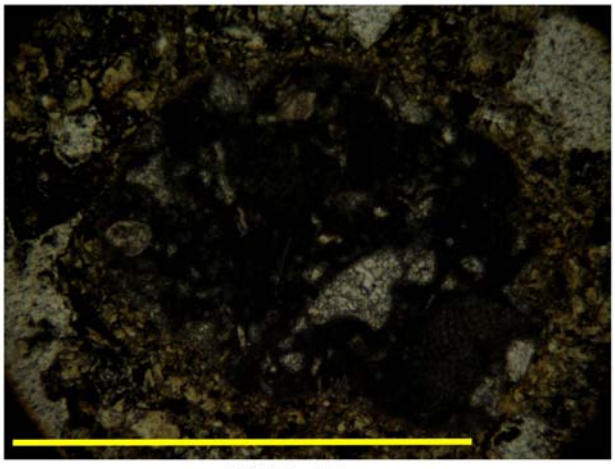

KC7-2B

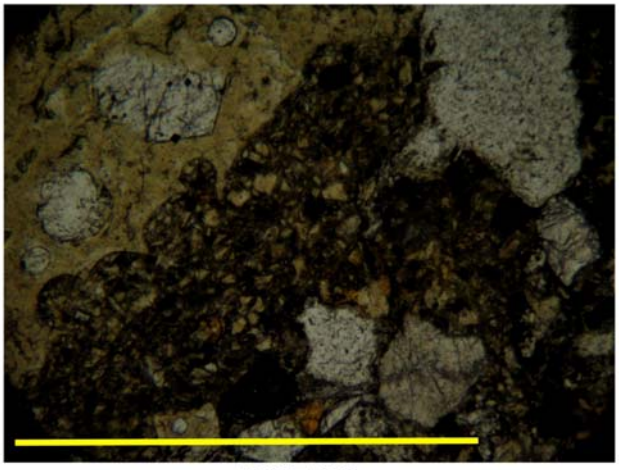

KC7-2C

Lf_b lithofacies

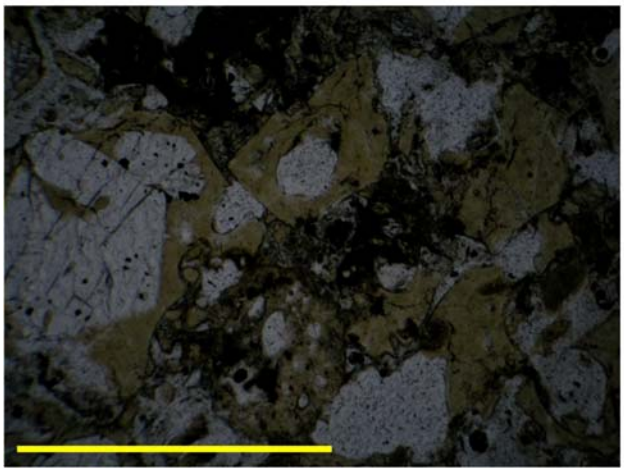

KC5-2A

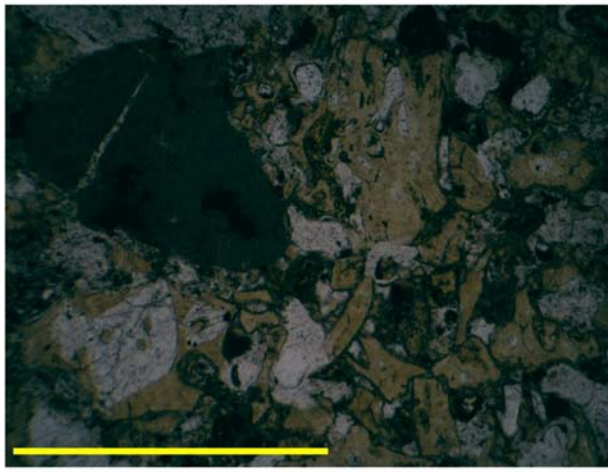

KC5-2B

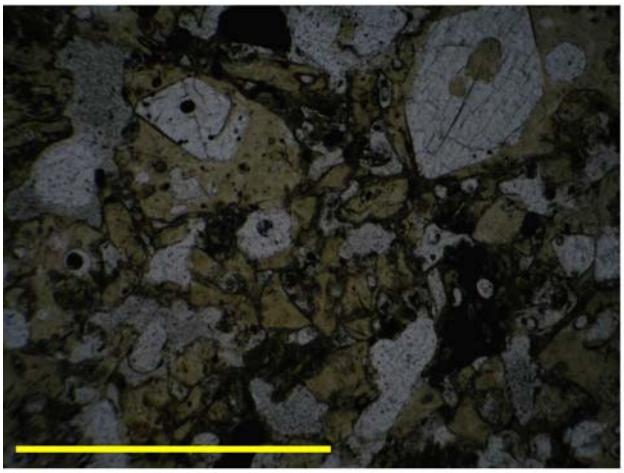

KC5-2C

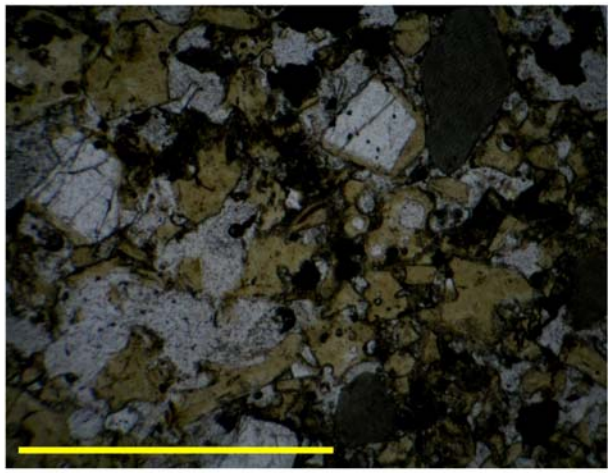

KC5-2D

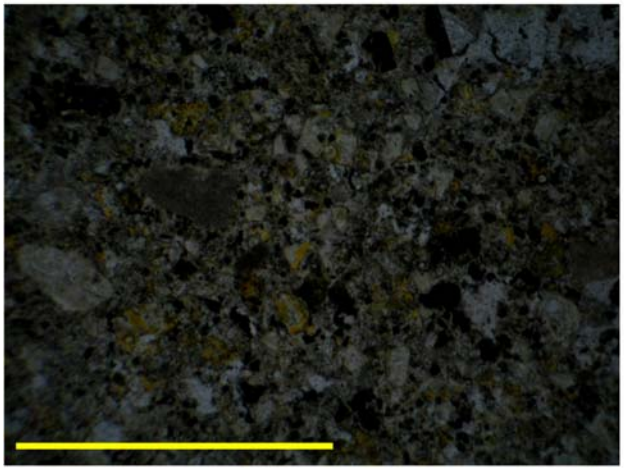

KC15-2A

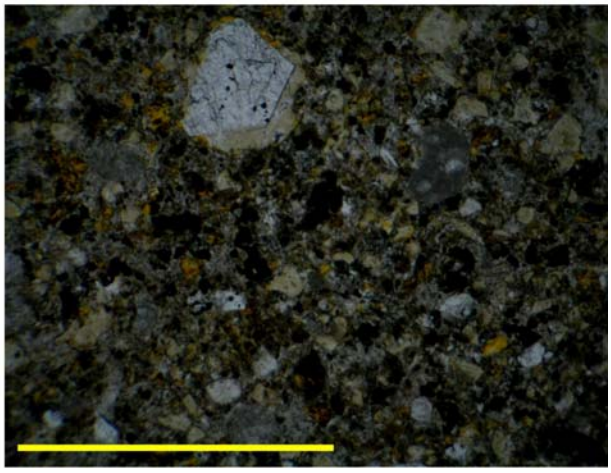

KC15-2B

Lf_b lithofacies

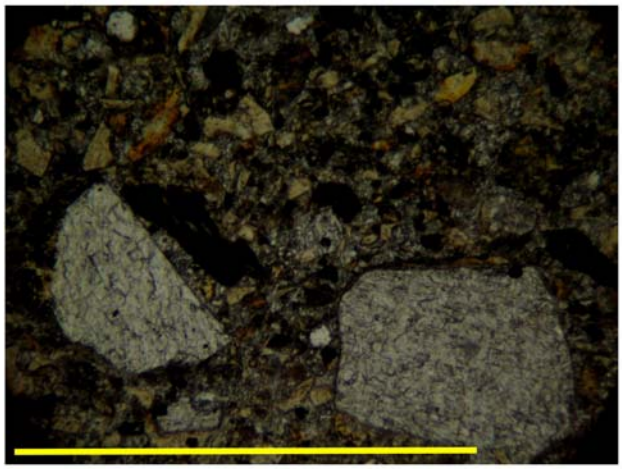

KC12-1A

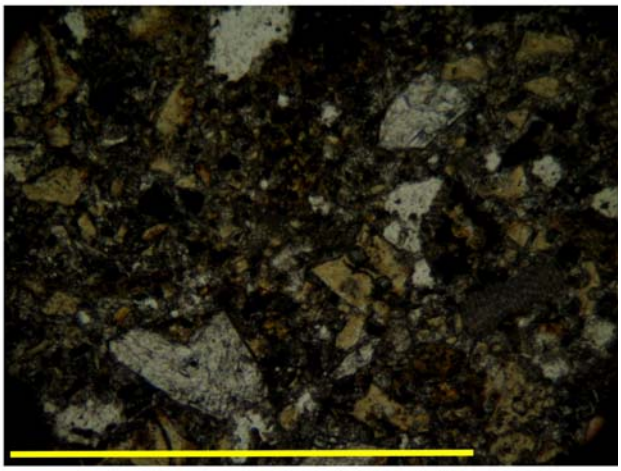

KC12-1B

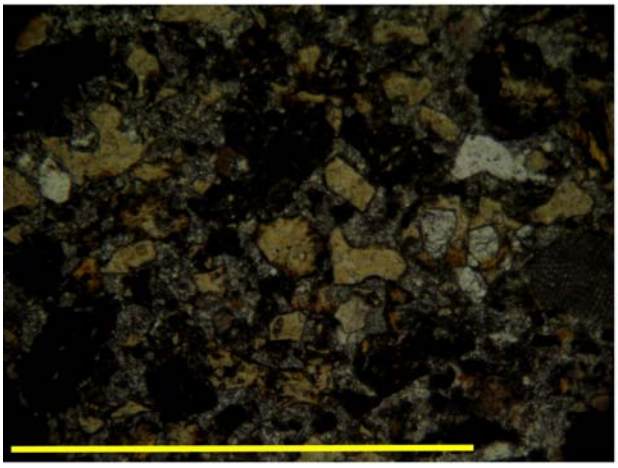

KC12-1C

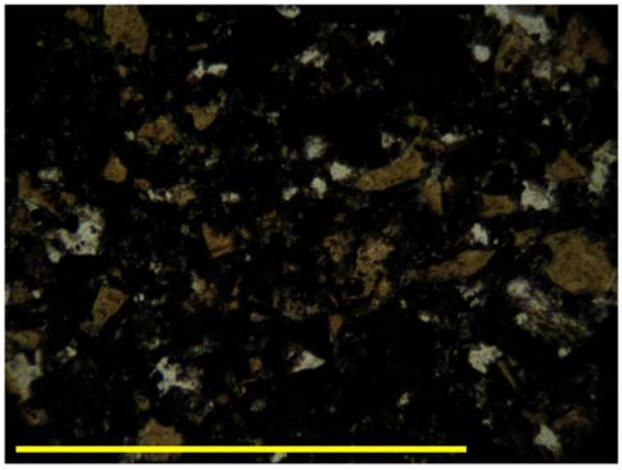

KC18-3A

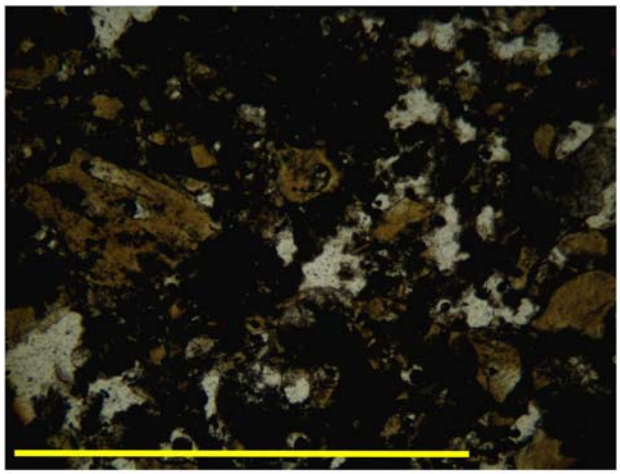

KC18-3B

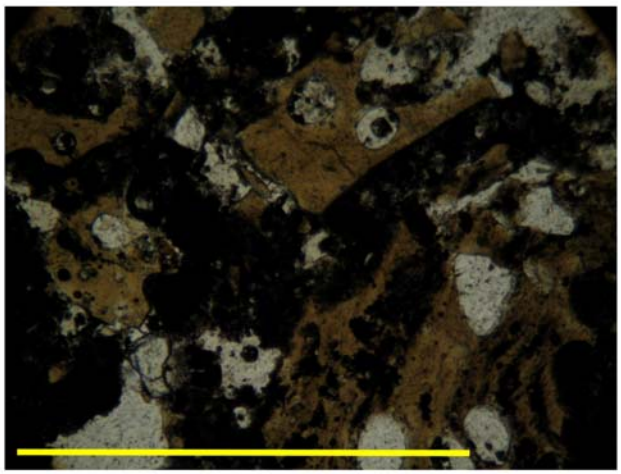

KC18-3C

Lf_b lithofacies

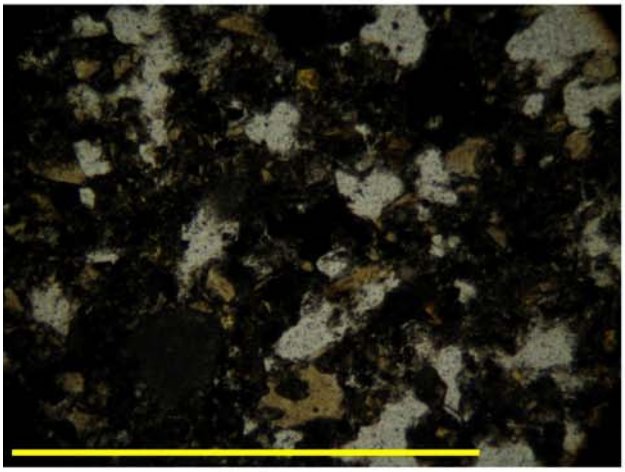

KC21-7A

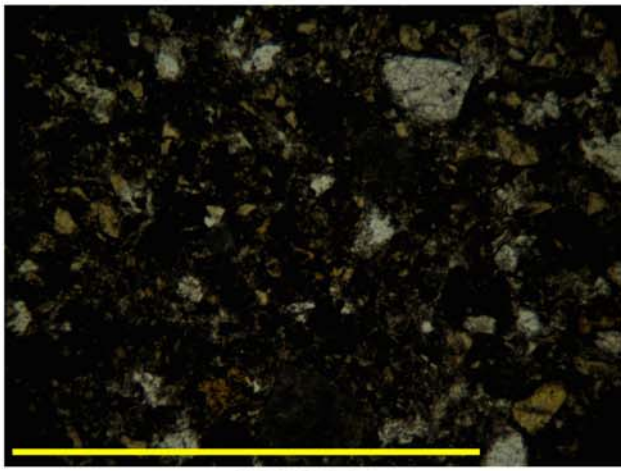

KC21-7B

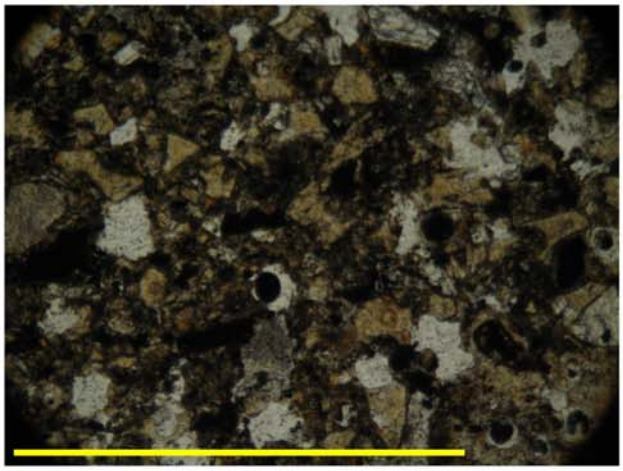

KC25-9A

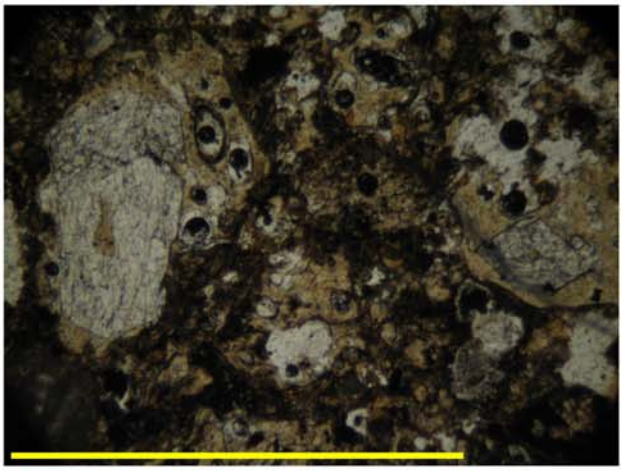

KC25-9B

Af_v lithofacies

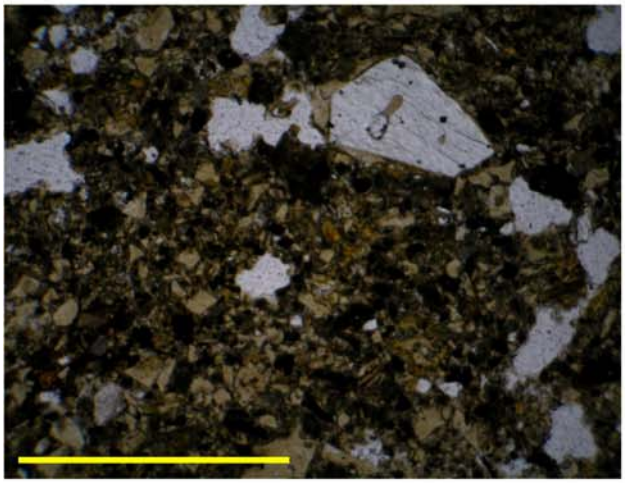

KC5-1A

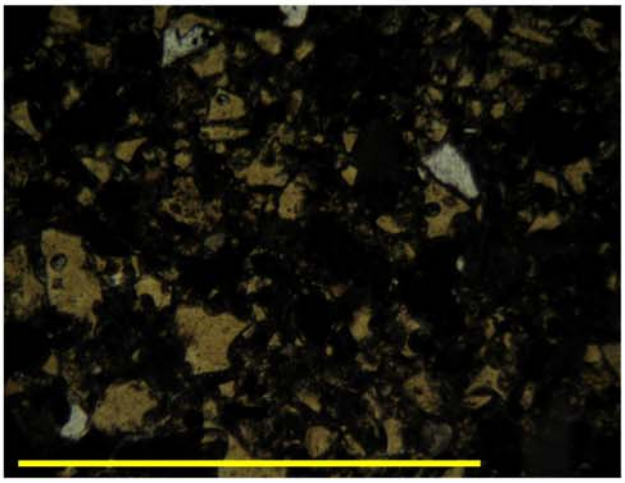

KC5-1B

Lf_m lithofacies

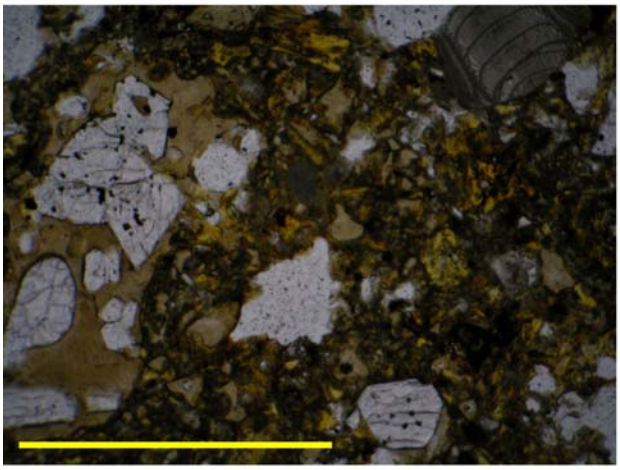

KC19-1A

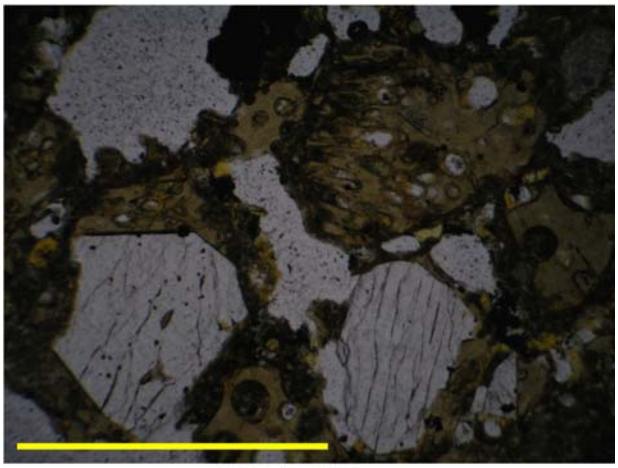

KC19-1B

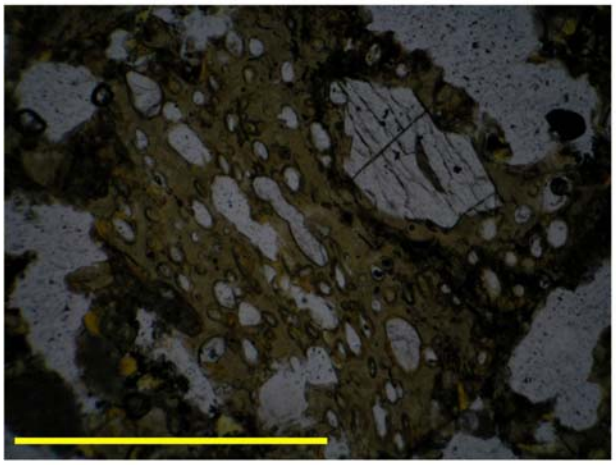

KC19-1C

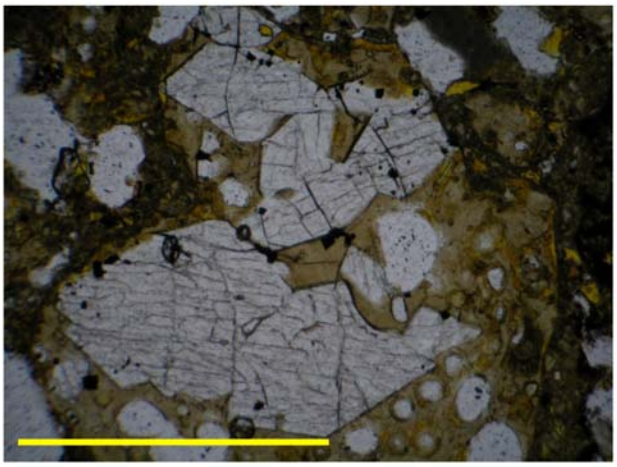

KC19-1D

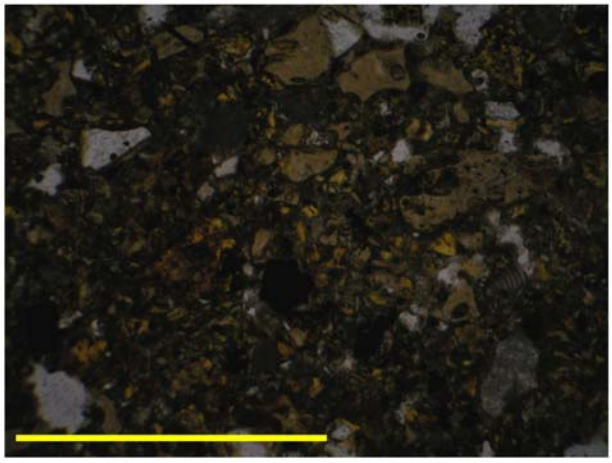

KC19-1E

Lc_m lithofacies

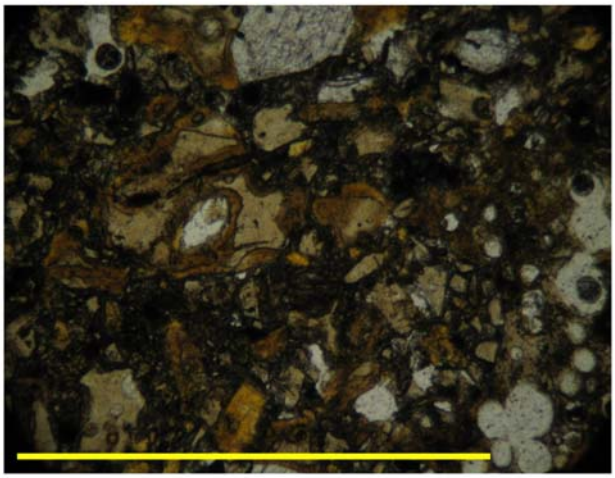

KC26-1A

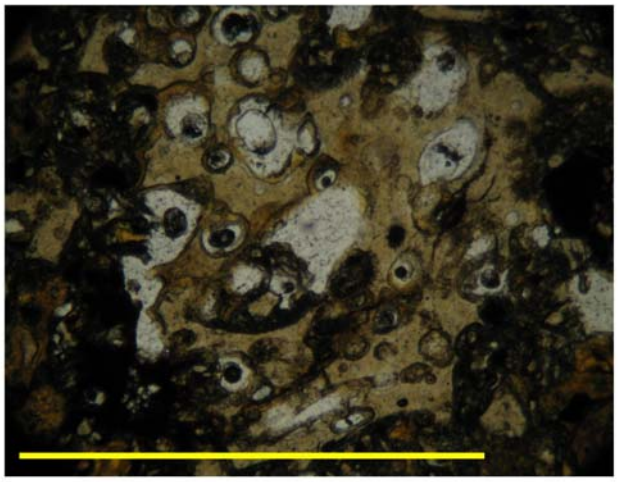

KC26-1B

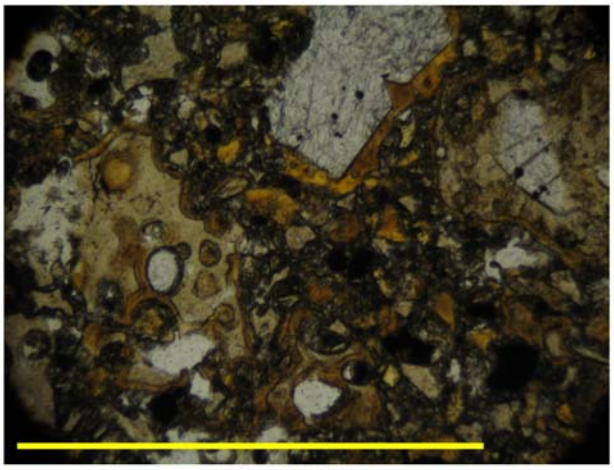

KC26-1C

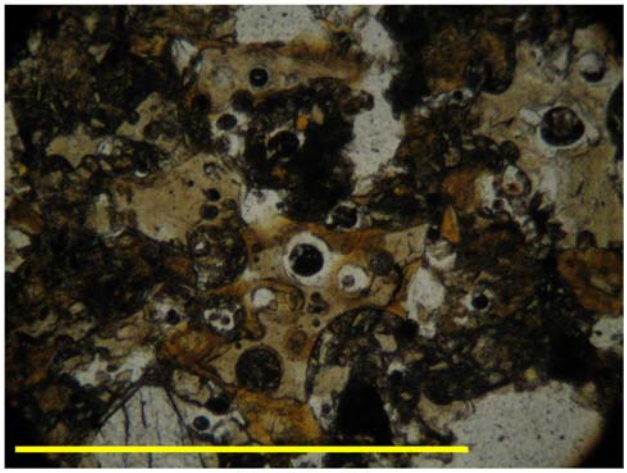

KC26-1D

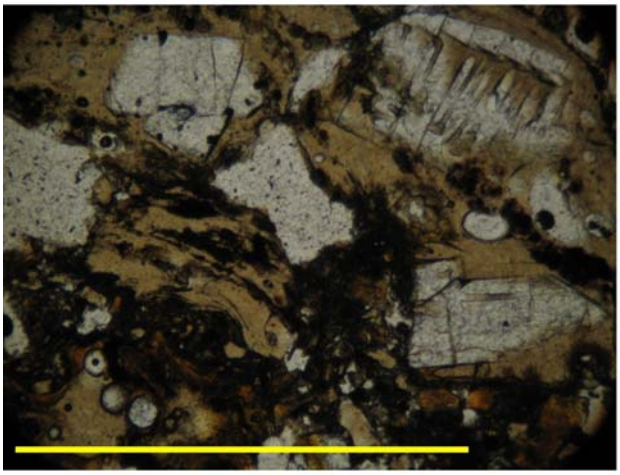

KC26-1E

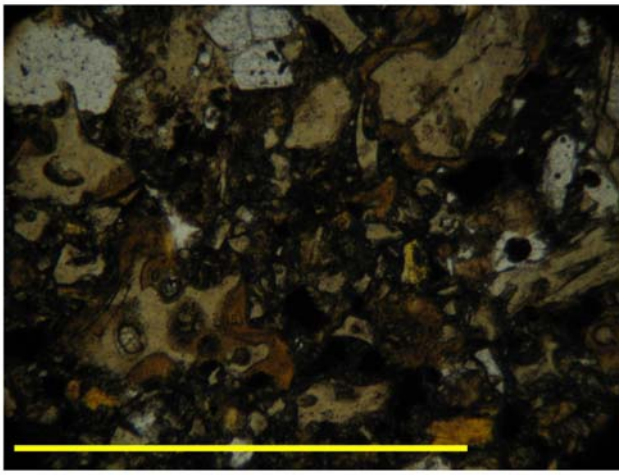

KC26-1F

BIBLIOGRAPHY

Baur, A.J., 1952, Soil and water conservation glossary, *Jour. Soil and Water Conserv*., **7**: 41-52, 93-104, 144-156.

Bennett, S.J., Casali, J., Robinson, K.M., and Kadavy, K.C., 2000, Characteristics of actively eroding ephemeral gullies in an experimental channel, *Transactions of the American Society of Agricultural Engineers*, **43**: 641-649.

Beverage, J.P. and Culbertson, J.K., 1964, Hyperconcentrations of suspended sediment, *J. Hydr. Div., American Society of Civil Engineers*, **90**, no. HY6:117-126.

Blong, R.J., 1970, The development of discontinuous gullies in a pumice catchment, *Am. J. Sci*., **268**: 369-383.

Boggs, S., Jr., 1995, Principles of Sedimentology and Stratigraphy, 2nd edition, Prentice-Hall, New Jersey, 774 pp.

Brantley, S.R. and Waitt, R.B., 1988, Interrelations among pyroclastic surge, pyroclastic flow, and lahars in Smith Creek valley during first minutes of 18 May 1980 eruption of Mount St. Helens, USA, *Bull. Volcanol*., **50**: 304-326.

Brice, J.C., 1966, Erosion and deposition in the loess-mantled Great Plains, Medicine Creek drainage basin, Nebraska, U.S. Geological Survey, Professional Paper 352-H: 255-339.

Bryan, R.B., 2000, Soil erodibility and processes of water erosion on hillslopes, *Geomorphology*, **32**: 385-415.

Bull, S.W. and Cas, R.A.F., 2000, Distinguishing base-surge deposits and volcaniclastic fluviatile sediments: an ancient example from the Lower Devonian Snowy River Volcanics, south-eastern Australia, *Sedimentology*, **47**: 87-98.

Calder, E.S., Sparks, R.S.J., and Gardeweg, M.C., 2000, Erosion, transport and segregation of pumice and lithic clasts in pyroclastic flows inferred from ignimbrite at Lascar Volcano, Chile, *J. Volcanol. Geotherm. Res*., **104**: 201-235.

Carey, B., Gray, J., and Seagrave, C., 2001, Gully erosion. Queensland Department of Natural Resources and Mines fact sheet, Natural Resource Sciences.

Carey, S.N., 1991, Transport and deposition of tephra by pyroclastic flows and surges. In: Fisher, R.V. and Smith, G.A. (eds) Sedimentation in volcanic settings, Soc. Sed. Geol. (SEPM) Special Publication 45: 39-57.

Carson, M.A. and Kirkby, M.J., 1972, Hillslope Form and Process, Cambridge University Press, New York, pp. 188-230.

Cas, R.A.F. and Wright, J.V., 1987, Volcanic Successions Modern and Ancient, Allen and Unwin, London, 528 pp.

Cole, P.D., Guest, J.E., Duncan, A.M., Pacheco, J.-M., 2001, Capelinhos 1957-1958, Faial, Azores: deposits formed by an emergent surtseyan eruption, *Bull. Volcanol.*, **63**: 204-220.

Colgate, S.E. and Sigurgeirsson, H., 1973, Dynamic mixing of water and lava, *Nature*, **244**: 552-555.

Collins, B.D. and Dunne, T., 1986, Erosion of tephra from the 1980 eruption of Mount St. Helens, *Geol. Soc. Am. Bull.*, **97**: 896-905.

Corradini, M.L., 1981, Phenomenological modeling of the triggering phase of small-scale steam explosion experiments, *Nucl. Sci. Eng.*, **78**: 154-170.

Costa, J.E., 1984, Physical geomorphology of debris flows. In: Costa, J.E. and Fleisher, P.J. (eds) Developments and Applications of Geomorphology, Springer-Verlag, Berlin, pp 268-317.

Crandell, D.R., 1971, Postglacial lahars from Mount Rainier Volcano, Washington, US Geol Surv Prof Pap 677: 1-73.

Dole, R.R. and Dalrymple, G.B., 1973, Potassium-argon ages and paleomagnetism of the Waianae and Koolau volcanic series, Oahu, Hawaii, *Geol. Soc. Am. Bull.*, **84**: 1217-1242.

Dunne, T., 1980, Formation and controls of channel networks, *Progress in Physical Geography*, **4**: 211-239.

Easton, W.H. and Olson, E.A., 1976, Radiocarbon profile of Hanauma Reef, Oahu, Hawaii, *Geol. Soc. Am. Bull.*, **87**: 711-719.

Enos, P., 1977, Flow regimes in debris flow, *Sedimentology*, **24**: 133-142.

Fairchild. L.H., 1987, The importance of lahar initiation processes. In: Costa, J.E. and Wieczorek, G.F. (eds) Debris Flows/Avalanches: Process, Recognition, and Mitigation. Geol Soc Am, Reviews in Engineering Geology VII, pp 51-61.

Favis-Mortlock, D.T., Boardman, J., Parsons, A.J., amd Lascelles, B., 2000, Emergence and erosion: a model for rill initiation and development, *Hydrological Processes*, **14**: 2173-2205.

Fiedler, A., Fröhlich, G., Müller, G., Benz, R., Bürger, M., Schwalbe, W., and Unger, H., 1980, Theoretische und experimentelle Untersuchungen zur Dampfexplosion. IKE 2 BMFT RS 206, 72 pp.

Fisher, R.V., 1977, Erosion by volcanic base-surge density currents: U-shaped channels, *Geol. Soc. Am. Bull.*, **88**: 1287-1297.

Fisher, R.V., 1979, Models for pyroclastic surges and pyroclastic flows, *J. Volcanol. Geotherm. Res.*, **6**: 305-318.

Fisher, R.V., 1983, Flow transformations in sediment gravity flows, *Geology*, **11**: 273-274.

Fisher, R.V. and Schmincke, H.-U., 1984, Pyroclastic Rocks. Springer-Verlag, Berlin, 472 pp.

Fisher, R.V. and Waters, A.C., 1970, Base surge bed forms in maar volcanoes, *Am. J. Sci.*, **268**: 157-180.

Francis, P., 1993, Volcanoes: A Planetary Perspective. Oxford University Press, New York, 443 pp.

Freundt, A. and Bursik, M., 1998, Pyroclastic flow transport mechanisms, In: Freundt, A. and Rosi, M. (eds) From Magma to Tephra: Modeling Physical Processes of Explosive Volcanic Eruptions, Elsevier, Amsterdam, 318 pp.

Glicken, H., Meyer, W., and Sabol, M.A., 1989, Geology and ground-water hydrology of Spirit Lake Blockage, Mount St. Helens, Washington, with implications for lake retention, U.S. Geol. Surv. Bulletin 1789: 1-33.

Gramlich, J.W., Lewis, V.A. and Naughton, J.J., 1971, Potassium-argon dating of Holocene basalts of the Honolulu volcanic series, *Geol. Soc. Am. Bull.*, **82**: 1399-1404.

Green, J. and Short, N.M., 1971, Volcanic landforms and surface features, a photographic atlas and glossary. Springer-Verlag, New York, 522 pp.

Hay, R.L. and Iijima, A., 1968, Petrology of palagonite tuffs of Koko Craters, Oahu, Hawaii, *Contr. Mineralogy and Petrology*, **17**: 141-154.

Heiken, G., 1972, Morphology and petrography of volcanic ashes, *Geol. Soc. Am. Bull.*, **83**: 1961-1988.

Heiken, G. and Wohletz, K., 1985, Volcanic Ash. University of California Press, Berkeley, 246 pp.

Heiken, G. and Wohletz, K., 1991, Fragmentation processes in explosive volcanic eruptions. In: Fisher, R.V. and Smith, G.A. (eds) Sedimentation in volcanic settings, Soc. Sed. Geol. (SEPM) Special Publication 45: 19-26.

Higgins, C.G., Hill, B.R. and Lehre, A.K., 1990, Gully development. In: Higgins, C.G. and Coates, D.R. (eds) Groundwater Geomorphology: The Role of Subsurface Water in Earth-Surface Processes and Landforms, Geol. Soc. Am. Special Paper, 252: 139-155.

Honnorez, J. and Kirst, P., 1975, Submarine basaltic volcanism: morphometric parameters for discriminating hyaloclastites from hyalotuffs, *Bull. Volcanol*., **39**: 441-465.

Horton, R.E., 1945, Erosional development of streams and their drainage basins: Hydrophysical approach to quantitative morphology, *Bull. Geol. Soc. Am*., **56**: 275-370.

Janda, R.D., Scott, K.M., Nolan, K.M., and Martinson, H.A., 1981, Lahar movement, effects, and deposits. In: Lipman, P.W. and Mullineaux, D.R. (eds), The 1980 eruptions of Mount St. Helens, Washington, U.S. Geol. Surv. Prof. Pap. 1250: 461-478.

Johnson, A.M., 1970, Physical processes in geology, Freeman, Cooper and Company, San Francisco, 577 pp.

Jones, J.A.A., 1990, Piping effects in humid lands. In: Higgins, C.G. and Coates, D.R. (eds) Groundwater Geomorphology: The Role of Subsurface Water in Earth-Surface Processes and Landforms, Geol. Soc. Am. Special Paper, 252: 111-138.

Keiffer, S.W. and Sturtevant, B., 1988, Erosional furrows formed during the lateral blast at Mount St. Helens, May 18, 1980, *J. Geophys. Res*., **93**: 14793-14816.

Knighton, D., 1998, Fluvial Forms and Processes: A New Perspective. Oxford University Press, New York.

Kokelaar, B.P., 1983, The mechanism of Surtseyan volcanism, *J. Geol. Soc. London*, **140**: 939-944.

Kokelaar, B.P., 1986, Magma-water interactions in subaqueous and emergent basaltic volcanism, *Bull. Volcanol.*, **48**: 275-289.

Laity, J.E. and Malin, M.C., 1985, Sapping processes and the development of theater-headed valley networks in the Colorado Plateau, *Geol. Soc. Am. Bull.*, **96**: 203-217.

Langenheim, V.A.M. and Clague, D.A., 1987, Stratigraphic framework of volcanic rocks of the Hawaiian Islands, U.S. Geol. Surv. Prof. Pap. 1350: 55-84.

Leat, P.T. and Thompson, R.N., 1988, Miocene hydrovolcanism in NW Colorado, USA, fuelled by explosive mixing of basic magma and wet unconsolidated sediment, *Bull. Volcanol.*, **50**: 229-243.

Leys, C., 1983, Volcanic and sedimentary processes during formation of the Saefell tuff-ring, Iceland, *Trans. Royal Soc. Edinburgh: Earth Sciences*, **74**: 15-22.

Lorenz, V., 1974, Vesiculated tuffs and associated features, *Sedimentology*, **21**: 273-291.

Lorenz, V., 1987, Phreatomagmatism and its relevance, *Chem. Geol.*, **62**: 149-156.

Lowe, D.R., 1982, Sediment gravity flows II: Depositional models with special reference to the deposits of high-density turbidity currents, *Jour. Sed. Petr*., **52**: 279-297.

Lowe, D.R., Williams, S.N., Leigh, H., Connor, C.B., Gemmell, J.B., and Stoiber, R.E., 1986, Lahars initiated by the 13 November 1985 eruption of Nevado del Ruiz, Colombia, *Nature*, **324**: 51-53.

Macdonald, G.A. and Abbott, A.T., 1970, Volcanoes in the sea: The geology of Hawaii, University of Hawaii Press, Honolulu, 441 pp.

Machado, F., Parsons, W., Richards, A., and Mulford, J., 1962, Capelinhos eruption of Fayal Volcano, Azores, 1957-1958, *J. Geophys. Res*., **67**: 3519-3529.

Maidment, D.R. (ed), 1993, Handbook of Hydrology, McGraw-Hill, Inc., New York.

Major, J.J. and Newhall, C.G., 1989, Snow and ice perturbations during historical volcanic eruptions and the formation of lahars and floods, *Bull. Volcanol.*, **52**: 1-27.

Manville, V., Hodgson, K.A., and White, J.D.L., 1998, Rheological properties of a remobilised-tephra lahar associated with the 1995 eruptions of Ruapehu volcano, New Zealand, *New Zealand Jour. Geol. Geophys.*, **41**: 157-164.

Merritt, E., 1984, The identification of four stages during micro-rill development, *Earth Surface Processes and Landforms*, **9**: 493-496.

Middleton, G.V., 1970, Experimental studies related to problems of flysch sedimentation, Geol. Assoc. Can. Sp. Paper 7: 253-272.

Moberly, R. and Walker, G.P.L., 1987, Coastal and volcanic geology of the Hanauma Bay area, Oahu, Hawaii, *Geol. Soc. Am. Centennial Field Guide, Cordilleran Section*: 5-10.

Moore, J.G., 1964, Giant submarine landslides on the Hawaiian Ridge, U.S. Geol. Surv. Prof. Paper 501 D: 95-98.

Moore, J.G., 1967, Base surge in recent volcanic eruptions, *Bull. Volcanol*., **30**: 337-363.

Moore, J.G., Nakamaru, K., Alcarez, A., 1966, The 1965 eruption of Taal Volcano, *Science*, **151**: 955-960.

Moore, J.G. and Sisson, T.W., 1981, Deposits and effects of the May 18 pyroclastic surge, In: Lipman, P.W. and Mullineaux, D.R. (Eds) The 1980 eruptions of Mount St. Helens, Washington, U.S. Geol. Surv. Prof. Pap. 1250: 421-438.

Mueller, W.U., Garde, A.A., and Stendal, H., 2000. Shallow-water, eruption-fed, mafic pyroclastic deposits along a Paleoproterozoic coastline: Kangerluluk volcano-sedimentary sequence, southeast Greenland, *Precambrian Res.,* **101**: 163-192.

Nairn, I.A., Wood, C.P., and Hewson, C.A.Y., 1979, Phreatic eruptions of Ruapehu: April 1975, *N.Z. Jour. Geol. Geophys*., **22**: 155-173.

Neall, V.E., 1976, Lahars – Global occurrence and annotated bibliography, Victoria University of Wellington, New Zealand, Publication 5, 18 pp.

Nejad, A.N. and Rezazadeh, S., 2002, Gully development in loess hilly area of Gorgan, northeast of Iran, *Proceedings of the 12th ISCO Conference*: 296-298.

Ollier, C.D., 1967, Maars: their characteristics, varieties, and definitions, *Bull. Volcanol*., **31**: 232-247.

Parker, G.G., Sr., Higgins, C.G., and Wood, W.W., 1990, Piping and pseudokarst in drylands. In: Higgins, C.G. and Coates, D.R. (Eds) Groundwater Geomorphology: The Role of Subsurface Water in Earth-Surface Processes and Landforms, Geol. Soc. Am. Special Paper 252: 77-110.

Peckover, R.S., Buchanan, D.J. and Ashby, D.E.T.F., 1973, Fuel-coolant interactions in submarine volcanism, *Nature*, **245**: 307-308.

Pierson, T.C., 1998, An empirical method for estimating travel times for wet volcanic mass flows, *Bull. Volcanol*., **60**: 98-109.

Pierson, T.C. and Costa, J.E., 1987, A rheological classification of subaerial sediment-water flows. In: Costa, J.E. and Wieczorek, G.F. (Eds) Debris Flows/Avalanches: Process, Recognition, and Mitigation, Geol. Soc. Am., Reviews in Engineering Geology VII: 1-12.

Pierson, T.C. and Scott, K.M., 1985, Downstream dilution of a lahar: Transition from debris flow to hyperconcentrated streamflow, *Water Resources Research*, **21**: 1511-1524.

Prothero, D.R. and Schwab, F., 1996, Sedimentary Geology: An Introduction to Sedimentary Rocks and Stratigraphy, W.H. Freeman and Company, New York, 575 pp.

Rauws, G., 1987, The initiation of rills on plane beds of non-cohesive sediments, *Catena Suppl*., **8**: 107-118.

Rosi, M., 1992, A model for the formation of vesiculated tuff by the coalescence of accretionary lapilli, *Bull. Volcanol.*, **54**: 429-434.

Rowley, P.D., Kuntz, M.A. and Macleod, N.S., 1981, Pyroclastic flow deposits, In: Lipman, P.W. and Mullineaux, D.R. (eds) The 1980 eruptions of Mount St. Helens, Washington, U.S. Geol. Surv. Prof. Pap. 1250: 489-512.

Sallenger, A.H., 1979, Inverse grading and hydraulic equivalence in grain-flow deposits, *Jour. Sed. Petr.*, **49**: 553-562.

Savat, J. and De Ploey, J., 1982, Sheetwash and rill development by surface flow. In: Bryan, R. and Yair, A. (Eds) Badland Geomorphology and Piping. Geo Books, University Press, Cambridge: 113-126.

Schmincke, H.-U., 1967, Graded lahars in the type sections of the Ellensburg Formation, south-central Washington, *Jour. Sed. Petr*., **37**: 438-448.

Schmincke, H.-U., 2004, Volcanism, Springer-Verlag, Berlin, 324 pp.

Schmincke, H.-U., Fisher, R.V. and Waters, A.C., 1973, Antidune and chute and pool structures in the base surge deposits of the Laacher See area, Germany, *Sedimentology*, **20**: 553-574.

Schumm, S.A., Mosley, M.P. and Weaver, W.E., 1987, Experimental fluvial geomorphology, Chichester, Wiley.

Scott, K.M., 1988, Origins, behavior, and sedimentology of lahars and lahar-runout flows in the Toutle-Cowlitz River system, U.S. Geol. Surv. Prof. Pap. 1447-A, 74 pp.

Selby, M.J., 1993, Hillslope Materials and Processes, Oxford University Press, Oxford, 451 pp.

Selby, M.J., 1994, Hillslope sediment transport and deposition. In: Pye, K. (ed) Sediment Transport and Depositional Processes. Blackwell Scientific Publications, UK, USA: 61-87.

Self, S. and Moberly, R., 1997, Phreatomagmatic volcanism and geology of southeast Oahu, *Cordilleran Section Meeting of the Geological Society of America, Kailula-Kona, May 21-23*, 1997: 1-34.

Shepherd, J.E. and Sturtevant, B., 1982, Rapid evaporation at the superheat limit, *J. Fluid Mech.*, **121**: 379-402.

Sheridan, M.F. and Updike, R.G., 1975, Sugar-loaf tephra – a Pleistocene rhyolitic deposit of base-surge origin in northern Arizona, *Geol. Soc. America Bull.*, **86**: 571-581.

Sheridan, M.F. and Wohletz, K.H., 1983, Hydrovolcanism: basic considerations and review, *J. Volcanol. Geotherm. Res.*, **17**: 1-29.

Sigurdsson, H., Carey, S.N. and Fisher R.V., 1987, The 1982 eruptions of El Chichon volcano, Mexico (3): physical properties of pyroclastic surges, *Bull. Volcanol*, **49**: 467-488.

Simpson, J.E. and Britter, R.E., 1979, The dynamics of the head of a gravity current advancing over a horizontal surface, *J. Fluid Mech.*, **94**: 477-495.

Smith, G.A., 1980, Non-magmatic historic eruptions and the origin of volcanic mudflows and floods of Mt. Pelée, Martinique, *Coompass*, **57**: 33-38.

Smith, G.A., 1986, Coarse-grained nonmarine volcaniclastic sediment: Terminology and depositional processes, *Geol. Soc. Am. Bull.*, **97**: 1-10.

Smith, G.A. and Lowe, D.R., 1991, Lahars: Volcano-hydrologic events and deposition in the debris flow-hyperconcentrated flow continuum. In: Fisher, R.V. and Smith, G.A. (Eds) Sedimentation in volcanic settings, Soc. Sed. Geol. (SEPM) Special Publication 45: 59-70.

Smith, R.L., 1960, Ash flows, *Geol. Soc. Am. Bull.*, **71**: 795-842.

Sohn, Y.K., 1995, Geology of Tok Island, Korea: eruptive and depositional processes of a shoaling to emergent island volcano, *Bull. Volcanol.*, **56**: 660-674.

Sohn, Y.K., 1996, Hydrovolcanic processes forming basaltic tuff rings and cones on Cheju Island, Korea, *Geol. Soc. Am. Bull.*, **108**: 1199-1211.

Sohn, Y.K. and Chough, S.K., 1992, The Ilchulbong tuff cone, Cheju Island, South Korea: depositional processes and evolution of an emergent, Surtseyan-type tuff cone, *Sedimentology*, **39**: 523-544.

Sparks, R.S.J., 1976, Grain size variations in ignimbrites and implications for the transport of pyroclastic flows, *Sedimentology*, **23**: 147-188.

Sparks, R.S.J., Barclay, J., Calder, E.S., Herd, R.A., Komorowski, J.-C., Luckett, R., Norton, G.E., Ritchie, L.J., Voight, B., and Woods, A.W., 1997, Generation of a debris avalanche and violent pyroclastic density current on 26 December (Boxing Day) 1997 at Soufriere Hills Volcano, Montserrat. In: Druitt, T.H. and Kokelaar, B.P. (Eds) The Eruption of Soufriere Hills Volcano, Montserrat, from 1995 to 1999, *Geol. Soc. London Mem.*, **21**: 409-434.

Sparks, R.S.J. and Walker, G.P.L., 1973, The ground surge deposit: a third type of pyroclastic rock, *Nature*, **241**: 62-64.

Stearns, H.T., 1985, Geology of the state of Hawaii, Second edition, Pacific Books, California, 335 pp.

Stearns, H.T. and Vaksvik, K.N., 1935, Geology and groundwater resources of the island of Oahu, Hawaii, *Bull. Hawaii Div. Hydrography*, **1**: 1-479.

Sturtevant, B. and Frost, D., 1984, Effects of ambient pressure on the instability of a liquid boiling explosively at the superheat limit. In: Proceedings of the Symposium on Fundamentals of Phase Change: Boiling and Condensation, Am. Soc. Mech. Eng. Winter Annual Meeting 1984.

Suzuki-Kamata, K., 1988, The ground layer of Ata pyroclastic flow deposit, southwest Japan – evidence for the capture of lithic fragments, *Bull. Volcanol*., **50**: 119-129.

Talbot, J.P., Self, S. and Wilson, C.J.N., 1994, Dilute gravity current and rain-flushed ash deposits in the 1.8 ka Hatepe Plinian deposit, Taupo, New Zealand, *Bull. Volcanol.*, **56**: 538-551.

Thorarinsson, S., 1964, Surtsey, the new island in the North Atlantic, Viking Press, New York, 47 pp.

Thorarinsson, S., Einarsson, Th., Sigvaldason, G., and Elisson, G., 1964, The submarine eruption off the Vestmann Islands 1963-64: A preliminary report, *Bull. Volcanol*., **27**: 435-445.

Valentine, G.A. and Fisher, R.V., 1993, Glowing avalanches: new research on volcanic density currents, *Science*, **259**: 1130-1131.

Vallance, J.W., 2000, Lahars. In: Sigurdsson, H., Houghton, B.F., McNutt, S.R., Rymer, H. and Stix, J. (eds) Encyclopedia of Volcanoes, Academic Press, San Diego, USA: 601-616.

Vallance, J.W. and Scott, K.M., 1997, The Osceola Mudflow from Mount Rainier: Sedimentology and hazard implications of a huge clay-rich debris flow, *Geol. Soc. Am. Bull.*, **109**: 143-163.

Vespermann, D. and Schmincke, H.-U., 2000, Scoria cones and tuff rings. In: Sigurdsson, H., Houghton, B.F., McNutt, S.R., Rymer, H. and Stix, J. (eds) Encyclopedia of Volcanoes, Academic Press, San Diego, USA: 683-696.

Waitt, R.B., Jr., Pierson, T.C., MacLeod, N.S., Janda, R.J., Voight, B., and Holcomb, R.T., 1983, Eruption-triggered avalanche, flood, and lahar at Mount St. Helens: Effects of winter snowpack, *Science*, **221**: 1394-1397.

Waldron, H.H., 1967, Debris flow and erosion control problems caused by the ash eruptions of Irazú Volcano, Costa Rica, U.S. Geol. Surv. Bulletin 1241-I, 37 pp.

Walker, G.P.L., 1984, Characteristics of dune-bedded pyroclastic surge bedsets, *J. Volcanol. Geotherm. Res.*, **20**: 281-296.

Walker, G.P.L. and Croasdale, R., 1972, Characteristics of some basaltic pyroclasts, *Bull. Volcanol.*, **35**: 303-317.

Waters, A.C. and Fisher, R.V., 1971, Base surges and their deposits: Capelinhos and Taal Volcanoes, *J. Geophys. Res.*, **76**: 5596-5614.

Wentworth, C.K., 1926, Pyroclastic geology of Oahu, Bernice P. Bishop Museum Bulletin 30, 121 pp.

White, J.D.L., 1991, The depositional record of small, monogenetic volcanoes within terrestrial basins. In: Fisher, R.V. and Smith, G.A. (eds) Sedimentation in volcanic settings, Soc. Sed. Geol. (SEPM) Special Publication 45: 155-171.

White, J.D.L. and Houghton, B.F., 2000, Surtseyan and related phreatomagmatic eruptions. In: Sigurdsson, H., Houghton, B.F., McNutt, S.R., Rymer, H. and Stix, J. (eds) Encyclopedia of Volcanoes, Academic Press, San Diego, USA: 495-511.

Wilson, C.J.N. and Houghton, B.F., 2000, Pyroclast transport and deposition. In: Sigurdsson, H., Houghton, B.F., McNutt, S.R., Rymer, H. and Stix, J. (eds) Encyclopedia of Volcanoes, Academic Press, San Diego, USA: 545-554.

Wilson, C.J.N. and Walker, G.P.L., 1982, Ignimbrite depositional facies: the anatomy of a pyroclastic flow, *J. Geol. Soc. Lond.*, **139**: 581-592.

Wilson, C.J.N. and Walker, G.P.L., 1985, The Taupo eruption, New Zealand I. General aspects, *Phil. Trans. R. Soc. Lond.*, A. **314**: 199-228.

Winchell, H., 1947, Honolulu Series, Oahu, Hawaii, *Geol. Soc. Am. Bull.*, **58**: 1-48.

Wohletz, K.H., 1986, Explosive magma-water interactions: Thermodynamics, explosion mechanisms, and field studies, *Bull. Volcanol.*, **48**: 245-264.

Wohletz, K.H., 1998, Pyroclastic surges and compressible two-phase flow. In: Freundt, A. and Rosi, M. (eds) From Magma to Tephra: Modeling Physical Processes of Explosive Volcanic Eruptions, Elsevier, Amsterdam, 318 pp.

Wohletz, K.H., 2003, Water/magma interaction: Physical considerations for the deep submarine environment. In: White, J.D.L., Smellie, J.L., and Clague, D.A. (eds.) Explosive Subaqueous Volcanism, American Geophysical Union, Geophysical Monograph 140: 25-49.

Wohletz, K.H. and Crowe, B.M., 1978, Development of lahars during the 1976 activity of La Soufriere de Guadeloupe, F.W.I., *Geol. Soc. Am. Abstracts with Programs*, **10**: 154.

Wohletz, K.H. and McQueen, R., 1981, Experimental hydromagmatic volcanism, *Amer. Geophys. Union Trans.*, EOS, **62(45)**: 1085.

Wohletz, K.H. and Sheridan, M.F., 1981, Rampart crater ejecta: experiments and analysis of melt/water interactions, *NASA Tech. Memor*. 82385: 134-136.

Wohletz, K.H. and Sheridan, M.F., 1982, Melt/water interactions: series II experimental design, *NASA Tech. Memor.*, 84211: 169-171.

Wohletz, K.H. and Krinsley, D.H., 1983, Scanning electron microscopic analysis of basaltic hydromagmatic ash. In: Whaley, W.B. and Krinsley, D.H. (eds), SEM in Geology, Geoabstracts, Norwich, England.

Wohletz, K.H. and Sheridan, M.F., 1983, Hydrovolcanic explosions II: evolution of basaltic tuff rings and tuff cones, *Am. J. Sci*., **283**: 385-413.

Zimanowski, B., 1998, Phreatomagmatic explosions. In: Freundt A. and Rosi, M. (eds.), From Magma to Tephra: Modeling Physical Processes of Explosive Volcanic Eruptions, Elsevier, Amsterdam, 25-53.

Zimanowski, B., Büttner, R., and Lorenz, V., 1997a, Premixing of magma and water in MFCI experiments, *Bull. Volcanol.*, **58**: 491-495.

Zimanowski, B., Büttner, R., Lorenz, V., and Häfele, H.G., 1997b, Fragmentation of basaltic melt in the course of explosion volcanism, *J. Geophys. Res*., **102**: 803-814.

Zimanowski, B. and Büttner, R., 2003, Phreatomagmatic explosions in subaqueous volcanism. In: White, J.D.L., Smellie, J.L., and Clague, D.A. (eds.) Explosive Subaqueous Volcanism, American Geophysical Union, Geophysical Monograph 140: 51-60.